The cell biology underlying juvenile ceroid lipofuscinoses (Batten disease)

Alessandra Calvi

A thesis submitted to the University of London for the degree of Doctor of Philosophy

February 2008

General and Adolescent Paediatric Unit
Institute of Child Health
University College London
The Rayne Building
5 University Street
London WC1E 6JJ

MRC Laboratory for Molecular Cell Biology
University College London
Gower Street
London WC1E 6BT

ProQuest LLC
789 East Eisenhower Parkway
P.O. Box 1346
Ann Arbor, MI 48106-1346

Declaration

I, Alessandra Calvi, confirm that the work presented in this thesis is my own. Where information have been derived from other sources, I confirm that this has been indicated in the thesis.

Abstract

The juvenile form of Batten Disease (JNCL) is an autosomal recessive neurodegenerative disease caused by mutations in the CLN3 protein, an integral membrane protein of unknown function. The hallmark of JNCL is the accumulation of storage material in lysosomes consisting predominantly of subunit c of mitochondrial ATP synthase.

CLN3 protein is present primarily in endosomes and lysosomes in non-neuronal cells, whereas in neuronal cells it is also reported to be in presynaptic vesicles and along the neurites. The current best evidence is that it traffics through the endoplasmic reticulum and Golgi apparatus to the endosome and lysosome, sorted by a dileucine motif which binds the adaptor complexes AP-1 and AP-3.

The effects of loss of CLN3 protein function on membrane trafficking were investigated in the *Cln3*$^{\Delta ex1\text{-}6}$ knockout mouse model and in human cell lines deficient for CLN3 due to siRNA-mediated gene silencing. Morphological analysis and immunostaining of CLN3-deficient fibroblasts and neurons revealed the presence of normal lysosomes but also an accumulation of aberrant organelles of autophagic origin.

Endocytic tracer analysis indicated that the aberrant organelles accumulate due to a defect in fusion between autophagosomes and lysosomes. Phagocytic defects involving a failure to recruit late endocytic markers were also defined. Together these findings indicate a similar defect in both these cellular pathways, involving defective maturation of autophagosomes and phagosomes which is accompanied by accumulation of undigested material in CLN3-deficient cells.

As well as impairments in the mechanism of endosome fusion with autophagosomes and phagosomes, defects in an additional cellular mechanism were detected in CLN3-deficient cells. The route of protein trafficking from the trans-golgi network (TGN) to endosomes is interrupted after CLN3 gene silencing, resulting in retention of the cation-independent mannose-6-phosphate receptor in the TGN accompanied by defective processing of lysosome hydrolases.

This investigation of the cellular pathology underlying Batten disease reveals a role for CLN3 in two distinct but related cellular pathways: autophagyc and phagocytosis and it also plays a role in TGN to endosome trafficking. This contributes to the understanding of the cellular phenotype underlying CLN3/Batten disease and most likely other forms of neuronal ceroid lipofuscinosis.

Contents

List of figures

List of tables

1 Introduction

1.1 Neuronal ceroid lipofuscinoses (NCL) or Batten disease

The neuronal ceroid lipofuscinoses (NCLs) are a genetically heterogeneous group of recessively inherited disorders which collectively form the most common neurodegenerative diseases of childhood, with an incidence as high as 1:12,500 live births (Santavuori, 1988) (Rider and Rider, 1999){the neuronal ceroid lipofuscinoses, H.H. Goebel, Eds}. There are at least ten clinically defined related NCL subtypes, and with the recent confirmation that cathepsin D and MFSD8 deficiency causes a human NCL subtype, a total of eight NCL genes have been characterised (Cooper, 2003) (Siintola et al., 2007; Siintola et al., 2005; Steinfeld et al., 2006).

Recently mutations in chloride channels CLC-6 and CLC-7 present in late endosomes and lysosomes have also been proposed as NCL-causing genes (Kasper et al., 2005; Poet et al., 2006).

NCL disorders are lysosomal storage disorders characterized by widespread intracellular accumulation of autofluorescent lipopigment in patient's tissues. NCL brains show neuronal cell atrophy and neuronal loss including a neuronal loss in the retina {the neuronal ceroid lipofuscinoses, H.H. Goebel, Eds}.

NCLs have traditionally been diagnosed based on the age at onset and distinct ultrastructure of the storage material. Four forms of NCL were initially identified, classified as infantile (INCL); late-infantile (LINCL); juvenile (JNCL) and adult (ANCL). Various late-infantile subgroup variants have been defined (Table 1-1) (Kyttala et al., 2006).

Patients suffer from uncontrollable seizures, visual failure, cognitive and motor decline and ultimately premature death. At present there is no effective therapy (Cooper, 2003) (Dyken, 1988).

Table 1-1 NCL classification

Clinical subtype	Gene	Protein	Storage phenotype
Congenic	Cat D	Cathepsin D aspartic protease	GROD Saposin A+D/subunit c
Infantile	CLN1	Palmitoyl protein thioesterase 1	GROD Saposin A+D
Late-infantile, 1. Classic	CLN2	Tripeptidyl peptidase 1	CL Subunit c
2. Finnish variant	CLN5	Soluble lysosome protein	FP/CL Subunit c
3. Variant	CLN6	ER membrane protein	FP/CL Subunit c
4. Turkish	CLN7	MFSD8 putative transporter	FP/CL ?
5. N. epilepsy/EMPR	CLN8	ER-ERGIC membrane protein	RL Subunit c
Juvenile	CLN3	Late endosome, lysosome membrane protein	FP Subunit c

1.1.1 Pathology of NCLs

The characteristic feature of NCL pathology is the intra-lysosomal accumulation of autofluorescent proteolipid in the brain and other tissues (Koenig, 1964) (Haltia et al., 1973) (Goebel, 1995). By electron microscopy, the electron dense accumulations have different appearances, depending on the NCL subtype. The ultrastructural morphology of the storage inclusions is used diagnostically and these subtypes have been classed as granular osmiophilic deposits (GRODs), curvilinear profiles (CL), rectilinear

profiles (RL) and fingerprint bodies (FP). Some NCL forms have a mixture of FP and CL/RL (Goebel et al., 1999).

The storage material present in the lysosomes is composed of a lipid-protein complex. The protein content varies and consists predominantly of either subunit c of the mitochondrial ATP synthase complex (F0/F1-ATP-ase) in subtypes CLN2, 3, 4, 5, 6, 7, 8, or predominant of saposins A and D in CLN1 (Palmer et al., 1992).

Mitochondrial ATP synthase subunit c is normally found as a component of the mitochondrial ATP synthase complex located on the inner mitochondrial membrane. It is encoded by two genes *P1* and *P2* (Ezaki et al., 1995). In both sheep models and patients with NCL, unmodified subunit c accumulates in cells but these two genes have normal sequence and mRNA expression levels (Medd et al., 1993). In addition the rate of oxidative phosphorylation in NCL cells is normal (Ezaki et al., 1995; Palmer et al., 1992) suggesting that the subunit c accumulation is not due to its malfunction.

1.1.2 Juvenile Batten disease

The juvenile-onset form of NCL (JNCL), also known as Juvenile Batten disease is the most frequent subtype. JNCL is caused by mutations in the *CLN3* gene which encodes the CLN3 protein The morphology and ultrastructure of the storage is of fingerprint bodies (Figure 1.1).

Figure 1.1 Fingerprint profile of the storage material characteristic of JNCL.
Electron micrograph of storage fingerprint profile present in a patient with mutation in the CLN3 protein. Image by Dr Juhani Rapola.

1.2 CLN3

The *CLN3* gene located on chromosome 16p12.1 was isolated by positional cloning in 1995, and has been shown to be responsible for JNCL by the identification of disease-causing mutations (Batten disease consortium, 1995) . There are now a total of 41 characterised *CLN3* mutations (http://www.ucl.ac.uk/ncl/). A founder effect is seen in JNCL and the most common mutation of the *CLN3* gene occurs in over 90% of patients. This is a 1 kb deletion in the genomic DNA, which removes exons 7 and 8. This mutation results in a truncated protein due to the loss of amino acids 154-438, and the introduction of 28 novel amino acids at the C terminal (Batten disease consortium, 1995).

The *Cln3* gene consists of 15 exons and encodes a protein of 438 amino acids which has no known homology to other proteins. The *CLN3* protein is conserved across all eukaryotes including *C.elegans* and yeast (Taschner et al., 1997). The function of CLN3 is not known, as discussed further in section 1.3.3.

There have been several computer prediction based models published of the structure of CLN3, each proposing that the protein is an integral membrane protein (Phillips et al., 2005). The topology has been predicted to comprise between five to

eight transmembrane spanning regions (Janes et al., 1996) (Mitchison et al., 1997) (Ezaki et al., 2003) (Mao et al., 2003a) and more recent studies support six transmembrane domains with the both the C termini and N termini positioned towards the cytosol (Kyttala et al., 2004) (Storch et al., 2004) (Figure 1.2).

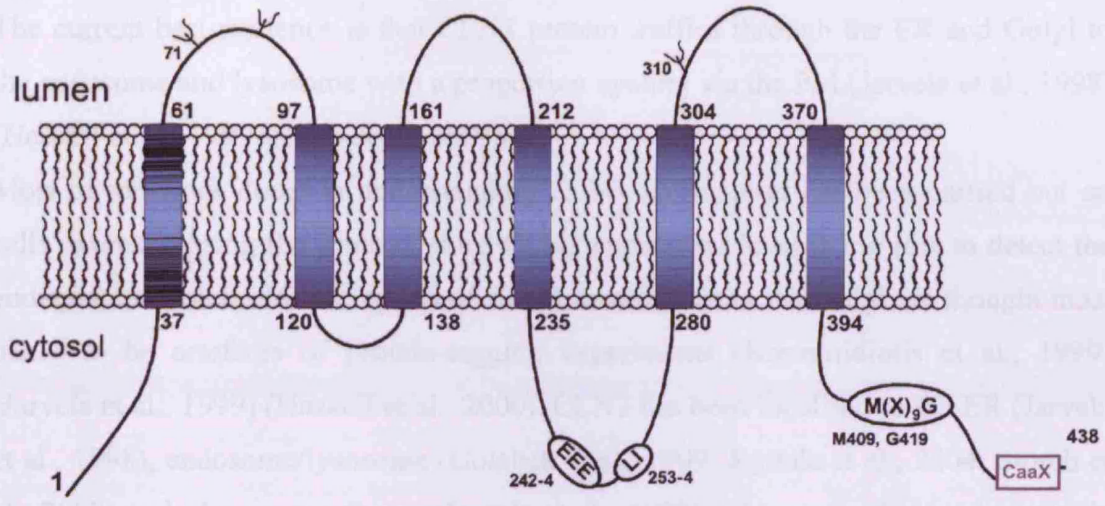

Figure 1.2. CLN3 structure
The topology of the 438 amino acid CLN3 protein is shown with the 6 transmembrane spanning regions and two lysosomal targeting motifs (in circles) reported in Kyytala et.al., 2004. Both N and C termini are exposed towards the cytosol. The two N-glycosylation sites and C-terminal farnesylation site (CaaX) reported by Storch et. al., 2007 are also shown.

Originally several motifs were identified in CLN3 that could give clues to structure and function. These were: four putative N-glycosylation sites, 2 O-glycosylation sites, 2 glycosaminglican attachment sites, 2 cAMP and cGMP dependent protein kinase phosphorylation sites, 6 protein kinase C phosphorylation sites, 8 casein kinase II phosphorylation site, 12 N-myristoylation sites and a farnesylation site at the C-terminal (Batten disease consortium, 1995). CLN3 appears to be reatively heavily glycosylated. Glycosylation of lysosomal enzymes targets them to the lysosome and may protect them from being degraded. A glycosylation motif was indentified at the N terminus. N-linked glycosylation sites can be important for the right localization of a

protein (Jarvela et al., 1998). CLN3 has two lysosomal targeting motifs (Ezaki et al., 2003) (Kyttala et al., 2004) (Storch et al., 2004) .

1.2.1 CLN3 localization and trafficking

Several groups have studied the localization of the CLN3 protein with varying results. The current best evidence is that CLN3 protein traffics through the ER and Golgi to the endosome and lysosome with a proportion cycling via the PM (Jarvela et al., 1998) (Haskell et al., 1999) (Mao et al., 2003a).

Most of the work done on understanding CLN3 localization has been carried out on cells overexpressing the protein, since CLN3 expression level is too low to detect the endogenous protein. Initial reports of CLN3 localization in the Golgi are thought most likely to be artefacts of protein-tagging experiments (Kremmidiotis et al., 1999) (Jarvela et al., 1999) (Haskell et al., 2000). CLN3 has been localised to the ER (Jarvela et al., 1998), endosome/lysosome (Golabek et al., 1999; Kyttala et al., 2004; Storch et al., 2007) and plasma membrane (Jarvela et al., 1999) (Mao et al., 2003a) in somatic cells.

In neuronal cells CLN3 has been proposed to be in synaptic vesicles (Haskell et al., 1999), the nucleus and the cytoplasm (Margraf et al., 1999). Other work carried out analyzing retinal neurons provides evidence that CLN3 is targeted to the neuronal synapse (synaptosomes) but excluded from synaptic vesicles (Luiro et al., 2001).

Detection of murine endogenous CLN3 has been reported in immortalized cerebellar neuronal precursor cells lines (Fossale et al., 2004) and in mouse retinal cells (Luiro et al., 2001). The endogenous protein was shown to co-localise with the lysosomal marker LAMP1 but more markedly with the early endosomal antigen EEA1 and the late endosomal marker Rab7 (Fossale et al., 2004). Limited overlap was observed with transferrin receptor, which is a marker of recycling early endosomes.

Lysosomal targeting of CLN3 appears to be facilitated by two targeting motifs, an unconventional motif in the C-terminal cytosolic tail consisting of a methionine and a glycine separated by nine amino acids [M(X)9G], and a more conventional dileucine-type motif in a cytoplasmic loop domain preceded by an acidic patch (Mao et al.,2003)

(Kyttala et al., 2004) (Storch et al., 2004). Deletion of both lysosomal targeting motifs abolishes targeting of the CLN3 protein to the lysosomes (Kyttala et al., 2005). Recently, a C terminal prenylation motif was also proposed as a facilitator of lysosomal targeting (Storch et al., 2007).

A small proportion of CLN3 has been reported to be present at the plasma membrane, and this suggests that at least some CLN3 may recycle through the plasma membrane en route to the endocytic system (Jarvela et al., 1998). On the other hand studies on embryonic testicular carcinoma cells in which expression of the μ3A subunit of the adaptor protein AP-3 had been silenced, showed upregulation of CLN3 at the plasma membrane demonstrating that at least a proportion of CLN3 likely goes to the lysosomes directly under normal circumstances in a AP-3 dependent manner (Mao et al., 2003b).

Evidence has been presented that the CLN3 dileucine motif binds both the adaptors AP-1 and AP-3 in vitro, and that the dileucine targeting motif alone is not able to sort CLN3 when one of the two adaptors is impaired (Kyttala et al., 2005). In fact CLN3, when its sorting depends on the dileucine motif, accumulates within the Golgi in AP-3 deficient fibroblasts. In AP-1 deficient fibroblasts it is mistargeted into transferrin positive structures and the plasma membrane. Therefore it is most likely that CLN3 traffics from the Golgi to the endosomes via AP-1 or AP-3 and is subsequently sorted from the endosomes to lysosomes via AP-1 or AP-3. Whichever adaptor proteins are specifically involved, CLN3 traffics to the endosomes before going to the final destination, which is the lysosome.

However it should be noted that another study disagreed with these finding, showing that CLN3 does not interact with AP-1, AP-3 or the GGAs (Storch et al., 2004).

1.3 Mouse models for Juvenile Batten disease (JNCL)

To facilitate studies on Batten disease pathogenesis and treatment, Cln3-deficient mice were created by homologous recombination and targeted disruption of the murine *Cln3* gene.

Four mouse models of juvenile onset NCL have been created so far by different gene targeting strategies. *Cln3* knockout mice were made by insertion mutation using the neomycin selectable marker cassette to disrupt the *Cln3* gene by replacement of exon 1-6 (Mitchison et al., 1999) or of exon 7-8 (Katz et al., 1999). A more subtle mutation was created to make *Cln3* knock-in mice using *cre-lox* technology, such that *Cln3* exon 7 and 8 were deleted, replaced by a single *loxP* site that was left in intronic sequence between exon 6 and 9 (Cotman et al., 2002). This is a genetically accurate model, exactly mimicking the major CLN3 1 Kb deletion, which removes exon 7 and 8 .

Recently a new reporter knock out mouse model was produced by insertion of a neomycin-ß galactosidase cassette to disrupt the gene by replacement of exon 1-8 and simultaneously report gene expression from the endogenous *Cln3* promoter. This allows study of CLN3 expression during embryogenesis and development to correlate the expression of CLN3 with the behaviour of the animals (Eliason et al., 2007).

All the mice models are viable and fertile but die prematurely with a late stage neurological phenotype recapitulating cell biological and pathological features of Batten disease (Cotman et al., 2002; Katz et al., 1999; Mitchison et al., 1999) (Eliason et al., 2007). Two of the models are not yet characterized (Eliason et al., 2007; Katz et al., 1999).

1.3.1 *Cln3* $^{\Delta ex1/6}$ mice as a model to study CLN3

The mouse model used in this thesis was the exon 1-6 deletion model mentioned in the previous paragraph (Mitchison et al., 1999) (hereafter referred to as '*Cln3* KO'). *Cln3* KO mice reproduce many of the features which characterize patients with JNCL. The mice start accumulating storage material from the age of 3 weeks, but do not display obvious clinical symptoms until around 16 months of age (Mitchison et al., 1999). Mice die around 18-20 months (Pontikis et al., 2004).

The storage material is autofluorescent and positive for the subunit c of the mitochondrial ATPase, similarly to JNCL patients.

Widespread degeneration and loss of neurons occurs in the central nervous system from 7 months, predominantly the cortex and cerebellum and this is accompanied by hypertrophy of many interneurons in the hippocampus.

Deterioration of vision due to retinitis pigmentosa is typically the first clinical sign to manifest in children with Juvenile Batten disease from the age of 4-8 years. One of the primary insults within the retina is the death of photoreceptors (Bensaoula et al., 2000). In *Cln3* KO mice retinal function appears relatively well preserved (Seigel et al., 2002) but there are deficits in optic nerve conduction accompanying degenerative loss of cells within the central visual processing regions of the brain, and this is proposed to precipitate the visual deterioration associated with CLN3 deficiency. A selective loss of the large retina-recipient projection neurons within the dorsal portion of the lateral geniculate was also observed (Weimer et al., 2006).

At the organelle level in addition to the presence of the storage of material, which accumulates in the cells, abnormal mitochondria were observed in brain tissue by electron microscopy investigation (Jolly et al., 2002).

Other reported findings from analysis of the mouse brains indicated decreased activity of glutamic acid decarboxylase resulting in elevated glutamate levels (Chattopadhyay et al., 2002). Also AMPA receptor function was found to be enhanced in cerebellar granular cells and suggested CLN3 could have a role directly or indirectly affecting the cycling of the receptor (Kovacs et al., 2006).

Currently, there is debate over the mechanism of neuronal cell death with evidence of both apoptosis and autophagy (Mitchison et al., 2004). In particular autophagy was reported in the mouse model around 12 months of age with findings that degenerating neurons from cortex were crowded with autophagic vacuoles and did not present any sign of apoptosis (Mitchison et al., 2004).

In the retina it appears clear that photoreceptors die by apoptosis (Seigel et al., 2002).

1.3.2 *Cln3* knock-in mouse (*CLN3*$^{\Delta ex7/8}$)

To investigate the common *CLN3* 1 Kb mutation, an identical genomic DNA deletion (the elimination of the exons 7 and 8) was introduced into the murine *CLN3* homologue, to create *Cln3*$^{\Delta ex7/8}$ knock-in mice (Cotman, 2002).

Like *Cln3* KO mice, *Cln3*$^{\Delta ex7/8}$ mice exhibit typical JNCL cellular features including accumulation of mitochondrial ATPse subunit c positive storage material in fingerprint-like inclusions. However, the neurological deficits are more marked and the mice also have a worse survival span, indicating a more severe classical phenotype. It is suggested that some features such as retinal degeneration in this mouse may be connected with the different strain background in addition to the different mutation and different housing. The knock-in mice were on 129/Sv-CD1 strain, while the *Cln3* KO were on 129/Sv-C57BL isogenic or mixed strain, and the CD1 strain is known to have visual deficits (Cotman, 2002). However, the possibility remains that the severity of the phenotype is connected to the specific mutation.

Homozygous *Cln3*$^{\Delta ex7/8}$ mutant mice displayed storage accumulation in peripheral cells and brains, evident from the E19.5 embryonic stage in liver, cerebellum, in neurons of the dentate gyrus and in the subventricular zone of the lateral ventricle. Degeneration of retinal neurons, CNS reactive astrocytosis, neurological deficits and reduced survival were also observed. This suggests that the disease starts before birth and this process does not perturb normal CNS development, but instead causes the demise of mature neurons(Cotman et al., 2002) as also proposed for the *Cln3* knock out mouse model.

RT-PCR amplification of *Cln3* mRNA from *Cln3*$^{\Delta ex7/8}$ peripheral tissue and brains showed that the common mutation yields multiple stable mRNA splice variants. The longest mutant cDNA is predicted to encoding a truncated 38kDa protein comprising the N terminus (exons 1-6) and C terminus (exons 9-15) of the *Cln3* gene, with a novel 29-residue midsection encoded by a frameshifted exon 6. If mutant *Cln3* protein exists and is expressed from these splice variants, this could create a different effect on cell homeostasis to that arising from complete absence of the protein, which is the

presumed situation in the *Cln3* KO mouse though RT-PCR analysis of the *Cln3* knock out model is not completed so there is no direct comparison yet. However, since adequate antibodies are not yet available to detect endogenous protein, there is no definitive proof of presence or absence of mutant protein in any of the *Cln3* mutant mice.

1.3.3 CLN3 functions

The function of the CLN3 protein remains unclear. The hallmark of JNCL is the accumulation of subunit c of the mitochondrial ATPase. For this reason several groups investigated the degradation capacity of CLN3 deficient cells with particular focus on the processing of the enzymatic activity of cathepsin D, which is required for subunit c degradation (Kominami et al., 1995) . Defects in cathepsin D processing were found but give conflicting results. In HEK cells overexpression of the CLN3 protein tagged to GFP revealed a higher level of the precursor and intermediate forms of cathepsin D whilst CLN3 knock down induced with antisense transfection resulted in an increased amount of the mature form (Golabek et al., 2000).

In contrast, immortalized cerebellar cells from the $Cln3^{\Delta ex7/8}$ mouse showed a reduced precursor and mature forms but an elevated intermediate form of cathepsin D (Cao et al., 2006). The difference between the two cells lines could be due to use of antisense RNA in the first case and the use of 1kb deletion cells in the second giving different cellular effects. Indirect immunofluorescence of cathepsin D in $Cln3^{\Delta ex7/8}$ cerebellar cells showed more perinuclear and less cytoplasmic punctate signal than in the wild type suggesting defective targeting to lysosomes. Analysis of the growth media did not shown altered levels of cathepsin D, excluding an increase in secretion and their cathepsin D total enzymatic activity was not different from the wild type (Fossale et al., 2004).

These results suggest that altered distribution and levels of mature cathepsin D enzyme do not appear to give rise to an enzyme defect that could be responsible for subunit c accumulation. More recent knockdown studies did not indicate a great cathepsin D

processing alteration but a slight decrease in mature enzyme was noted in fibroblasts derived from CLN3 1kb deletion patients (Pohl et al., 2007).

1.3.3.1 The CLN3 protein influences Lysosomal pH

The role of CLN3 in pH regulation has been debated with varying results depending on the cell and mutation type investigated. The yeast protein Btn1p is 39% identical and 59% similar to CLN3(Pearce and Sherman, 1997). Btn1p localizes to the vacuole, which is the equivalent to the lysosome (Croopnick et al., 1998; Gachet et al., 2005).. In the fission yeast *S.Pombe*, Btn1p traffics to the vacuole membrane via early endocytic and pre-vacuolar compartments in a Rab7-dependent manner (Gachet et al., 2005). An *S. cerevisiae* yeast strain lacking the Btn1 protein was shown to have a lower than normal vacuolar pH during early growth that becomes normalized by later growth stages (Pearce et al., 1999). Studies on human CLN3 have also revealed that mutation of CLN3 results in a disruption of lysosomal pH. HEK293 cells transfected with antisense-oriented CLN3 cDNA demonstrated significantly lower pH than non treated controls (Golabek et al., 2000). However in JNCL patient cells the intracellular/lysosomal pH has been shown to be elevated rather than reduced (Holopainen et al., 2001), and in Btn1 deficient *S.Pombe* mutant fission yeast strain the vacuoles are also more alkaline. In the *S.Pombe* Btn1 yeast model, Btn1-deficiency results in enlarged vacuole size, and overexpression of Btn1p reduced both vacuole diameter and pH in a complementary manner (Gachet et al., 2005).

1.3.3.2 Role of CLN3 in arginine transport

The *S. cerevisiae* yeast strain lacking Btn1p was shown to have a defect in inward vacuolar transport of arginine and this defect was shown to be complemented by expression of human CLN3, suggesting that altered vacuolar/lysosomal pH might be a consequence of altered transport of small molecules into the vacuole(Kim et al., 2003). However, the physiological significance of arginine transport into the vacuole (rather than out) is not known. Btn1p and CLN3 do not share sequence homology to any

known transporter, therefore CLN3/Btn1p may not actually transport arginine but rather may play a role in the regulation of transport at the lysosomal/vacuolar membrane. Lysosomal arginine transport is ATP, vATPase and cation-dependent. In cells from JNCL patients there is also evidence of a defect in arginine transport into the lysosomes, resulting in depleted internal lysosomal arginine levels (Ramirez-Montealegre and Pearce, 2005). This defect seems CLN3-specific, since it is not seen in INCL or Niemann-Pick patients.

1.3.3.3 Other proposed functions for CLN3

It has been proposed that CLN3 function could be connected to maintenance of the integrity of the cytoskeleton. The overexpression of CLN3 induces aggregation of the microtubule binding protein HOOK1 (Luiro et al., 2004), which was shown to be upregulated in Btn1-deficient *S.cerevisiae* (Pearce et al., 1999). It was suggested that perhaps CLN3 mediates HOOK1 dissociation from the microtubules, providing a link between CLN3 and the cytoskeleton. CLN3 was shown to weakly interact with HOOK1 which in turn interacts with Rab7, Rab9 and Rab11 (Luiro et al., 2004).

CLN3 was also found to interact in an vitro binding assay with CLN5, a soluble mannose-6-phosphate modified lysosomal protein of unknown function (Isosomppi et al., 2002). Mutations in CLN5 cause late-infantile Batten disease (Vesa et al., 2002).

CLN3 has recently been proposed to have a novel palmitoyl protein Δ-9 desaturase function, implying it could function as a degradative enzyme that converts membrane associated palmitoylated proteins to their respective palmitoylated derivatives. Palmitoyl protein Δ-9 desaturase activity is deficient in the *Cln3* mouse KO (Narayan et al., 2006) and intermediate levels were detected in heterozygotes (Narayan et al., 2007).

The CLN3 C-terminus is reported to interact with calsenilin. Calsenilin is increased in the Cln3 KO mouse signifying that CLN3 negatively regulates its cellular levels. Calsenilin is a multifunctional Ca^{2+} binding protein that interacts with presenilins and mediates calcium mediated apoptosis. An increase of calcium concentration causes

significant dissociation of calsenilin from CLN3. CLN3 could therefore suppress calsenilin-induced cell death (Chang et al., 2007).

1.4 Autophagy

1.4.1 The importance of autophagy in Batten disease

In the *Cln3* KO mouse model a loss of neurons occurs in the brains (Mitchison et al., 1999; Pontikis et al., 2004; Weimer et al., 2006). To investigate the process of death undergone by the neuronal cells, a detailed morphological investigation of the brain from the Cln3 KO mouse was made few years ago in a collaboration between Hannah Mitchison and Mark Turmaine (Anatomy, UCL).

Surprisingly, no sign of apoptosis was revealed after analysing the most severely affected regions of neuronal loss in the brains. Cells in the thalamus, hippocampus and cerebellum did not appear to contain any of the typical morphological signs including apoptotic bodies, cytoplasmic and chromatin condensation and DNA fragmentation characteristic of apoptosis. Interestingly, detailed EM analysis of degenerating and dying neurons revealed the presence of autophagosomes in the cytoplasm. Microglia cells which are the professional phagocytes of the brain also appeared swollen and full of inclusions containing membraneous plus fingerprint profiles suggesting a successful engulfment of material but incapacity to degrade it. Astrocytes, in contrast, did not contain such huge storage accumulations.

The CLN3 autophagy phenomenon was confirmed during the course of the work presented in this thesis in immortalized cerebellar cell derived from the $Cln3^{\Delta ex7/8}$ mice where LC3-II, an autophagosomal marker, was increased in the deficient cells (Cao et al., 2006). Cerebellar cells transfected with GFP tagged LC3 and fed with lysotracker to stain the endocytic pathway showed less colocalization of the two markers in CLN3 deficient cells than in wild type controls suggesting less encounters of the autophagosomes with the endocytic pathway (Cao et al., 2006).

Since autophagy, a pathway that regulates mitochondrial turnover, was perturbated by deficiency of CLN3, this led to the conclusion that defects in autophagy could be the cause of the abnormal accumulation of the mitochondrial ATPase subunit c when CLN3 is deficient.

1.4.2 The autophagic pathway

Cytoplasmic components are degraded within the lysosome by microautophagy, chaperone-mediated autophagy and macroautophagy. In microautophagy, complete cytosolic regions are sequestered directly by the lysosome. This involves formation of invaginations of lysosomes to engulf components direcly, without any intermediate vesicles (Shintani and Klionsky, 2004). Chaperone mediated autophagy is applied only to cytosolic proteins with a specific lysosomal targeting motif. These are selectively recognised by a chaperone in the cytosol which delivers the proteins to the lysosome (Martinez-Vicente and Cuervo, 2007). A specific receptor recognizes the substrate and helped by a chaperone inside the lysosome, the substrate will get degraded. (Dunn, 1990b)

In mammalian cells macroautophagy (from now on referred to as autophagy) is an important survival mechanism during short term starvation (Eskelinen et al., 2002).

The process of autophagy consists of four different steps: induction; formation of the autophagosome; docking and fusion of the newborn organelle with the lysosome; autophagic material break down (Klionsky and Emr, 2000).

After an induction signal, autophagy starts when a flat membrane cisterna called a phagophore or isolation membrane wraps around a portion of cytoplasm, engulfing cytosol and the organelles in it. The origin of the phagophore remains to be discovered (Klionsky, 2005). The phagophore closes itself into a double membrane-bound vacuole, forming an initial autophagosomal organelle (Klionsky and Emr, 2000) (Mizushima et al., 2002). The autophagosome undergoes a process of maturation which includes contacts with the endocytic pathway consisting of fusion events with early endosomes and multivesicular bodies (AVl) (Liou et al., 1997) (Berg et al., 1998). At the end of this maturation process, the mature autophagosome (AVl) fuses

completely or kiss and run with a lysosome (Jahreiss et al., 2008) allowing the lysosomal hydrolases to start the process of degradation of the internal autophagosomal material for eventual recycling of nutrients back to the cells.
Autophagy can be selective or non selective. During selective autophagy, only some cargos are sequestered into autophagosomes and they contain little bulk cytosol. Selective autophagy has been reported so far in cases where bacteria and peroxisomes are being degraded. In non selective autophagy, autophagosomes primarily contain bulk cytoplasmic material (Xie and Klionsky, 2007).

Autophagic vacuoles can be characterized on the basis of the maturation process into early autophagic vacuoles containing morphologically intact cytoplasm and organelles, and late autophagic vacuoles containing partially degraded cytoplasm (Dunn, 1990a; Dunn, 1990b; Dunn, 1994).

The sequestration process started by the autophagosomes is orchestrated by a series of autophagy related genes (Atg), first identified in yeast, and it is regulated by the mTOR kinase pathway. The activity of mTOR is controlled by insulin and other growth factors through the phosphatidylinostiol 3-kinase (PI-3) pathway. In normal conditions mTOR allows translation, ribosome biosynthesis and inhibits autophagy but in starvation conditions mTOR is inhibited, permitting autophagy. In this way mTOR acts as a master regulator of the balance between protein synthesis and degradation (Raught et al., 2001).

A protein called Beclin which is localized at the TGN is important for autophagosome formation, where its association with PI-3K can produce PI3P (Kihara et al., 2001).

1.4.3 ATG genes

The ATG genes governing the autophagy pathway were discovered using yeast mutants defective in autophagy and have been discovered from studies of the biosynthetic cytoplasm to vacuole targeting (Cvt) pathway (Klionsky et al., 2003). Atg genes are listed in Table 1-2.

Cloning of Atg genes revealed that they are all novel, except for Atg6 which was found to be identical to Vps30, a protein required for the sorting of carboxypeptidase Y (CPY) to the vacuole (Kametaka et al., 1998). Atg6/Vps30 has distinct functions in the autophagic and vacuolar protein sorting pathway.

The byosynthetic Cvt and degradative autophagy pathways are similar and share most of the Atg components (Harding et al., 1996). The Cvt pathway sequesters within double membrane bound vesicles (Cvt vesicle) at least two specific cargos, aminopepidase and mannosidase, which are synthesized in the cytosol, for their transport into the vacuole. In these vesicles the cytosol is excluded (Yorimitsu and Klionsky, 2005) (Figure 1.3). The Cvt pathway is not known outside yeast.

Table 1-2 Atg genes

Yeast name	Human homologue	Role in autophagy
ATG1		Induction
ATG2		Autophagosome formation (association with ATG9)
ATG4		Autophagosome formation (Atg8 conjugation system)
ATG5	hATG5	Autophagosome formation (Atg12 conjugation system)
ATG6	Beclin	Autophagosome formation (forms a complex with Atg14)
ATG7	HsGSA/haPG	Autophagosome formation (Atg12 and Atg8 conjugation system)
ATG8	MAP1LC3	Autophagosome maturation
ATG9	ATG9	Autophagosome formation
ATG10		Autophagosome formation (association with Atg12)
ATG12	hAPG12	Autophagosome formation
ATG13		Induction
ATG14		Autophagsome formation (complex with Atg6)
ATG16		Autophagosome formation (association with Atg12-Atg5 complex)

Figure 1.3 Biosynthetic cytoplasm to vacuole targets (Cvt pathway) in yeast
Modified from (Klionsky, 2005).

During nutrient-rich conditions the protein kinase TOR inhibits the autophagic pathway but starvation inhibits TOR, allowing the formation of autophagic vacuoles. In yeast, there are two conjugation machineries (Figure 1.4). One (System I, Figure 1.4) begins with Atg7 which activates Atg10 to conjugate Atg5 with Atg12. Atg16 is assembled to the complex Atg12-Atg5.

In the other system (System II, Figure 1.4) Atg7 is activated and transfers Atg8, previously prepared by Atg4, to Atg3 after the conjugation of Atg8 to phosphatidylethanolamine (PE). The two complexes Atg12-Atg5-Atg16 and Atg8-PE localize at the initial autophagosomal membrane (PAS) for the formation of the autophagic vacuole {Yorimitsu, 2005 #118}.

The proteins Atg12 and Atg5 are implicated in the formation of the autophagosomal membrane but they are not present in the sealed autophagosome (Suzuki et al., 2001) (Kim et al., 2002). It is not know at present if a similar pathway and set of complexes is present in mammalian cells as well.

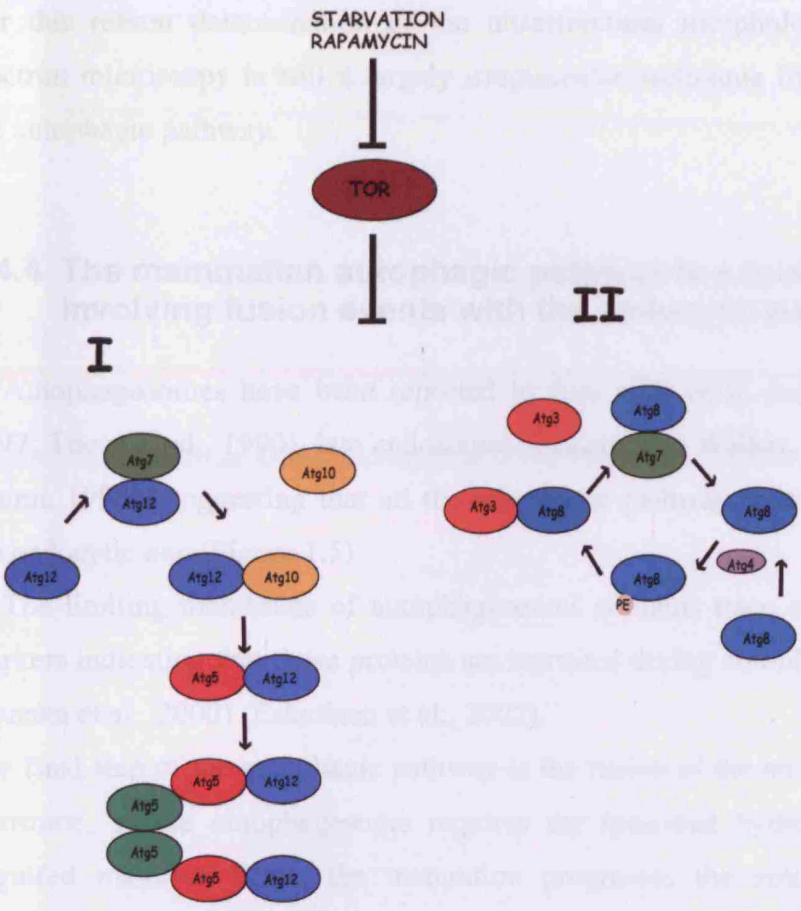

Figure 1.4 The two Atg conjugation machinery in yeast

Most of the Atg proteins are conserved in mammals. The best analysed is ATG8 and the mammalian homolog of ATG8 is called microtubule associated protein 1 light chain 3, or LC3. LC3 plays a role in the formation of the autophagosome (Kabeya et al., 2000). LC3 is cytosolic but after processing by ATG7 it become membrane bound and localizes with the initial membrane and early autophagosomes similarly to the

yeast system II process (Figure 1.4). During maturation of the early autophagosome the LC3 on the external membrane is cleaved off and the LC3 on the inner membrane stays trapped inside until rapidly degraded by the lysosomal hydrolases after lysosome fusion (Kabeya et al., 2000).

At present LC3 is the only marker available to label mature autophagic vacuoles. For this reason determination of the ultrastructural morphology of autophagy by electron microscopy is still a largely irreplaceable technique for the investigation of the autophagic pathway.

1.4.4 The mammalian autophagic pathway is a multi step pathway involving fusion events with the endocytic pathway

Autophagosomes have been reported to fuse with early endosomes (Liou et al., 1997; Tooze et al., 1990), late endosomes (Lucocq and Walker, 1997) and lysosomes (Dunn, 1990b) suggesting that all the autophagic pathway is intimately connected to the endocytic one (Figure 1.5).

The limiting membrane of autophagosomes contains trace amounts of lysosomal markers indicating that these proteins are recruited during autophagosomal maturation (Tanaka et al., 2000) (Eskelinen et al., 2002).

The final step of the autophagic pathway is the fusion of the autophagosome with the lysosome, as the autophagosome requires the lyosomal hydrolases to degrade its engulfed material. While the maturation progresses the autophagosome acquires lysosomal markers including Rab7, Lamp1 but loses LC3 (Jager et al., 2004)

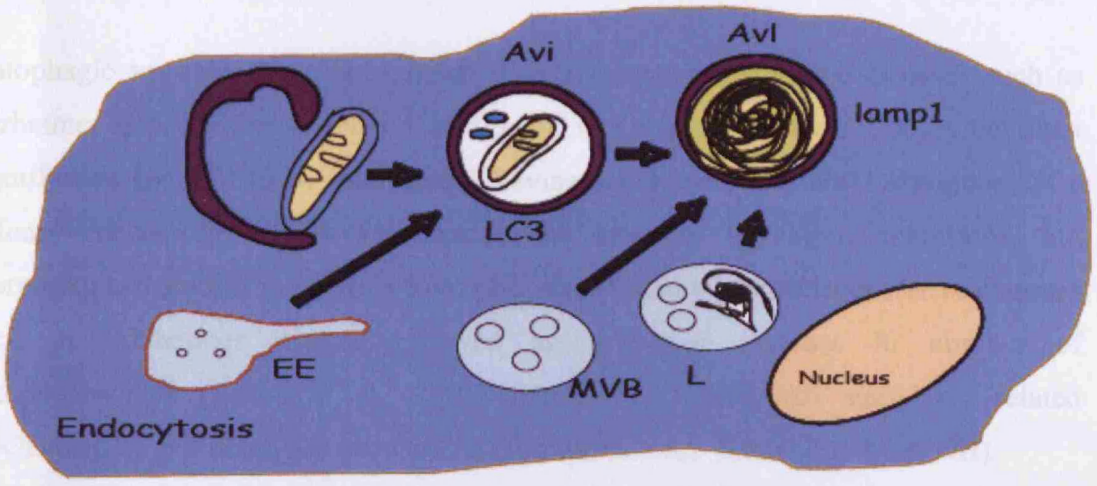

Figure 1.5 Endocytic and autophagic pathways are connected

EE (early endosomes), MVB (multivesicular bodies) and L (lysosomes) fuse with Avi (early autophagosomes) and Avl (late autophagosomes)

Intact microtubules are fundamental for autophagosomal maturation and their motility. Use of vinblastine or nocodazole, drugs that prevent polymerization of microtubules, induce accumulation of autophagosomes that do not contain hydrolases, suggesting a role for the microtubules in fusion of autophagosomes with lysosomes (Kochl et al., 2006).

pH seems to be important for fusion of autophagosomes with lysosomes; initially autophagosomes have the same pH as the surrounding cytoplasm, but during maturation their pH becomes acidic preceeding any delivery of the lysosomal enzymes (Dunn, 1990a) (Punnonen et al., 1992). Treatment with bafilomycin, an inhibitor of the lysosomal proton pump that maintains the lysosome at the optimal pH for lysosomal hydrolases to work, disrupts pH and stimulates accumulation of autophagic structures. This suggests that fusion between autophagosomes and lysosomes is inhibited by bafalomycin (Mousavi et al., 2001; Yamamoto et al., 1998) and that lysosomal pH plays a role in the fusion process.

1.4.5 Autophagy and neurodegeneration: neuronal cell death or protection against it?

Autophagic vacuoles have been noted in many neurodegenerative diseases such as Alzheimer and Parkinson (Nixon et al., 2005; Rubinsztein et al., 2005), but their significance has still to be interpreted (Levine and Kroemer, 2008). Autophagy is a defence mechanism which can rescue the cells in starvation conditions, but morphological studies in neurons from patients affected by neurodegenerative diseases such as Alzheimer disease, showed an abnormal increase in number of autophagosomes (Nixon et al., 2005) (Yu et al., 2005). An autophagy related mechanism of cell death has been called programmed cell death type II (PCDII).

PCDII differs from apoptotic programmed cell death (PCDI) because dying cells are full of autophagic vacuoles and they do not present with apoptotic features such as cytoskeleton collapse, cell shrinkage, membrane blebbing or cromatin condensation. Furthermore autophagy uses lysosomal enzymes and the dying cells employ the endogenous lysosomal machinery (Shintani and Klionsky, 2004).

In Alzheimer disease autophagosomes accumulate progressively to become the predominant organelle in neurons, their presence reflecting autophagy activation and the impaired maturation of autophagosomes to autophagolysosomes (Nixon et al., 2005). Autophagy is also crucial in Huntington disease, where fusion between autophagosomes and lysosomes is impaired and increases aggregation of the Huntington protein in cells. Rapamacyin treatment which stimulates autophagy reduces htt accumulation and neurodegeneration in fly and mouse models for Huntington disease(Ravikumar et al., 2004).

The impairment of the maturation of autophagosomes to autolysosomes also leads to a continuous autophagic build up in Pompe disease (Fukuda et al., 2006).

1.5 Phagocytosis

The characteristic accumulation of storage material observed in JNCL has been found in all cells of the body including microglia in the brain. Microglial cells, are scavengers cells that remove the damaged neurons by phagocytosis, in the *Cln3* KO mouse they present a large accumulation of storage material which appears to be properly internalized by these cells, but not digested efficiently.

Phagocytosis is a receptor mediated process of professional phagocytic cells, such as neutrophils or macrophages and it is used for the elimination of foreign particles and apoptotic bodies(Vieira et al., 2002).

Phagocytosis is initiated by the clustering of surface receptors upon interaction with the relevant ligand. A well known family of phagocytosis receptors are the FcIIλ Receptors (FcR) which bind to opsonized pathogens.

Newly formed phagosomes are relatively inert but as soon as the phagosomal membrane seals, interactions between phagosomes and endocytic components start, in a fashion that recapitulates the endocytic sequence (Vieira et al., 2002). The phagosomes initiate a dynamic fusing activity with repeated, transient fusion events in which they acquire endocytic markers allowing their maturation. This ultimately yields, after fusion with a lysosome, a phagolysosome (Tjelle et al., 2000).

Ten minutes after the fission of the phagosome from the PM, the phagosome has already acquired EEA1 and Rab5 through kiss and run events with sorting endosomes (Duclos et al., 2000). Early fusion events involve the activity of the type III PI-3K, which generates phosphatidylinositol 3-phosphate (PI3P) on the phagosomal membrane. Inhibitors of PI-3K activity were found to diminish EEA1 recruitment to newly formed phagosomes and block phagosomal acquisition of late endocytic properties, indicating that generation of PI3P plays a role in phagosomal maturation (Fratti et al., 2001).

As expected, SNARE proteins also participate in phagosomal maturation; syntaxin 13 at the initial stage and syntaxin 7 recruited later (Collins et al., 2002).

Twenty minutes after phagosomal sealing, the phagosome has lost all its early endocytic markers and acquired late endocytic markers such as Lamp1 and Rab7

through fusion with lysosomes. Lamp1 and Lamp2 have recently been reported to be important for the complete maturation of the phagosomes (Huynh et al., 2007). The connection between the phagocytic, endocytic and autophagic pathways is shown in Figure 1.6.

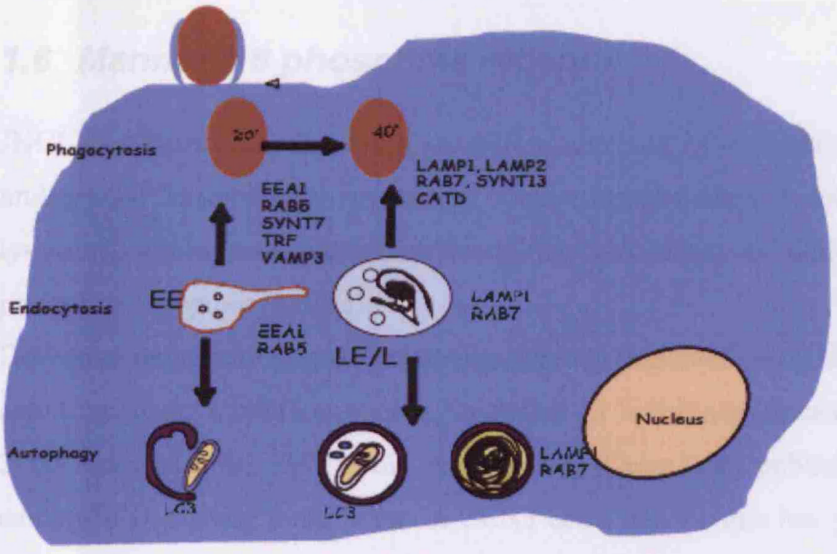

Figure 1.6 Phagocytic, Endocytic and Autophagic pathways
EE indicate early endosomes, LE/L indicate late edosomes/lysosome.

1.5.1 Modified non professional phagocytic cells as a system to study phagocytosis

To study phagosomal maturation, a new approach has been used in recent years, where non-professional phagocytic cells are transfected with FcIIλ receptor, conferring phagocytic capability to those cells. Such cells are able not only to internalize phagosomes but these phagosomes can also mature by endocytic fusion(Downey et al., 1999).

It has been reported that cells such as COS cells or mouse embryonic fibroblasts, when transfected with FcIIλ, are able to internalize latex beads opsonized with IgG via phagosomes and the beads acquire endocytic markers, allowing the study of the maturation of the phagosomal membrane, by monitoring the phagosomal acquisition of endocytic proteins.

1.6 Mannose 6 phosphate receptor

JNCL is a lysosomal storage disease characterized by a prominant accumulation of undegraded material in lysosomes. Cells degrade their lysosomal content using lysosomal hydrolases, which arrive to the lysosomes by delivery via mannose 6 phosphate receptors (MPRs).

Defective cathepsin D processing was already reported in cells from JNCL patients and *Cln3* mice models suggesting a defect in hydrolase processing (Golabek et al., 2000; Fossale et al., 2004; Pohl et al., 2007). There is no published evidence yet that cathepsin D activity is deficient in CLN3 cells, and no-one has yet directly examined trafficking of this model. In order to examine this aspect of lysosome function, part of our investigation to determine the function of CLN3 focused on trafficking of the mannose 6 phosphate receptor (CI-MPR) which is responsible for delivery of lysosomal hydrolases to the lysosome.

1.6.1 CI-MPR and CD-MPR

Soluble lysosomal hydrolases become postranslationally modified by the addition of mannose residues at the TGN where they are then recognized by the mannose 6-phosphate receptors for targeting to the lysosome(Kornfeld and Mellman, 1989).

In mammalian cells there are two types of mannose 6 phosphate receptor, the 46-kDa cation independent mannose 6-phosphate receptor (CD-MPR) and the 300 k-Da cation dependent mannose 6-phosphate receptor (CI-MPR). Both receptors are type I

transmembrane proteins and they are involved in targeting of lysosomal hydrolases to the lysosomes (Pohlmann et al., 1995).

The association between ligand (hydrolase) and receptor (CI-MPR) is fundamental to the delivery of the enzyme to the lysosome and prevents the secretion of the lysosomal enzymes.

A detailed study of CI-MPR localization, done by electron microscopy analysing cryo-sections of HepG2 and BHK cells double transfected with CI-MPR and CD-MPR showed the presence of both receptors in TGN, recycling early endosomes, plasma membrane, late endosomes, and endosomes with many vesicles. The CD-MPR appeared to be concentrated in the associated tubules and vesicles, whereas the CI-MPR was more prominent in the central vacuole of endosomes(Klumperman et al., 1993). However both receptors have been found in the same coated buds at the TGN, suggesting that they use the same exit from the Golgi (Klumperman et al., 1993).

1.6.2 The CI-MPR route

The cycling of mannose 6 phosphate receptor follows a complicated cellular itinerary (Figure 1.7).

Endocytosed CI-MPR is delivered to the TGN via transferrin positive recycling early endosomes (REC) but leaves this compartment very rapidly such that at steady state only a small fraction of CI-MPR stays in the REC (Lin et al., 2004).

CI-MPR binds its hydrolase cargo at the TGN and the complex is packaged into transport carriers that deliver the receptor with its ligand to the prelysosomal endosomes (Lin et al., 2004).

A cluster of amino acids followed by a dileucine motif in the cytoplasmic tail mediates receptor sorting from the TGN to late endosomes, since it has been shown that mutations in this motif prevents. Lysosomal enzyme sorting by blocking association of the CI-MPR with coat proteins in the TGN(Tortorella et al., 2007).

To maintain efficient sorting and transport of the hydrolases, as soon as the MPR dissociates from the ligand, it must be prevented from degradation in the lysosome and is sent back to the TGN for a new cycle. Tail interacting 47-kDa protein (TIP47) binds

to the cytoplamic domains of both MPRs for this purpose and is required for their transport from endosomes to the TGN; it also binds to Rab9, increasing the affinity between TIP47 and CI-MPR. Rab9 positive vesicles have been visualized leaving the late endosomal compartment and fusing with the TGN (Barbero et al., 2002).

There is also evidence that AP-1 and PACS-1 are involved in MPR recycling. In cells lacking either AP-1 or PACS-1, MPRs accumulate in endosomes indicating that these proteins can have a role in MPR trafficking from the endosomes to the Golgi(Meyer et al., 2000).

The retrieval of CI-MPR from the endosomes to the TGN is also reported to be retromer dependent. Cells lacking mammalian VPS26, which is normally localized with EEA1 and Rab5, fail to retrieve CI-MPR resulting in its mislocalization at the PM and in early endosomes (Seaman, 2004).

CI-MPR but not CD-MPR is able to bind M6P-containing ligands at the PM. There are several ways by which the CI-MPR can reach the PM, one is via direct carriers from the TGN destined for the PM, another is by recycling from early endosomes/late endosomes (Riederer et al., 1994). Once at the cell surface the CI-MRP gets internalized rapidly.

1.6.3 CI-MPR exit from the TGN

CI-MPR recognizes the mannose 6 phosphate groups attached to lysosomal hydrolases (Kornfeld, 1992). The receptor-ligand complex leaves the TGN segregated in tubulo-vesicular structures (Waguri et al., 2003) coated by clathrin (CCV) and the adaptor proteins AP-1 and GGAs.

The CI-MPR cytoplasmic cytosolic tail contains a dileucine motif that directs sorting from TGN to the endosome; it was thought that sorting of MPRs at the TGN was mediated by AP-1 but CI-MPR does not bind AP-1 with its dileucine motif (Honing et al., 1997). The CI-MPR cytosolic tail interacts with the VHS domain of the GGA proteins instead, as proved by yeast two hybrid system and GST pulldown assays (Puertollano et al., 2001). The overexpression of a dominant negative GGA1 VHS-

GAT domain caused accumulation of CD-MPR at the TGN suggesting that GGAs may be also required for CD-MPR exit from the TGN (Puertollano et al., 2001).

The 3 cytosolic GGAs proteins are recruited from the cytoplasm to the TGN where they then colocalize in the same coated buds (Ghosh et al., 2003b). Individual GGAs are recruited as monomers from the cytosol onto the Golgi in an ARF-GTP dependent manner and then form a complex which interacts with AP-1.

GGAs may bind MPRs in the trans Golgi network and bring them to AP-1 containing clathrin coated vesicles. Overexpression of CD8-CI-MPR enhances GGA recruitment (Hirst et al., 2007).

Transported via 60-100nm CCVs, CI-MPR and GGAs rapidly uncoat and fuse with the prelysosomal endosomes, into which the cargo is released. The amount of AP-1 bound to membranes and associated with clathrin-coated vesicles depends on the expression levels of MPRs (Le Borgne and Hoflack, 1997).

Dissociation of the CI-MPR and cargo is caused by the acidic environment of the endosomes. However for CD-MPR it was recently showed that the capacity to deliver the cargo hydrolases to the lysosomes does not depend on endosomal acidification (Probst et al., 2006).

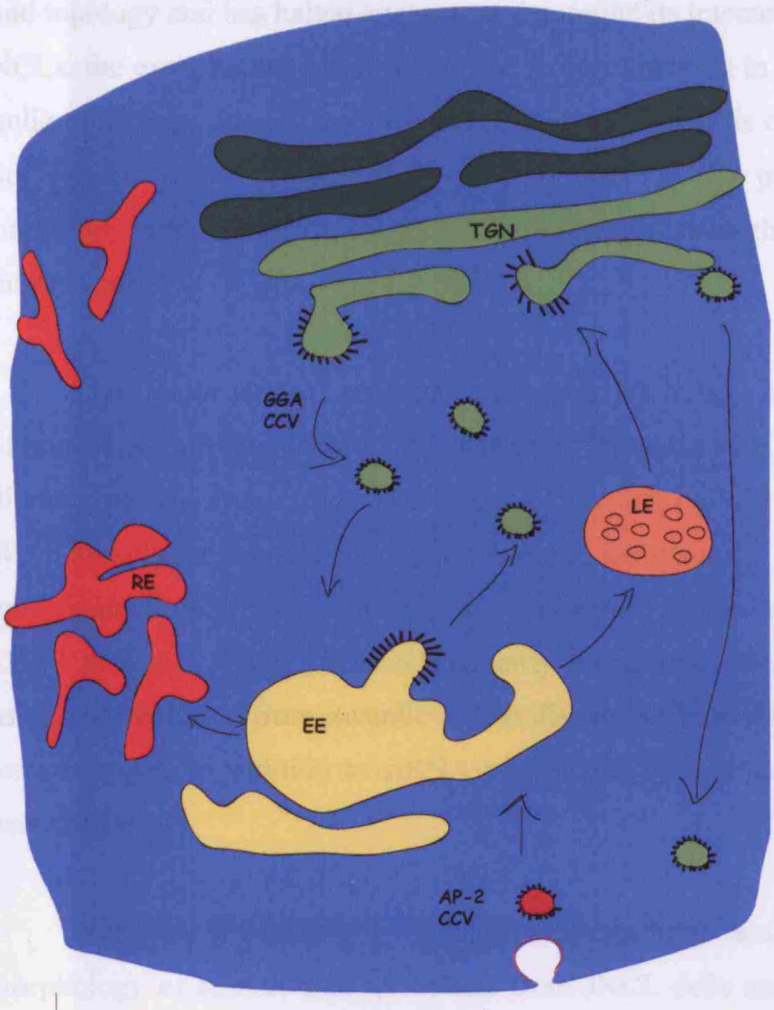

Figure 1.7 CI-MPR trafficking route

Aim of this thesis

The CLN3 protein was isolated as the cause of juvenile Batten disease or JNCL over ten years ago. However despite reasonably intensive efforts, the normal function of this protein and how this function is compromised by mutations to give rise to cellular dysfunction remains obscure. The lack of specific antisera that recognise the hydrophobic CLN3 protein, coupled with its low level ubiquitous expression, has made it difficult to arrive at a consensus on its intracellular location

and topology and has halted attempts to determine its interaction partners. As for other NCLs, the exact nature and origin of the storage material in JNCL is uncertain so that unlike for many other lysosome storage disorders, analysis of the storage material has not proven useful in providing a hypothesis for the protein's function, except suggesting a putative role for CLN3 in autophagy since the major protein stored is mitochondrial in origin.

The major aim of this study was to provide insight into the functional biology of the CLN3 protein in order to determine the molecular basis of juvenile Batten disease, starting from a characterisation of the cell biology of CLN3 deficient cells. With its cellular location and the nature of the disorder, the major focus was on investigating the primary endocytic and autophagic defects arising from the loss of the CLN3 protein. A study was made of early events associated with the loss of CLN3, using cells cultured from juvenile Batten disease patients and from the *Cln3* knockout mouse model, in addition to siRNA-treated cell lines where CLN3 gene expression was silenced.

Chapter 3 presents a detailed ultrastructural analysis of the changes in morphology of human skin fibroblasts from JNCL cells and fibroblasts and neurons from the *Cln3* KO mouse. Chapter 4 describes an extended investigation of the abnormal accumulation of autophagic structures that was detected in JNCL cells, aimed at understanding the reasons for this phenotype and the exact role of CLN3 in the autophagic pathway. It also includes work following on from this addressing the role of CLN3 in the related phagocytic pathway. Chapter 5 presents work following from cellular immunofluorescence studies and the observation of an altered distribution of the cation-independent mannose 6-phosphate receptor in JNCL cells. The nature of this apparent trafficking defect and the role CLN3 plays in governing correct function of the lysosome via this critical lysosomal hydrolase receptor is investigated. Chapter 6 links defects in the autophagic pathway arising from dysfunction of CLN3 to alterations in the distribution of CI-MPR, exploring the

connection between the trans Golgi network (TGN) and formation and maturation of autophagosomes.

2 Materials and methods

2.1 Cell culture

2.1.1 Cell lines and maintenance

The cells lines used in the thesis are listed in Table 2-1.

All the cells lines used were grown in Dulbecco's modified Eagle's medium (DMEM, Gibco /Invitrogen,Paisley, UK) plus 10% fetal calf serum (Biowest, Miami, Florida) and in Nunc tissue culture plastic dishes (Gibco/Invitrogen (Paisley, UK) at 37 C° and 5% CO_2.

Fibroblasts were grown in 10 cm plastic dishes and maintained at 80% confluency judged by eye. Mouse fibroblasts were passaged at a ratio of 1:2 and maintained for use to a maximum of three passages only. Human skin fibroblasts were passaged at a ratio of 1:2 and maintained for use to a maximum of 20 passages.

HeLa cells were maintained at almost full confluency and passaged at a ratio of 1:3.

Table 2-1 Cells lines used in this thesis

	ID	Overexpressed proteins	Source
Human primary fibroblasts from healthy control (used as WT)	Hs68		ECACC
	48BR		Peter Clingen,UCL
	1BR.3		"
	AGO		"
	HF523N		Elaine Aegius, Sara Mole,Uk
	HF524N		"
	HF526N		"
	HF527N		"
	HF528N		"
	HF529N		"
Human primary fibroblasts from 1KB deletion JNCL patients	HF 470Pa		GOS
	HF478Pa		Alfried Kohschutter,Germany
	HF479Pa		"
	HF480Pa		"
	HF481Pa		"
Mouse embryonic fibroblasts			Hannah Mitchison UCL, London
HeLa cells			Alan Hall, Sloan Kett. NY
HeLa cells		CD8-CI-MPR	
HeLa cells		EGFP-LC3	Aviva Tolkovsky,Cambridge

2.1.2 Preparation of mouse embryonic fibroblasts

Pregnant female mice at 13-14 days gestation were sacrified and embryos collected for dissection into phosphate-buffered saline (PBS) in a Petri dish. PBS consisted of 8g NaCl, 0.2g of KCl, 1.44g of Na_2HPO_4, 0.24g of KH_2PO_4 per litre, pH adjusted to 7.4. The head and viscera were removed from the embyos with forceps. The carcasses were plated in a fresh dish and minced, then the material was transferred into a solution of 0.25% trypsin (Gibco) in DMEM media (Gibco) in a 50 ml falcon tube, 2 mls per embryo. This was incubated at 37°C for 20 minutes, then triturated using a 5 ml pipette in order to break up the tissues. The supernatant was transferred to a new tube and an equal volume of growth media (Dulbecco's modified Eagle's medium (DMEM, Gibco)) supplemented with 10% fetal calf serum (Bioline) was added. Cells were counted and plated out at a density of 10^6 cells (or 0.5 embryo) per 10 cm culture dish.

2.1.3 Freezing and thawing cultured cells

Aliquots of $1x10^7$ cells were suspended in 1 ml of FCS supplemented with 10% DMSO. These were frozen overnight at -80°C. The aliquots were moved to liquid nitrogen for permanent storage. Individual aliquots were thawed rapidly at 37°C and placed in a 15cm dish with 25 ml pre-warmed medium.. Cells were then grown in fresh medium, and initially passaged two days post-thawing.

2.1.4 Transient transfections

For transient transfection experiments, cells were grown to 80% confluency and transfected by nucleofection with DNA or siRNA construct using a nucleofector device from Amaxa Biosystems.

Cell number, nucleofection program and DNA or siRNA concentration were used according to the nucleofection machine manufacturer's instructions found in the human skin fibroblasts, mouse embryonic fibroblasts or HeLa cells kit (Table 2-2).
Cells were grown for at least a further 24 hours before use in immunofluorescence or electron microscopy studies.
Constructs used in the thesis are listed in Table 2-3 for DNA constructs.
There are a number of different human CLN3 transcripts and therefore two oligonucleotides were designed to ensure the most complete gene knockdown. These were located in exon 6 and exon 10, both portions of the gene where all the CLN3 transcripts overlapped and in Table 2-4 for siRNA sequences (supplied by MWG).

Table 2-2 Transient transfections details

Cell type	Cell number	Nucleofector Program	DNA Concentration	siRNA Concentration
HeLa cells	1.10^6	A28	5 μg/μl	20μM
Human skin Fibroblasts	2.10^6	U23	3 μg/μl	
Mouse Emb. Fibr.	2.10^6	T20	5 μg/μl	

Table 2-3 DNA constructs used in this thesis

Construct	Source
CLN3-MYC	Thomas Braulke, University of Hamburg
CLN3-EGFP	Aija Kyttala, Biomedicum, University of Helsinki
CLN3-GFP	Sara Mole, UCL, London
CI-MPR-CD8	Matthew Seaman, University of Cambridge
FcIIλReceptor	Emmanuelle Caron, Imperial College, London
LC3-EGFP	Tamotsu Yoshimori, Japan
RAB7-EGFP	Cecilia Bucci, Italy

Table 2-4 Details of siRNA oligos used in this thesis

Target/siRNA	mRNA target sequence
CLN3 1 (exon 6)	GUGGGAUUUGUGCUGCUGGAA
CLN3 2 (exon 10)	CCAGCCUCUCCCUUCGGGAAA
Scrambled/control	AAUUCUCCGAACGUGUCACGU

2.1.5 Starvation

To obtain starvation conditions, cells were washed in PBS and incubated in Earl's salt balanced medium (EBSS) at 37 C° and 5% CO_2 for different time periods.

2.1.6 Preparation of CD8-CI-MPR stable cell lines

HeLa cells were transfected with CD8-CI-MPR using an Amaxa nucleofector device and grown in presence of 1:200 concentration G418 (Calbiochem – 3451812) until

mocks mostly dead. Cells were then splitted hard into 15cm dishes (1:10,000) to allow single colonies to be isolated.

Approximately 1 week later, trypsin soaked filter papers were placed onto the single colonies. Filter papers were transferred into 24 well format dishes. One clone (colony) per well and grown up until in 10 or 15cm well format (approximately 10 – 14 days).

Positive clones for CD8-CI-MPR were assessed by immunofluoescence:

2.2 FACS analysis

Cells were washed in PBS after removal of the growing medium, lifted in PBS 5mM EDTA and collected in a 10ml falcon tube. Subsequently cells were spun down at 1200rpm and the PBS 5mM EDTA removed. The cell pellet was resuspended in 100 μm FACS incubation buffer (PBS, 5% FCS and 0.1% azide), spun down again and resuspended in 100 μM FACS incubation buffer with secondary antibody. Cells were then incubated on ice for 30 minutes and after that spun down and resuspended in FACS fix (4% paraformaldheyde in PBS).

Quantitative analysis of fluorescence intensity was carried out using a FACSCalibur flow cytometer with 10,000 gated events analyzed. The relative fluorescence was determined by comparing HeLa cells expressing GFP (positive control) transfected 24 hours before the experiment against untreated HeLa cells (negative control).

2.3 Immunofluorescence microscopy

2.3.1 Indirect immunofluorescence

Cells were grown on 30mm diameter glass coverslips (VWR International) for immunofluorescence studies.

The coverslips with the adherent cells were washed in PBS and then fixed in 4% paraformaldehyde in PBS for 15 minutes at room temperature followed by

permeabilization with 0.1% saponin. Free aldehyde groups were then quenched with 50mM ammonium chloride in PBS for 15 minutes.

Subsequently the cells were labelled for 60 minutes with primary antibody in PGAS blocking buffer (0.01% saponin, 0.1% gelatin in PBS).

Detection was by secondary antibodies in PGAS for 45 minutes.

Primary and secondary antibodies used in this thesis are listed in Table 2-7.

Finally, the coverslips were washed again 3 times quickly in PBS and once in distilled water, mounted with Prolong antifade mountant (Molecular Probes) and viewed on a confocal scanner microscope MRC1024 or confocol microscope Leica SPE.

2.4 Phagocytosis assay

Cells were transfected with the Fc receptor construct using an Amaxa nucleofector device. After 24 hours cells were incubated in serum free media for various time points with 3 μM latex beads that had previously been opsonized with human IgG (overnight, rotating on ice in human serum). The phagocytosis was synchronized by spinning down the cells for 1 minute at 1400 rpm after addition of beads.

At the end of the time point, cells were stained, for 10 minutes on ice with secondary antibody against human anti IgG to stain all the external beads, then 4% PFA fixed and stained with secondary antibody anti human IgG (of a different fluorophore from the one used to label just the external beads) to label all the beads.

2.5 Molecular biology

2.5.1 Transformation of *E.coli*

Chemically competent cells (DH5α strain, Invitrogen, UK) were thawed quickly at room temperature and placed on ice. DNA constructs (1 μl of plasmids for amplification) to be transformed were placed in 1.5 ml microfuge tubes and mixed with 50 μl competent cell suspension. Tubes were tapped and placed on ice for 5 min.

Cells were 'heat shocked' by incubation at 42°C for 45 sec and were then immediately returned to ice for 5 min. Pre-warmed L-Broth (200 µl per transformation) was added and the cells were incubated with moderate agitation for 10 min (amplification). 200 µl of transformed bacteria were plated onto selective LB agar plates containing either ampicillin (50 µg/ml) or kanamycin (30 µg/ml) as required. Plates were incubated overnight at 37°C.

2.5.2 Bacterial DNA maxi prep

DNA was prepared using GenElute HP Plasmid Maxiprep Kit ® (Sigma) according to the manufacturers instructions. Elution of DNA was followed by an Ethanol precipitation. 500 µl of 3M NaOAc, pH 5.2 and 12.5 ml of 100% ice-cold EtOH were added to the 5 ml eluate. Tubes were centrifuged at 3400 x g for 30 min at 4°C. Supernatants were discarded and pellets were resuspended in 1 ml 70% ice-cold EtOH. After centrifugation at 5000 x g for 10 min, the supernatants were carefully discarded. Pellets were left to air dry and resuspended in 500 µl – 1 ml distilled water.

2.5.3 Polymerase chain reaction

DNA was amplified in a thermocycler. PCR reactions used a final volume of 20 µl containing 10 ng template DNA, 50µM dNTPs (Promega), 0.25 µl Taq polymerase (Promega) when testing for HeLa specific expression, or 0.25µl Pfu polymerase (Promega) for cloning, plus 20µM of each oligonucleotide primer (Invitrogen) and 2µl of the respective polymerase 10x buffer. DNA was amplified using reaction specific programmes with the following parameters: 1x at 95°C for 5 min, 30-35x [95°C for 1 min, 55-65°C for 1 min, 72°C for 1 to 3 min, depending on the length of product] and 1x 72°C for 10 min. PCR products were purified for cloning using the QIAquick® PCR Purification Kit (Qiagen) according to the manufacturers instructions.

2.5.4 RNA extraction

Cell were lysed in lysis buffer, plus β mercaptoethanol, included in the Qiagen RNeasy mini kit. The lysates were homogenised using the Qiashredder and then processed according to manufacturers instructions for the Qiagen RNeasy mini kit. RNA was eluted in 30µl of RNase free water.

2.5.5 Reverse transcription

RNA was reverse transcribed using the SuperScript™ III First-Strand Synthesis System for RT-PCR (Invitrogen). 10µl of RNA was used for each reaction and random hexamers were used as primers in this reaction to ensure total DNA amplification. Incubation times were according to manufacturers instruction.

2.5.6 DNA quantitation

The concentration and purity of DNA preparations were examined by optical density ($Abs_{260/280}$).

2.5.7 Real time PCR

DyNAmo™ SYBR® Green qPCR Kit was used to quantify the relative amount of DNA in the various samples. This kit is composed of a master mix containing modified Thermus brockianus DNA Polymerase, SYBR Green I dye, optimized PCR buffer, 5mM $MgCl_2$, dNTP mix including dUTP. Added to this were the gene specific primers either at 1.2µM or 1X final concentration for the Quantitect primers (Quagen) and the DNA samples, which were diluted to 150ng/µl. The sequences of the primers are set out in Table 2-5 and the cycling conditions in Table 2-6. All primers were designed to produce a product that encompasses two exons to ensure that no genomic

DNA contaminated the cDNA preparations and the amplicons were 100-200 base pairs.

Table 2-5 Primers used in the real time PCR

Target	Sequence
CLN3	QuiagenHs_CLN3_1_SGQuantiTectPrimerAssay(NM_000086)
Actin	**forward:** GCGAGAAGATGACCCAGAT
	reverse: TGGTGGTGAAGCTGTAGCC

Table 2-6 Cycling conditions used for the real time PCR

Step #	Purpose	Temperature	Time
1	Initial denaturation	95°C	10 mins
2	Denaturation	94°C	10 secs
3	Annealing	55°C	15 secs
4	Extension	72°C	20 secs
5	Fluorescence measurement	72°C and 77°C	1 sec each
Steps number 2-5 are repeated 39 times			
6	Final extension	72°C	8 mins
7	Melting curve	72°C -95°C	approx. 20 mins
8	Reannealing	72°C	8 mins

The melting curve was used to check the specificity of the amplified product. Primers that formed more than one product were discarded. The relative knockdown for each

product was determined by comparing the cycle number at which the amount of PCR product exponentially increases (C(t)) between knockdown and mock transfected cDNA sample using the $2^{-\Delta\Delta C(t)}$ method (Livak and Schmittgen, 2001).

$\Delta C(t)$ gene specific = knockdown C(t) – mock C(t)

$\Delta C(t)$ housekeeping = knockdown C(t) – mock C(t)

$\Delta\Delta C(t) = \Delta C(t)$ gene specific - $\Delta C(t)$ housekeeping

In all siRNA experiments, <90% knock down of CLN3 expression was confirmed using the exon 6 and exon 10 siRNAs together by real time PCR.

2.6 Antibodies

Details of all the primary antibodies used in this thesis are presented in Table 2-7.

Details of all the secondary antibodies used in this thesis are presented in Table 2-8.

Table 2-7 Primary antibody used in this thesis

Antibody	Species/Isotype	Source
CathepsinD	Mouse (CTD-19)	Abcam
CD8	Mouse	Matthew Seaman, Cambridge
CD8	Mouse (UCHT4)	Ancell
CI-MPR	Rabbit	Peter Loebel
LC3	Mouse	Yoshimori, Japan
EEA1	Mouse	BD Transduction laboratories
GFP	Rabbit	LMCB, EM unit
HRP	Rabbit (B0144)	DAKO
Lamp1	Mouse (H4A3)	Developmental studies Hybridoma Bank
Lamp1	Rat (CD107a)	PharMingen
Lamp1	Rabbit (ab19294)	Abcam
LBPA	Mouse	Juan Gruenberg
LC3	Rabbit	Yoshimori, Japan
Lgp120	Rabbit	Colin Hopkins, Imperial
Myc	Rabbit (sc-789)	Santa Cruz biotechlogy
Rab11	Rabbit (71-5300)	Zymed laboratories (Invitrogen)
TGN46	Sheep (AHP500)	AbD SEROTEC
Syntaxin 8	Mouse	Andrew Peden, Cambridge
Subunit c	Rabbit	Eiki Kominami, Japan
Transferrin Rec.	Mouse (H68.4)	Zymed laboratories (Invitrogen)

Table 2-8 secondary antibody used in this thesis

Antibody	Source
Donkey α Mouse Alexa Fluor® 488	Invitrogen/Molecular Probes
Donkey α Mouse Alexa Fluor® 594	
Donkey α Sheep Alexa Fluor® 594	
Donkey α Sheep Alexa Fluor® 488	
Donkey α Rabbit Alexa Fluor® 488	
Donkey α Rabbit Alexa Fluor® 594	
Donkey α Mouse Cy5	Jackson Laboratories
Donkey α Sheep Cy5	
Donkey α Rabbit Cy5	

2.7 Electron microscopy

Electron microscopy samples were analyzed with a G2 Spirit transmission electron microscope and SIS Morada CCD camera.

2.7.1 Sample preparation for conventional electron microscopy

Cells were grown in glass coverslips to subconfluency and fixed in 2% paraformaldehyde and 1.5% gluteraldehyde, both reagents from TAAB Laboratories (Aldermaston, Berks, UK) and Agar Scientific (Stanstead, UK) in 0.1M sodium cacodylate buffer for 20 minutes at room temperature after being washed briefly in PBS. Cell were subsequently briefly washed in sodium cacodylate buffer 0.1M, pH 7.6

and postfixed in 1% osmium tetroxide and 1.5% potassium ferrocyanide for one hour at 4C and then washed again in sodium cacodylate buffer 0.1M.

The coverslips were incubated in 1% tannic acid in 0.05M sodium cacodylate, washed in sodium sulphate for 5 minutes and finally rinsed in water to start the process of dehydration by serial incubations of 5 minutes, twice each in 70% ethanol, 90% ethanol and 100% ethanol. The coverslips were then immersed in a mixture of 1:1 propylene oxide and Epon 812 for 1 hour, which was then replaced with 100% Epon to continue the embedding. The epon was changed twice in 4 hours and the coverslips were mounted in previously hardened blocks and baked overnight in an oven at 60 degrees.

The following day, the coverslips were detached from the block by immersion in liquid nitrogen and the cells were cut in ultra-thin sections on an Ultracut (UCT) ultramicrotome (Leica Microsystems, Vienna, Austria) at room temperature and stained with lead citrate.

2.7.1.1 Epon composition for sample embedding

TAAB 812 19.2 ml
DDSA 7.6 ml
MNA 13.2 ml
DMP-30 0.8 ml

2.7.2 Horseradish peroxidase (HRP) feeding

Cells grown on glass coverslips were incubated for 90 minutes in Horseradish peroxidise (HRP, Type V, Sigma) at a concentration of 4mg/ml. The medium with HRP was then replaced with 2% paraformaldehyde and 1.5%glutaraldehyde fixative, and the location of the HRP was revealed by addition of diaminobenzidine and hydrogen peroxide.

Then cells were postfixed with Osmium tetroxide and processed for electron microscopy as described above.

2.7.3 Coupling of Zenon® Fab fragments to the CD8 antibody for electron microscopy study

The Zenon mouse IgG_{2a} labelling kit (Molecular Probes) was used to conjugate the CD8 antibody to HRP-Fab fragments.

HRP enzymes previously conjugated to Fab fragments were provided in the Zenon® molecular labelling kit. 1 μg of the CD8 antibody was added to 5 μl of the Zenon® mouse IgG_{2a} labelling reagent for 5 minutes; after which 5 μl of the non isotype specific Zenon® blocking reagent was added to the reaction mixture for a further 5 minutes according manufacture instructions.

The ready for use complex was added to 30 μl of media and used in feeding to allow internalization in the cells.

Figure 2.1 Zenon labeling kit

The Zenon labeling scheme. An unlabeled IgG is incubated with the Zenon labeling reagent, which contains an HRP-labeled Fab fragment (A). The labelled Fab fragment binds to the Fc portion of the IgG antibody (B), and excess Fab fragment is neutralized by the addition of a nonspecific IgG (C). The addition of nonspecific IgG prevents cross-labeling of the Fab fragment in experiments where multiple primary antibodies of the same type are present.

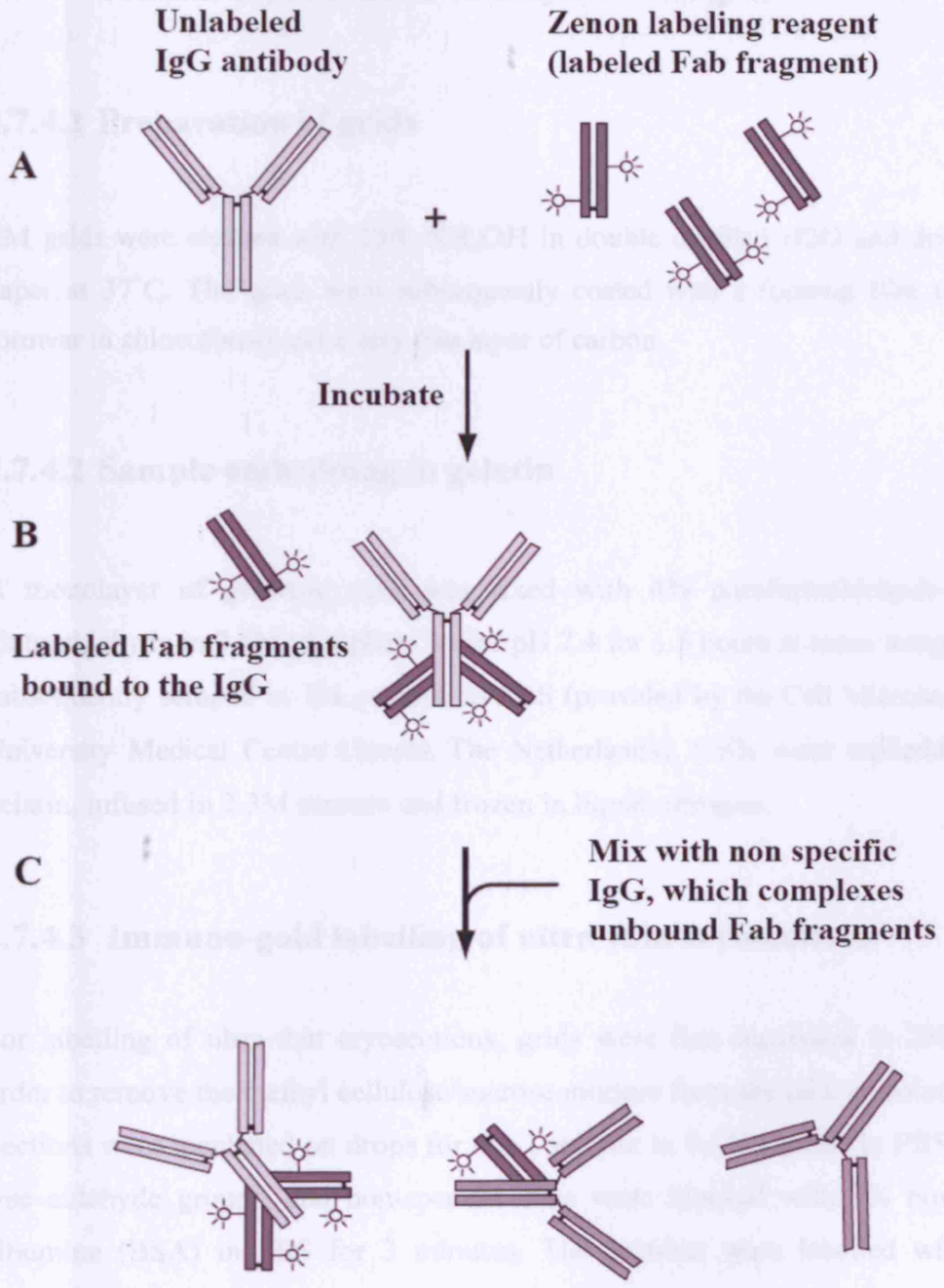
Unlabeled
IgG antibody
Zenon labeling reagent
(labeled Fab fragment)
A
+
Incubate
B
Labeled Fab fragments
bound to the IgG
C
Mix with non specific
IgG, which complexes
unbound Fab fragments

2.7.4 Ultrathin cryosections (Tokuyasu technique)

2.7.4.1 Preparation of grids

EM grids were cleaned with 25% NH_4OH in double distilled H2O and dried on filter paper at 37°C. The grids were subsequently coated with a formvar film (1.1% (w/v) formvar in chloroform) and a very thin layer of carbon.

2.7.4.2 Sample embedding in gelatin

A monolayer of growing cells was fixed with 4% paraformaldehyde and 0.2% gluteraldehyde in 0.1M phosphate buffer pH 7.4 for 1.5 hours at room temperature and subsequently scraped in 1% gelatine in PBS (provided by the Cell Microscopy Centre, University Medical Centre Utrecht, The Netherlands). Cells were embedded in 12% gelatin, infused in 2.3M sucrose and frozen in liquid nitrogen.

2.7.4.3 Immuno-gold labelling of ultra-thin cryosections

For labelling of ultra-thin cryosections, grids were first incubated in 2% gelatin in order to remove the methyl cellulose/sucrose mixture from the pick up solution.
Sections were incubated on drops for 4 x 1 minute in 0.1% glycine in PBS to quench free aldehyde groups, and non-specific sites were blocked with 1% bovine serum albumine (BSA) in PBS for 3 minutes. The sections were labelled with primary antibody diluted in 1%BSA/PBS for 60 minutes, rinsed for 4 x 2 minutes with PBS and incubated for 20 minutes with Protein A-colloid gold (PAG) conjugates in 1% BSA/PBS (15nm, Cell Microscopy centre, Utrecht, the Netherlands) PAG. Unbound PAG was removed by washing with PBS.
Labelling was stabilised by fixing with 1% Gluteraldehyde in PBS for 5 minutes. After 10 x 1 minute washes, sections were stained with 2% uranyl oxalate/acetate at

pH 7 for 5 minutes. The sections were rinsed in ice-cold ddH2O and incubated for 5 minutes in 1% methyl cellulose/2% uranyl acetate pH 4 on ice. Finally, grids were picked up with loops and dried at RT to form a thin support film of methylcellulose and uranyl acetate.

3 CLN3 is associated with defective autophagy

Juvenile Batten disease is caused by mutations in the CLN3 protein, which is over 90% of the cases is a 1kb deletion. The disease is characterized by the accumulation of subunit c of the mitochondrial ATPase in all the cells of the body. Previous work indicated that the storage material accumulates in lysosomes and it has a typical fingerprint aspect at the ultrastructural level.

CLN3 is a very hydrophobic protein which interacts with AP-1 and AP-3 to be targeted to the lysosomes. It was reported that CLN3 could traffic also via the PM.

Much of the functional work done on CLN3 originates from the yeast *S.cerevisiae* model and a link was made between the protein causing JNCL and intracellular protein trafficking (Chattopadhyay et al., 2003; Fossale et al., 2004; Gachet et al., 2005; Luiro et al., 2004).

The relationship between accumulation of storage material and lysosomal dysfunction is not clear.

In this chapter we investigated the CLN3 localization at the ultrastructural level and we attempted to discover the basic phentypes arising from CLN3 deficiency using fibroblasts and neuron cultures from the *Cln3* KO mouse and fibroblast cultures derived from JNCL patients with the 1kb deletion. The aim was to discover the early disease events from cells in culture for the first time in this laboratory, in order to gain an insight into the intracellular pathways distributed by CLN3 dysfunction. This work would form the basis of the follow-on research into the trafficking and degradation pathways described in subsequent chapters of the thesis.

3.1 CLN3 localization: Immunogold labelling of ultra-thin cryosections

Several groups have studied the localization of the CLN3 protein with varying results and the current best evidence is that CLN3 traffics through the ER and Golgi to the late endosomes and lysosomes (Haskell et al., 2000; Jarvela et al., 1998; Kida et al., 1999) (Ezaki et al., 2003) (Mao et al., 2003a). This is governed by two lysosomal targeting motifs (Kyttala et al., 2004; Storch et al., 2004). A C terminal prenylation motif is also required for efficient sorting to lysosomes (Storch et al., 2007). The CLN3 dileucine lysosome targeting motif binds to the adaptor complexes AP-1 and AP-3, suggesting that CLN3 can traffic through the plasma membrane and early endosomes even if the final destination is the lysosomes (Kyttala et al., 2005). This study was contested by another group, which found that CLN3 does not interact with AP-1, AP-3 or GGA3 adaptors (Storch et al., 2004). Localisation experiments reported so far have used overexpressed CLN3 since no antibody directed against the endogenous CLN3 has been successfully raised.

To obtain more details on the compartment in which CLN3 resides, HeLa cells were transfected with CLN3-GFP using an Amaxa nucleofector device, fixed 24 hours later and prepared for cryo sectioning. Immunolabeling of ultra-thin cryosections (70 nm) was carried out using a GFP antibody to detect CLN3 followed by protein A gold, size 10 nm (PAG_{10}).

As expected, CLN3 labelled the late endosomal and lysosomal population (Figure 3.1).

Representative cryosections from CLN3-GFP transfected HeLa cells are shown in Figure 3.2. Surprisingly, the CLN3 protein was also detected in endosomes containing multiple vesicles (panel A, B, E and F) and small vesicles of 30-40nm (panel B, C and E and Figure 3.1.) usually close to the plasma membrane. The endosomes with vesicles cannot be considered to be multivesicular bodies (MVBs) since the diameter of the structures where CLN3 is detected is below 200 nm and MVBs are usually around 500nm.

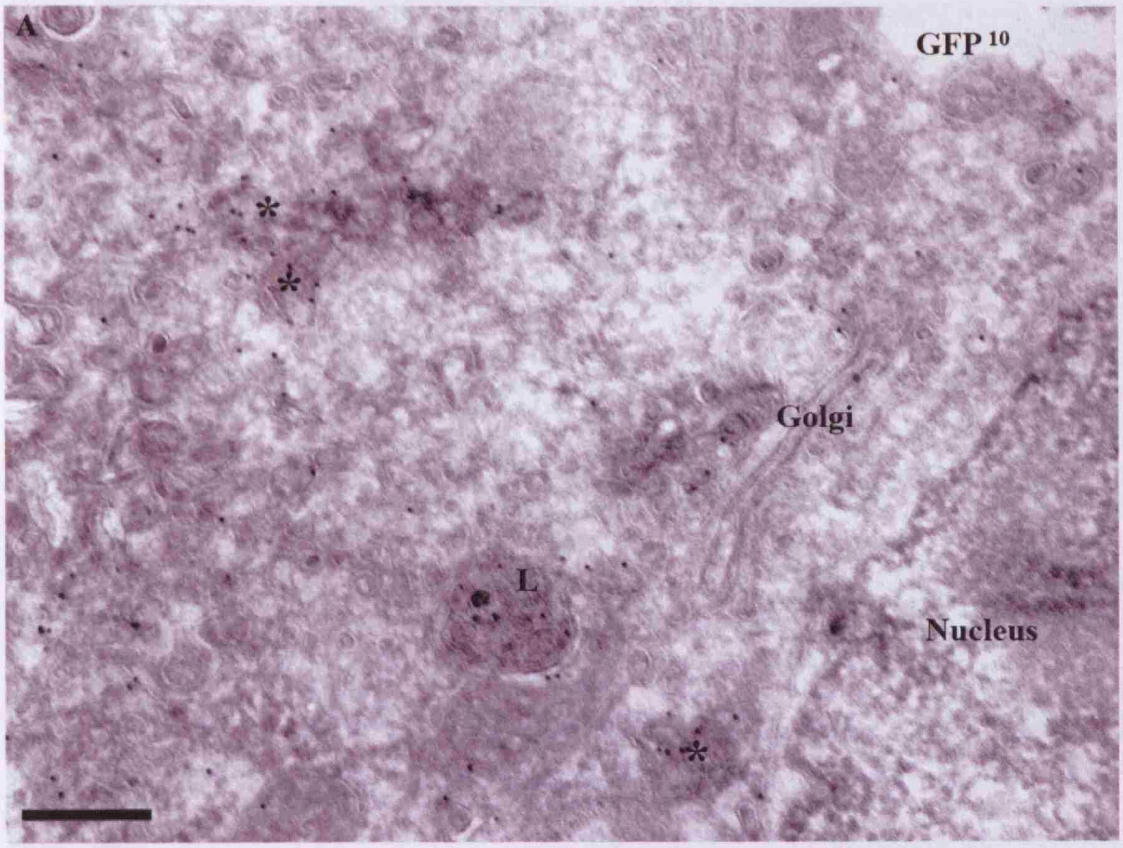

Figure 3.1 Ultra-thin cryosections Immunogold-labelled for CLN3

HeLa cells transfected with CLN3-GFP , 24 hours later 4% PFA fixed and cryo-sectioned then labelled with GFP. This image shows the Golgi area with CLN3 positive small vesicles (*), and a late endosome/lysosome (L).
Scale bar=500nm.

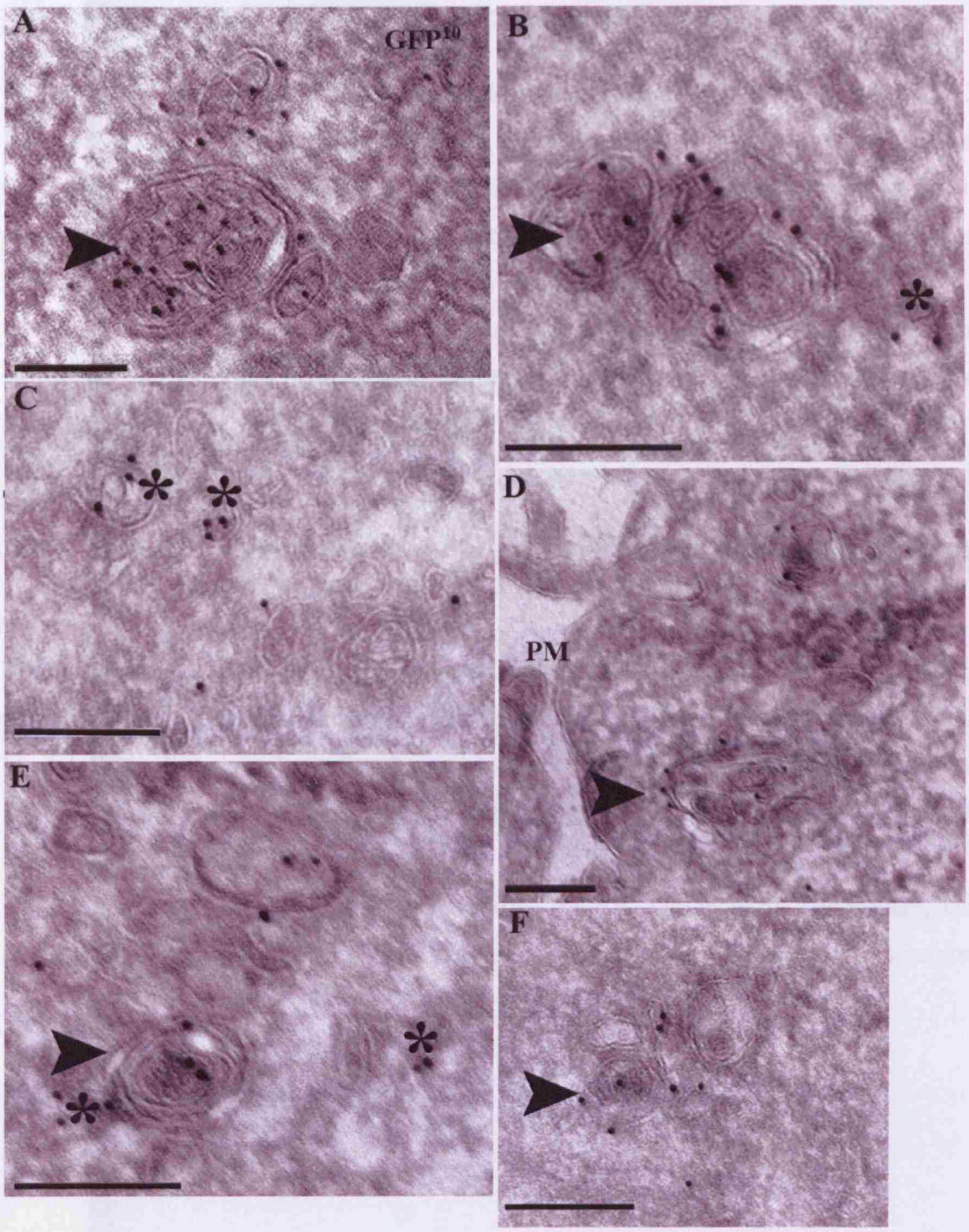

Figure 3.2 Ultra-thin cryosections immunogold-labelled for CLN3

HeLa cells were transfected with CLN3-GFP and 24 hours later 4% PFA fixed and cryo-sectioned then labelled with anti-GFP antibody. PM=plasma membrane. Arrow head= endosomes with few vesicles; * vesicles of 30-40 nm diameter. Scale bar=200nm.

3.2 *Phenotypes arising from CLN3 deficiency*

The strategy employed to search for basic phenotypes arising from loss of CLN3 function was to investigate the integrity, organization and distribution of cellular organelles by immunofluorescence analysis using various organelles markers. This screening was done in parallel with ultrastructural analysis performed using electron microscopy.

The cells used for this study were fibroblasts from the *Cln3* $^{ex\ 1\text{-}6\ \Delta}$ mice (referred to below as *Cln3* KO) and primary skin fibroblasts from JNCL patients homozygous for the common CLN3 1 kb deletion carried on >80% of cases.

3.2.1 Cellular organelle survey in primary fibroblasts cultured from JNCL homozygous 1.02 Kb deletion patients

To examine the role of CLN3 in cellular trafficking, immunofluorescence studies were performed to determine whether deficiency in the CLN3 protein impaired the localization of the markers listed in Table 3-1. Control and 1 kb deletion human fibroblasts were grown for not more than 20 passages and analysed by indirect immunofluorescence.

Cells were fixed and labelled with antibodies for ER, Golgi, early endosomes, late endosomes and lysosomes, recycling early endosomes and the autophagosomal marker LC3.

Table 3-1 Organelle markers used for human and mouse IF study

Organelle	Antibodies
Lysosomes and late endosomes	Lamp1 (Lgp120), CD63, Rab7, CI-MPR
Recycling early endosomes	Rab11, Rab4, Transferrin receptor
Early endosomes	EEA1, Rab5
Golgi	TGN46,TGN38, CI-MPR
ER	Calreticulin
Autophagosome	LC3

Staining with the endosomal, lysosomal (Figure 3.3) Golgi and ER markers (data not shown) did not reveal any morphological differences between wild type and mutant fibroblasts.

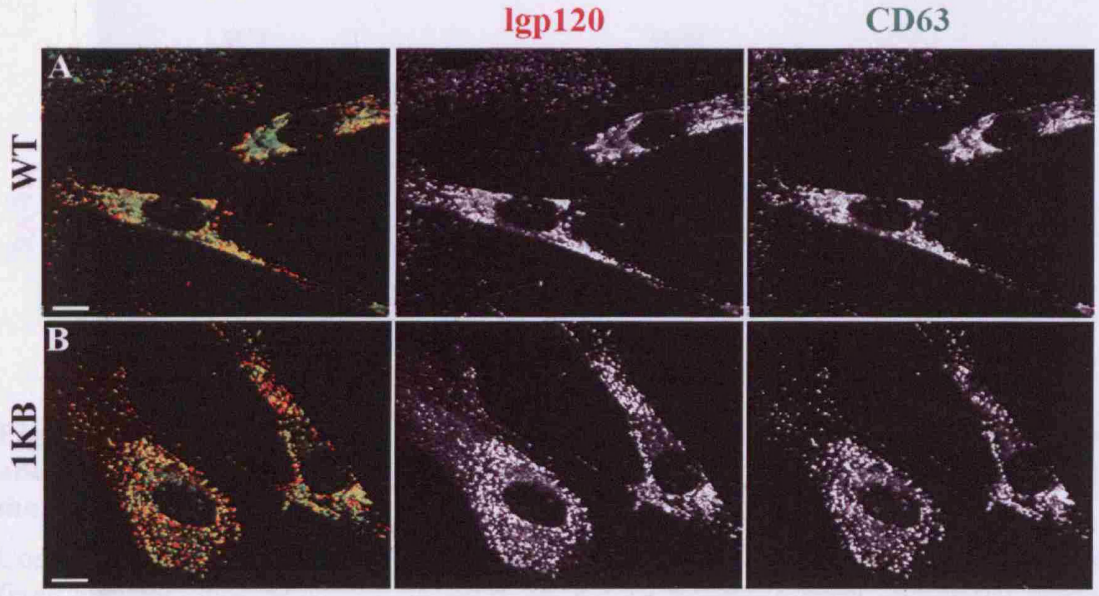

Figure 3.3 Immunofluorescence labelling of human skin fibroblasts from control and 1kb deletion patient for late endosomes/lysosomes

Control (panel A) and 1kb deletion JNCL (panel B) fibroblasts were fixed and immunolabelled for the late endosomal/lysosomal markers Lgp120 and CD63.
Scale bar=10μm

However a change was detected in the distribution of Rab11, Rab11 labelling showed a distinct difference in distribution between control and JNCL cells. In the mutant cells, Rab11 localization was accentuated in the perinuclear area in contrast with control cells, in which it was also distributed in peripheral endosomes (Figure 3.4).

In addition to these differences, the microtubular associated protein light chain III (LC3), which is an autophagosomal marker also displayed an altered localization in JNCL cells.

LC3 is a cytoplasmic protein, which gets recruited to the autophagic membranes during the autophagosomal maturation (Kabeya et al., 2000). In the wild type cells, the LC3 staining was mostly dispersed in cytoplasm and only occasionally appeared to be associated with punctate vesicles, which represent autophagosomes (Figure 3.5, first panel).

In JNCL, there was a stronger staining for LC3 and it appeared to be associated mostly to punctate vesicles, which were dispersed throughout the cytoplasm. This suggested that the autophagic pathway could be upregulated (Figure 3.5, second panel).

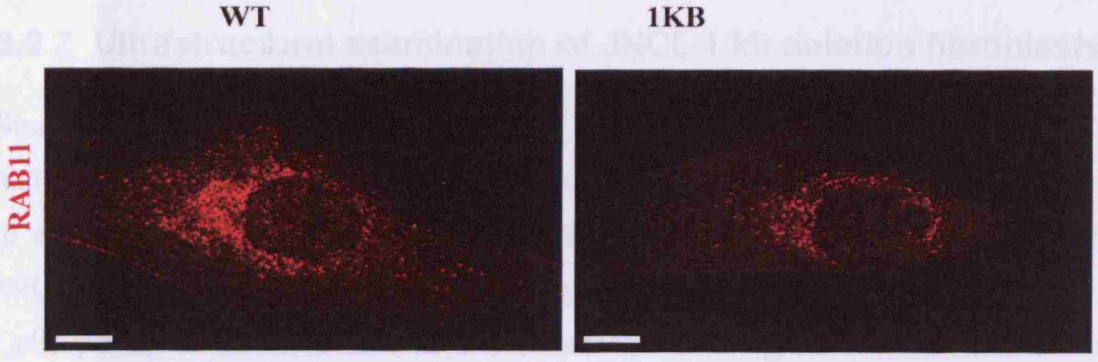

Figure 3.4 Immunofluorescence labelling of human skin fibroblasts from control and 1kb deletion patient for the early endosomal/recycling early endosome marker Rab11

Control (panel on the left) and 1kb deletion JNCL (panel on the right) fibroblasts were fixed and immunolabelled for the early endosomal/recycling early endosomal marker Rab11.
Scale bar=10μm

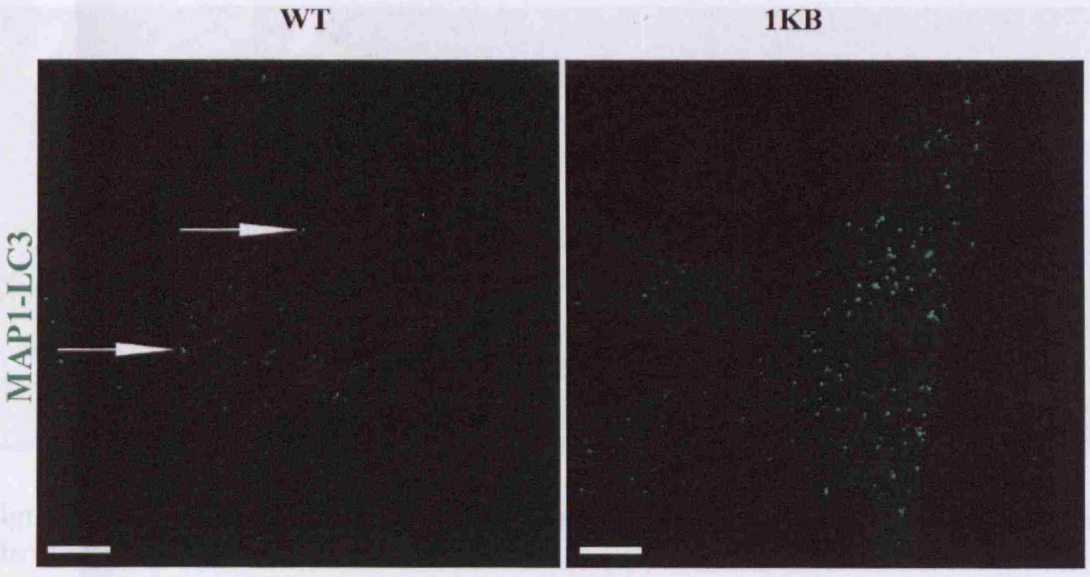

Figure 3.5 Immunofluorescence labelling of human skin fibroblasts from control and 1kb deletion patient for the autophagosomal marker LC3

Control (panel on the left) and 1kb deletion JNCL (panel on the right) fibroblasts were fixed and immunolabelled for the autophagosomal marker LC3.
Scale bar=10μm

3.2.2 Ultrastructural examination of JNCL 1 kb deletion fibroblasts

Since JNCL human skin fibroblasts showed defects in distribution of certain endocytic and autophagic markers used in the screening performed at the light level, we decided to extended the study to include an investigation of the cellular architecture of the JNCL 1kb deletion fibroblasts by morphological ultrastructural analysis.

Cells passaged not more than 20 times were grown on glass coverslips, fixed and processed for electron microscopy examination. A detailed survey of cellular organelle showed no differences. Lysosomes, endosomes, ER, Golgi and mitochondria were morphologically normal in JNCL fibroblasts. Since CLN3 is a late endosomal/lysosomal protein, careful attention was given to the lysosomes in particular. Panel A and panel B of Figure 3.6 shows wild type lysosomes, which are between 500 to 700 nm, electron dense and contain membrane whorls.

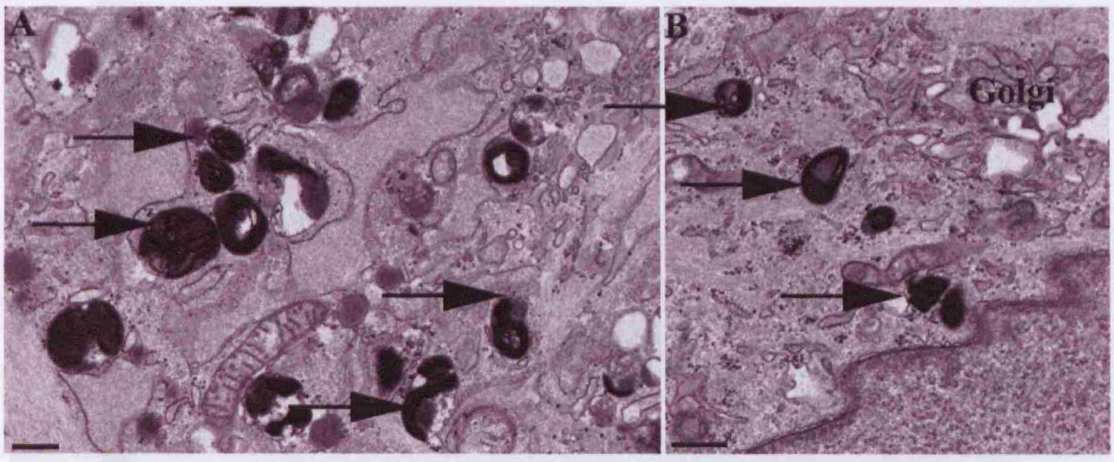

Figure 3.6 Electron micrographs of lysosomes from wild type human skin fibroblasts

Lysosomes are indicated by arrows

Scale bar=500nm

The lysosomes of the control human skin fibroblasts have the same appearance as those from a JNCL patient as shown in Figure 3.7, panel B. However in the JNCL fibroblasts, two additional organelle compartments were also observed. As shown in panels A and C (large arrow heads) of Figure 3.8, the first of these consist of organelles, which morphologically can be identified as components of the endocytic pathway. The shape of these organelles is more elongated than conventional endosomes and their internal structure is composed of 2 different contents suggesting that they are organelles in the process of fusing.

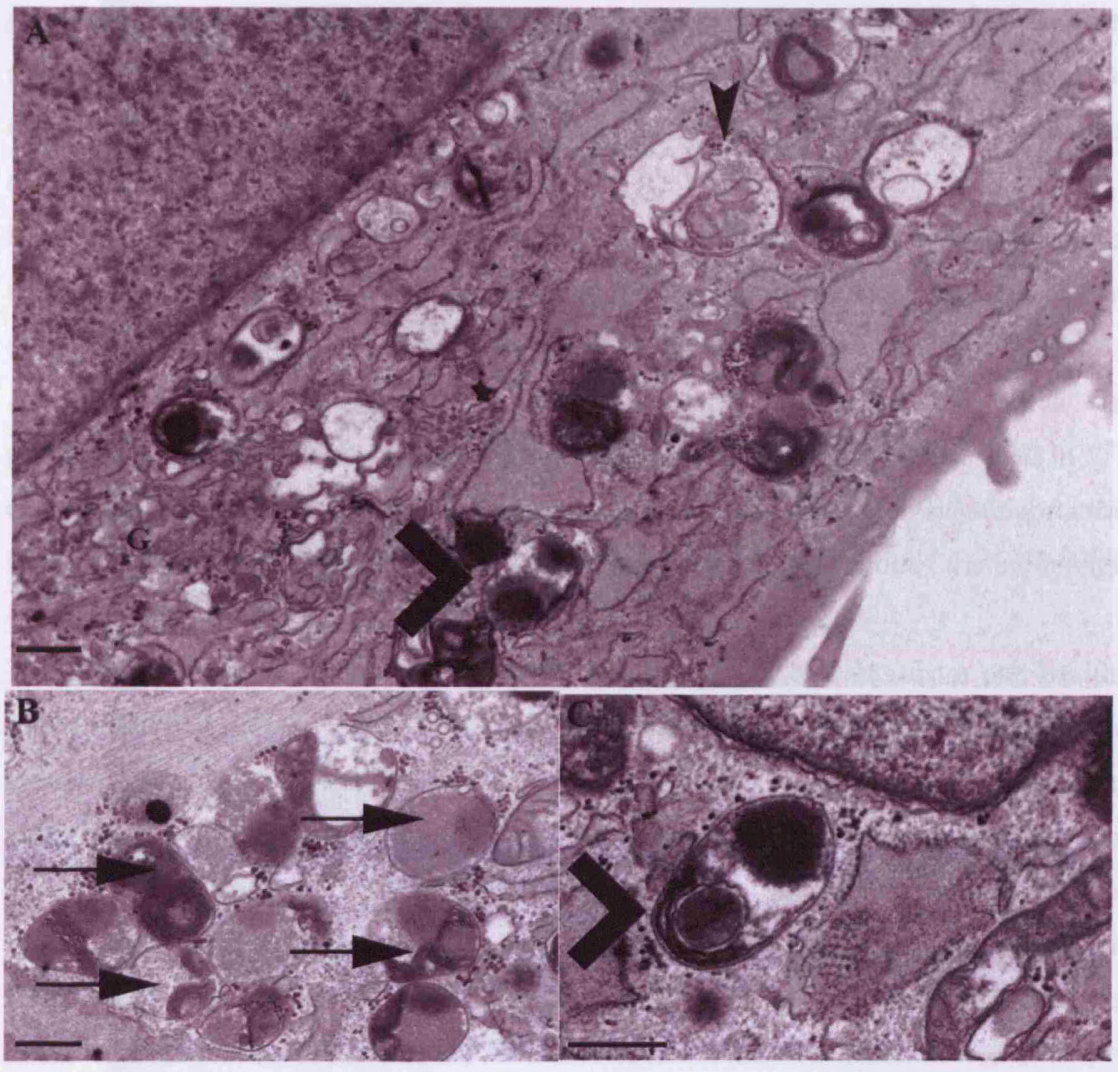

Figure 3.7 Electron micrographs of JNCL fibroblasts

The arrows indicates lysosomes. Large arrowhead indicates elongated endosomes. The small arrow head in A indicates an early autophagosome. Scale bar=500nm

The second and more expanded compartment consists of autophagosomes (Figure 3.7, small arrow heads). Examined in more detail early autophagosomes (Figure 3.8 panels A, B, C, E) were clearly identified by the classic double membrane (small arrow heads) which surrounds the organelles, and the still distinguishable cytoplasmic content indicative of a newly formed organelle. Newly forming phagophores were visible in the perinuclear area, in the process of entrapping cytoplasm (Figure 3.8,

panel B). In a representative example, close to one phagophore is another autophagosome but in a more advanced stage, as suggested by the increase in the electron density of this organelle (panel B). Many late autophagosomes were seen (panel B,D,F).

Early autophagosomes were often found in the vicinity of the late autophagosomes, and they were also most often positioned in the proximity of the Golgi area. More examples of autophagosomes are shown in the panels D and F of Figure 3.8.

As described in the section 3.2.1, the LC3 marker in mutated fibroblasts was prevalently associated with membranes rather then being mostly cytoplasmic as in WT cells, suggesting an accumulation of autophagic structures. EM analysis supports this finding, since it is immediately obvious that there is an enlargement of the autophagic compartment.

The morphological study illustrated so far was based on cell lines from one healthy individual (cell line called 1BR.3) and one 1kb JNCL patient (cell line called HF480Pa). To confirm the phenotype identified in the patient cell we carried out an analysis of additional cells lines derived from nine healthy individuals (cells lines called: 48BR, Hs68, AGO, HF523N-HF529N) and four other JNCL patients with the same common 1kb deletion (cell lines called HF470Pa, HF478Pa, HF479Pa, HF481Pa). Detailed electron microscopy examination using these additional samples provided evidence of major differences between fibroblast cell lines. Accumulation of autophagic structures was again observed uniquely in the new mutant cell lines and not controls, but a big heterogenity was detected in the new control cell lines. Morphologically most of the new cells lines (patient and controls) were different from each other. The endocytic pathway in particular presented major differences, some of the cells lines in fact presented an expanded lysosomal compartment with granular features.

Clearly there could be heterogeneity of the cell types in the primary skin cultures, and their cell cycle stages. The differences between cell lines could also be due to the provenance of the cells, differences between individuals and the methods of culturing the cells at the initial passages in different labs. Due to the difficulty of working with

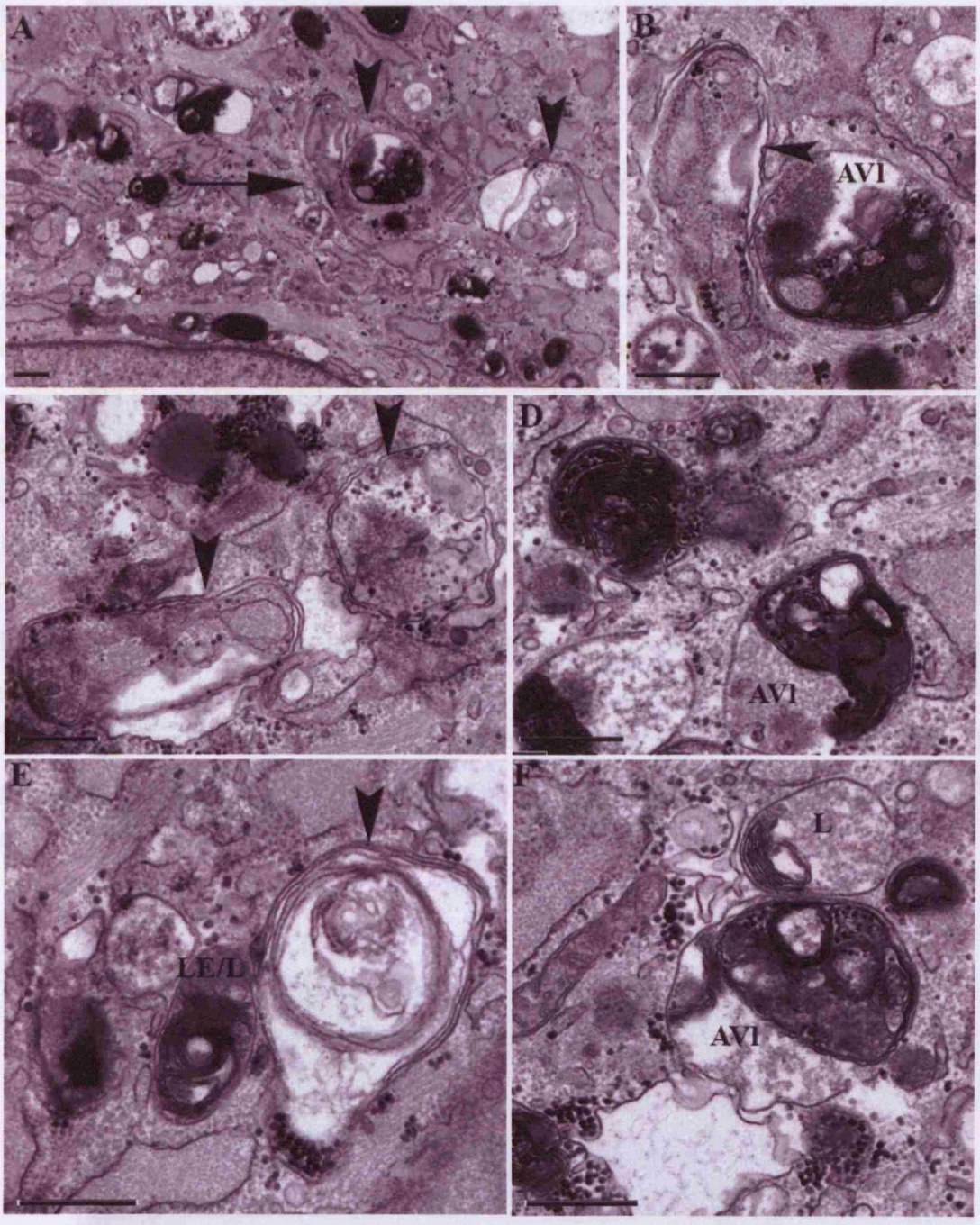

Figure 3.8 Electron microscopy investigation of autophagic compartment in JNCL human skin Fibroblasts

Early autophagosomes are indicated by arrowheads, late autophagosomes are labelled AVl. Late endosomes are labelled (LE) and lysosomes (L) were also found.
In panel B there is an enlargement of the phagophore represented in the centre of panel A. Scale bar=0.5 μm.

heterogeneous cell lines originating from different individuals and labs, the use of human skin fibroblasts was discontinued.

3.2.3 Survey of cellular organelles in *CLN3* KO mouse primary fibroblasts (MEFs)

In parallel to the study in human skin fibroblasts described in 3.2.1, a survey was carried out using the same main organelle markers listed in Table 3-1 in mouse embryonic fibroblasts (MEFs) from wild type (WT) and *Cln3* knock out mice (KO). Similarly to the findings for the human skin fibroblasts, few organelles appeared to be distributed differently in the wild type MEFs compared to the knock out MEFs. However some differences were observed, as follows.

The CI-MPR appeared to be present almost exclusively in the perinuclear region in the KO MEFs whereas in the WT MEFs it was also present in peripheral endosomes (Figure 3.9).

The early endosomal/recycling endosomal marker Rab11 was concentrated predominantly in the perinuclear region in the knock out MEFs whereas in the WT cells it was also observed in the peripherial endosomes (Figure 3.10).

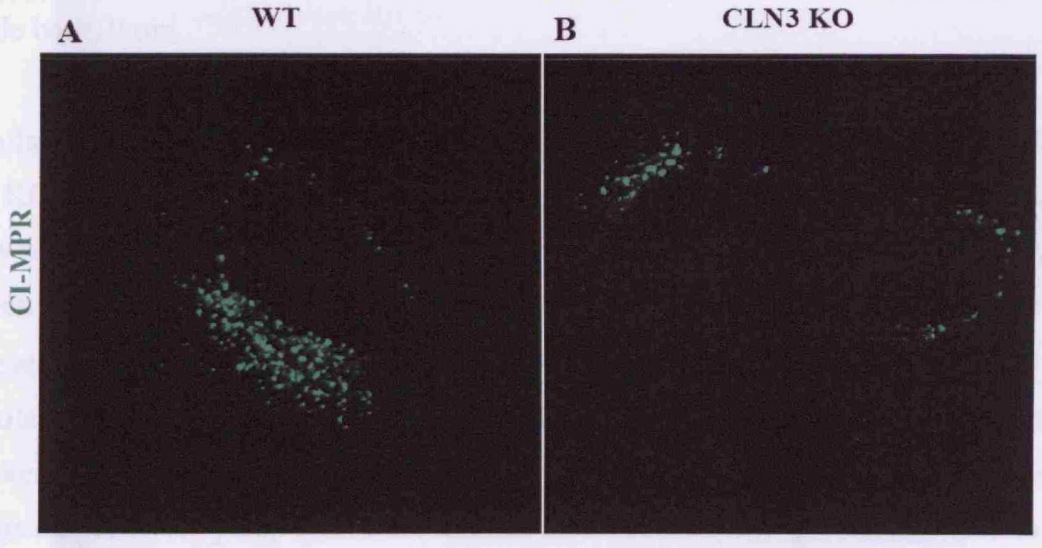

Figure 3.9 CI-MPR labelling of WT and CLN3 KO mouse embryonic fibroblasts.

Control (panel A) and CLN3 KO fibroblasts (panel B) were fixed and immunolabelled for the CI-MPR marker.
Scale bar=10 μm

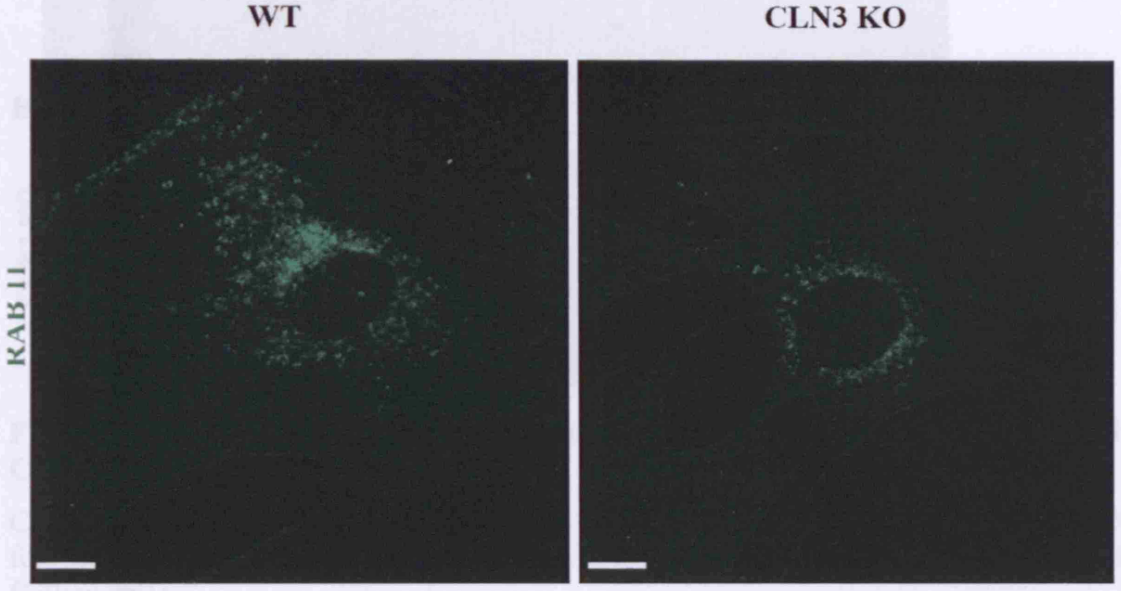

Figure 3.10 Indirect immunofluorescence of MEFs with Rab11

Control (panel on the left) and CLN3 KO (panel on the right) fibroblasts were fixed and immunolabelled for the early endosomal/recycling early endosomal marker Rab11.
Scale bar=10 μm

Similarly to the findings for human skin fibroblasts, no differences were observed in the KO MEFs for LAMP1 or any other lysosomal marker used (Figure 3.11 and not shown). Surprisingly no difference was observed with the Cathepsin D antibody, which was reported to be more perinuclear in the cerebellar cells from the *Cln3* $^{\Delta ex7/8}$ (Fossale et al., 2004).

Similarly to the 1kb JNCL fibroblasts, in the *Cln3* KO MEFs the autophagosomal marker LC3 stained the cell more strongly and was heavily concentrated in vesicles suggesting that autophagosomes accumulate in the KO cells (Figure 3.12) whereas in the WT it appeared to be more distributed in the cytoplasm.

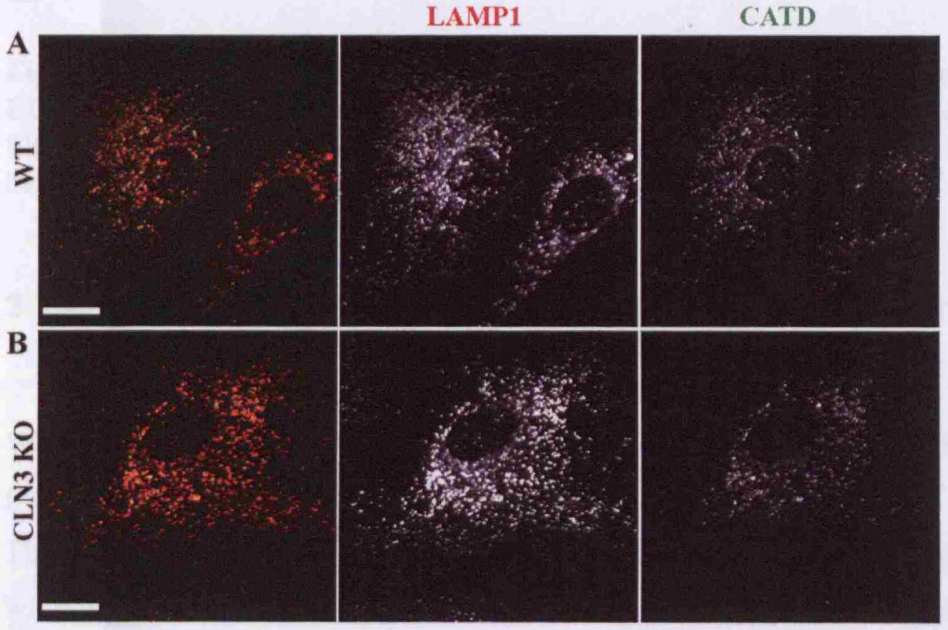

Figure 3.11 Indirect immunofluorescence of MEFs with the markers Lamp1 and Cathepsin D.

Control (panel A) and CLN3 KO (panel B) fibroblasts were fixed and immunolabelled for the late endosomal/lysosomal marker LAMP1 and for the lysosomal hydrolase Cathepsin D.
Scale bar=10μm

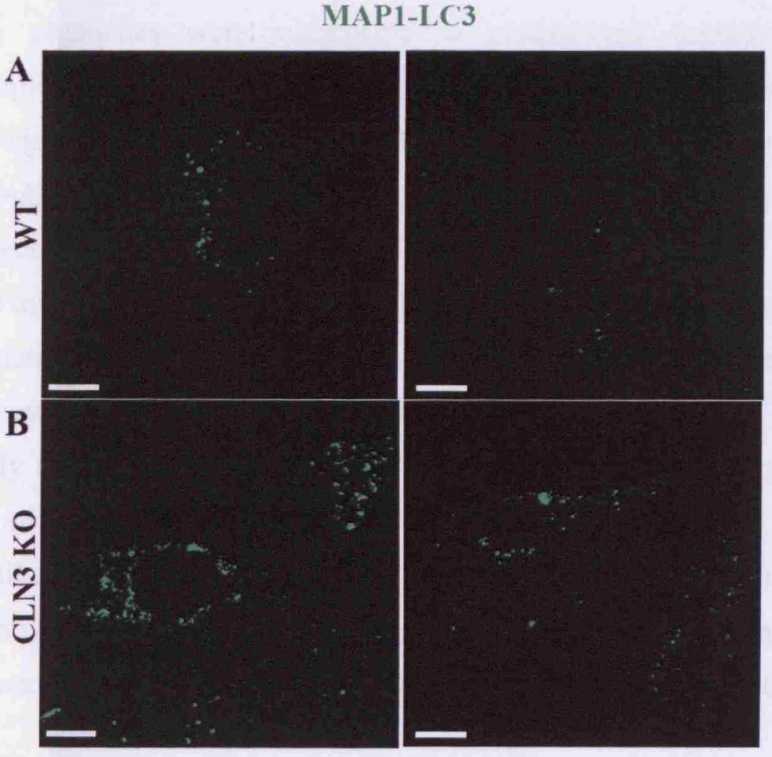

Figure 3.12 Indirect immunofluoresce of MEFs with the autophagosomal marker LC3. Control (both pictures, panel A) and CLN3 KO (both pictures, panel B) fibroblasts were fixed and immunolabelled for the autophagosomal marker LC3. Scale bar=10μm

3.2.4 Ultrastructural examination of CLN3 KO mouse primary fibroblasts (MEFs)

Wild type and *Cln3* knock out MEFs were grown for not more than four passages, fixed, embedded for electron microscopy and analyzed.

The ultrastructural morphology of the cellular organelles was carefully examined and wild type cells were compared with the KO cells. No differences were detected between KO cells and WT cells except for the presence of an abnormal compartment, present exclusively in the KO MEFs.

The compartment consisted of organelles over 1000nm in diameter, with internal membrane whorls and occasionally vesicles (Figure 3.13). Normal lysosomes were also present in the KO cells.

The organelles were autophagic in morphology containing partially or more completely degraded cytosolic material and organelles, suggesting they are part of an expanded autophagic population. The EM images were indicative of a malfunctioning autophagic pathway, similarly to that observed for the patient human skin fibroblasts in section 3.2.2.

The autophagic organelles in the KO MEFs were markedly bigger than any seen in the human skin fibroblasts. Most of them were observed to be in an advanced stage of maturation since the content was electron dense.

Early autophagic organelles were also found, but it was not possible to observe any cytoplasm as content (Figure 3.14).

Similarly to the human skin fibroblasts, no mitochondrial defects were observed. During the course of this study, two reports were published suggesting such defects in neuronal cells derived from the mice models (Fossale et al., 2004; Luiro et al., 2006).

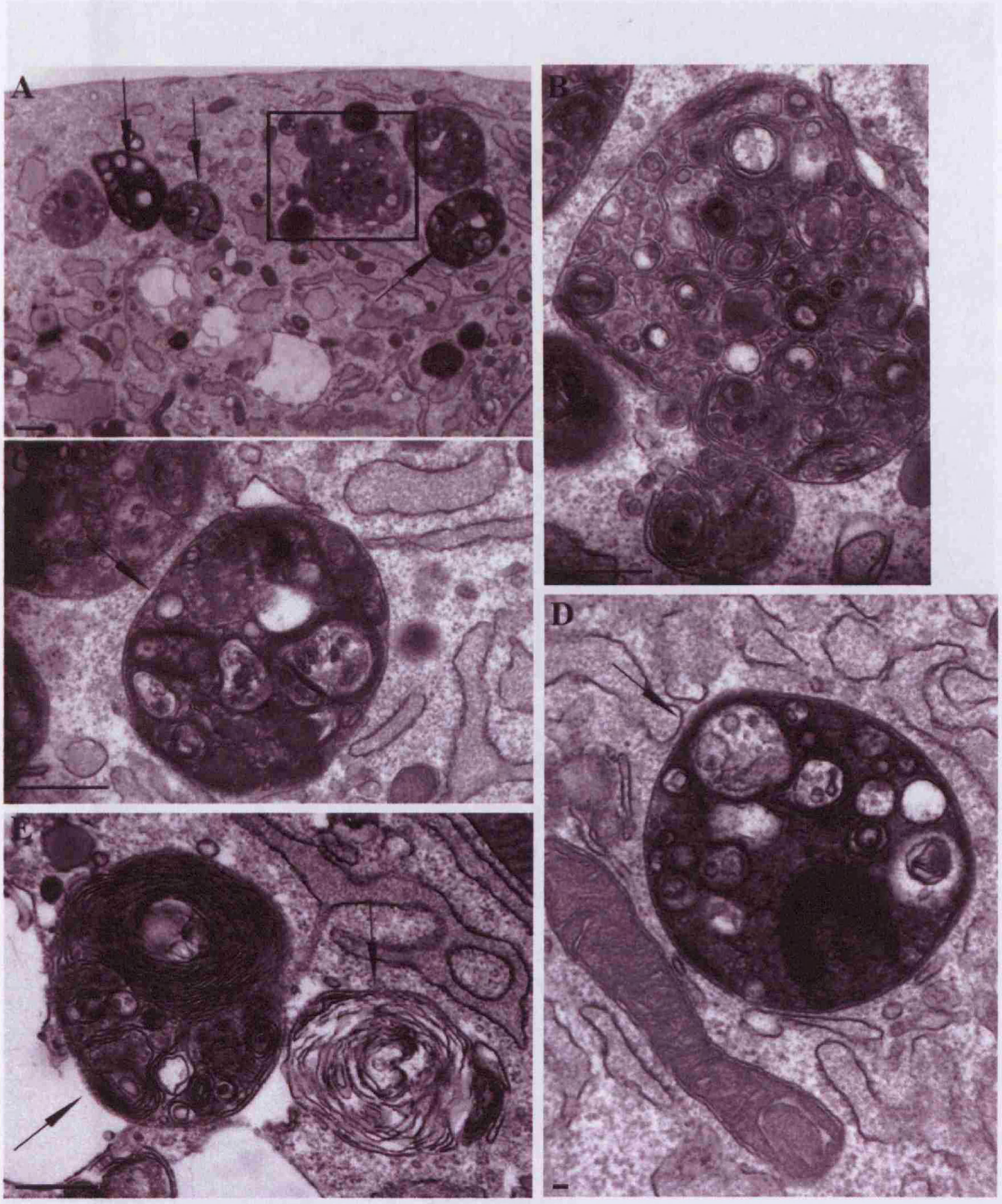

Figure 3.13 Electron microscopy analysis of mouse Cln3 KO fibroblasts

The arrows show late autophagic structures. Panel B is an enlargement of the autophagosome highlighted in panel A.
Scale bar=0.5 μm.

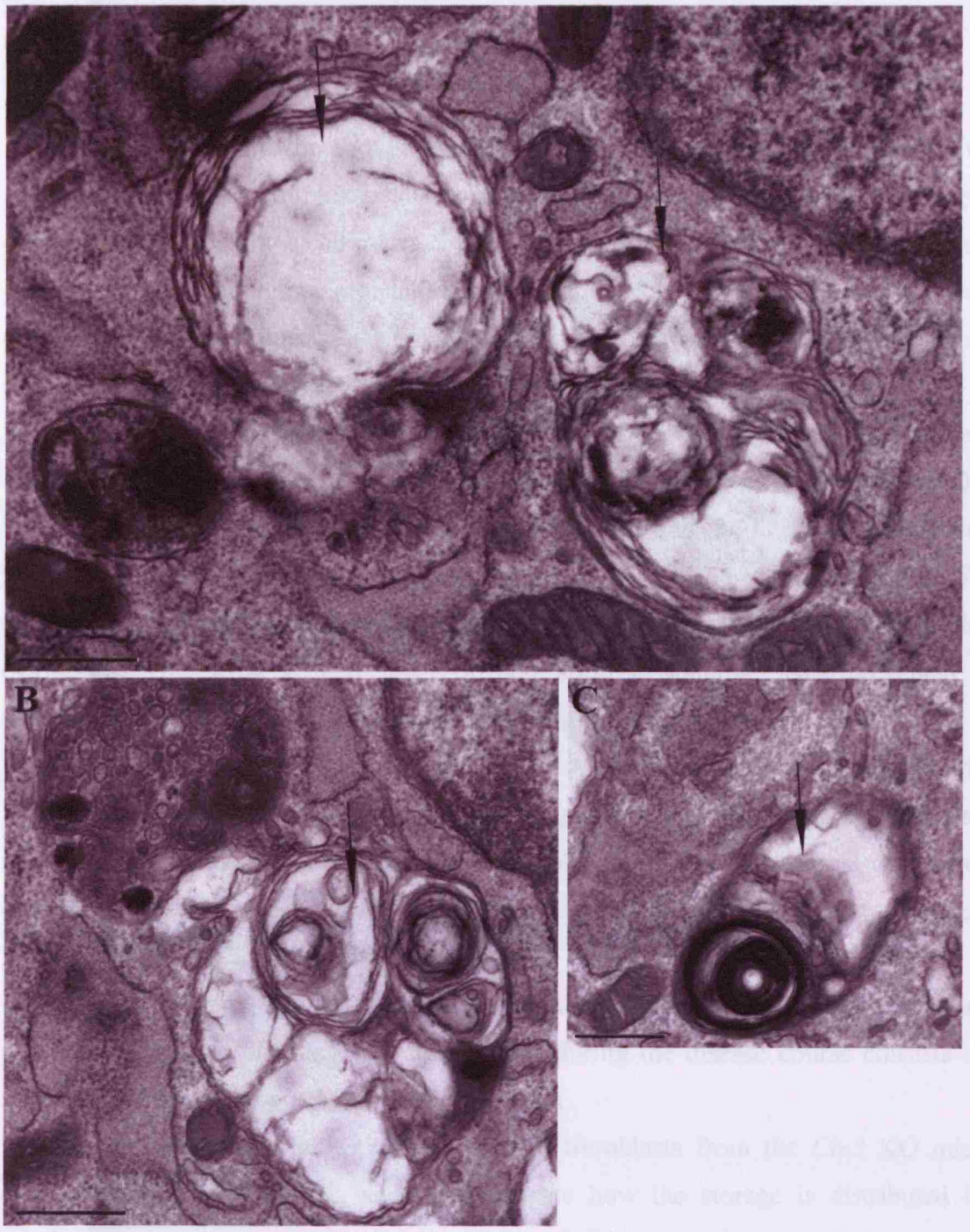

Figure 3.14 Electron Microcopy investigation of Cln3 KO fibroblast

Arrows indicate early autophagosomes.
Scale bar=0.5μm

3.2.4.1 Autophagosomes but not lysosomes are positive for subunit c in the CLN3 KO MEFs

To obtain more information about the abnormal compartments exclusively detected in the knock out mouse fibroblasts and to investigate further their putative autophagic origin, immunolabelling of ultra-thin cryosections from mouse primary fibroblasts was performed. Since the unique organelles share features with the endocytic compartment especially the late endosomes/lysosomes, and with autophagosomes, the markers selected for the analysis were LC3 and LAMP1 respectively.

Since the robust LC3 antibody available to us does not work on cryo samples, we used a construct encoding an EGFP tagged form of the LC3 protein kindly provided by Dr. T.Yoshimori. WT and KO MEFs were transfected and after 24 hours the cells were fixed and prepared for immunolabelling. A GFP antibody was used to detect the GFP tagged LC3. EM analysis showed that LC3 was relatively randomly distributed in the cytoplasm, suggesting a high level of non specific staining. This prevented a distinction between the real staining and the background (not shown).

Ultra-thin cyosections were also stained with LAMP1 to label late endosomes and lysosomes. Multivesicular bodies (Figure 3.15, panel A and B), lysosomes and also small vesicles (panel C) were positive for LAMP1. The autophagosomal organelles exclusively present in the KO fibroblasts present just few gold particles representing LAMP1 (Figure 3.15, panel D and Figure 3.16).

In the juvenile-onset form of Batten disease, the majority of the storage material protein content that progressively accumulates during the disease course consists of the mitochondrial ATP synthase subunit c protein .

In order to determine whether primary mouse fibroblasts from the *Cln3* KO mice display storage of subunit c, and to investigate how the storage is distributed in relation to the aberrant organelles in mutant MEFs, ultra-thin cryosections were stained with an anti subunit c antibody, kindly provided by Professor E.Kominami. Subunit c can also be used as a marker of autophagy since turnover of mitochondria is controlled by the autophagic pathway.

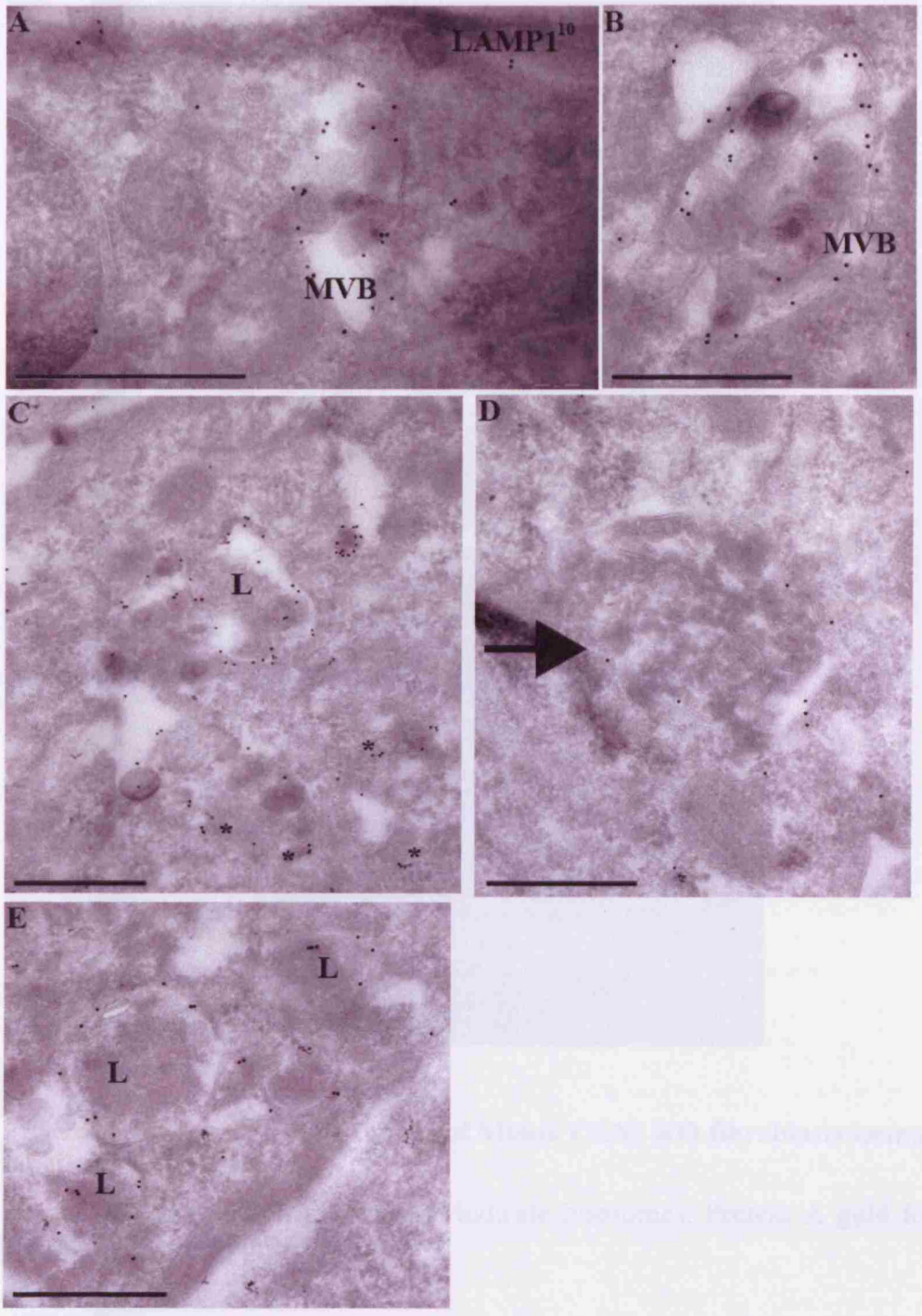

Figure 3.15 Ultrathin cryosections of CLN3 KO primary fibroblasts immunogold labelled for LAMP1

Arrows indicates autophagosome. Multivesicular bodies (MVB) and lysosomes (L) also indicated. * indicates small LAMP-1 positive vesicles.
Protein A gold for Lamp1, 10nm.
Scale bar=500nm.

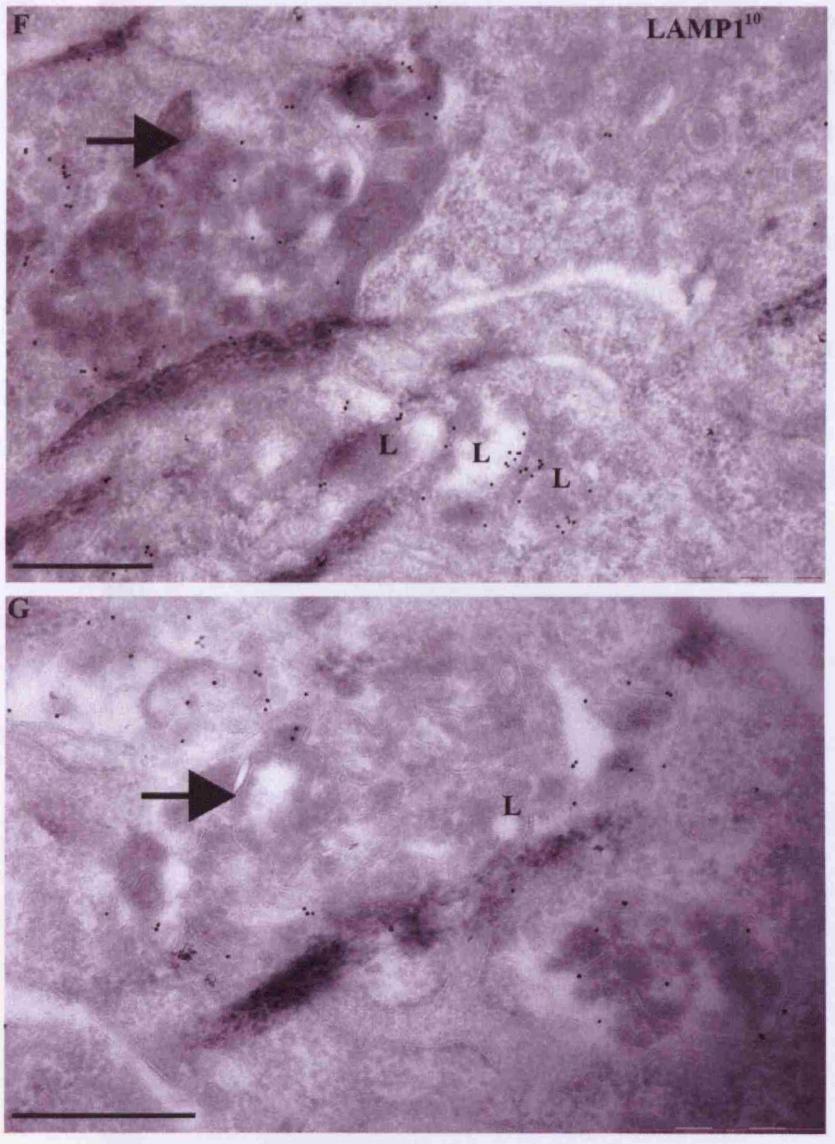

Figure 3.16Ultra-thin cryosections of Mouse CLN3 KO fibroblasts immunogold labelled for Lamp1.

Arrows indicate autophagosomes, L indicate lysosomes. Protein A gold for Lamp1, 10nm. Scale bar=500nM

Mitochondria are subject to regular turnover and they are directly removed via the autophagic pathway (Klionsky and Emr, 2000). In *Cln3* KO primary fibroblasts the subunit c protein was, as expected, present in the internal cristae of mitochondria (Figure 3.17, panel A and B). However, subunit c was also seen within the unique autophagic compartment of the mutant fibroblasts (panel C and D) and it was not present anywhere else. In contrast to Lamp1, subunit c heavily decorated the internal membrane of the unique compartment suggesting internalization of mitochondria within these structures.

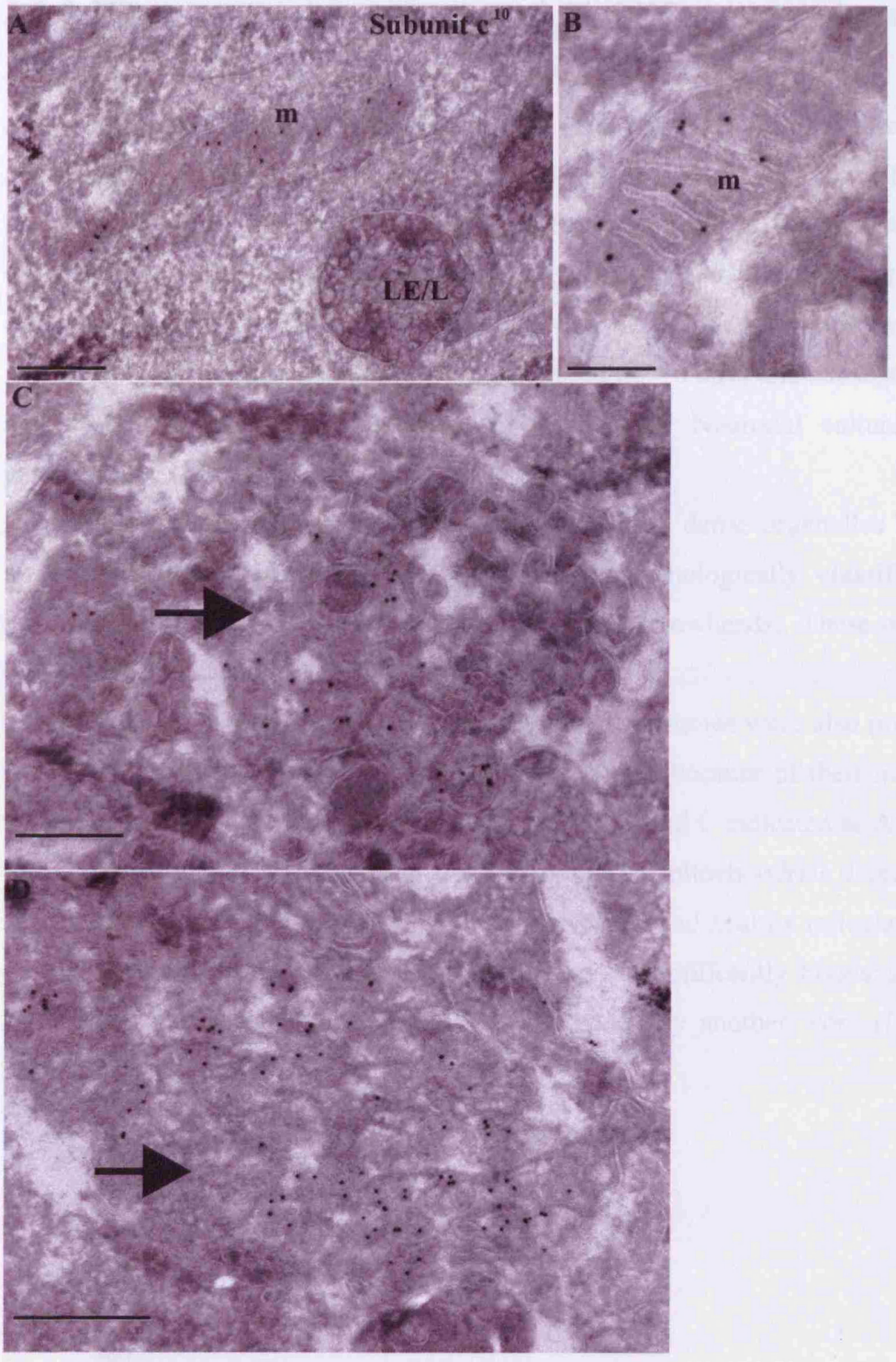

Figure 3.17 Subunit c immunolabelling of ultrathin cryosections of CLN3 KO mouse Fibroblasts

Arrows indicate autophagic organelles. LE/L indicate late endosomes/lysosomes
m indicate mitochondria
Scale bar=200nM

3.2.5 Ultrastructural examination of *Cln3* KO mouse primary neurons

JNCL is a neurodegenerative disease and the hallmark of the disease is the accumulation of the mitochondrial ATPse synthase in all the cells of the body. However the only cells that are clinically affected and die in the disease are in the CNS and the neural retina. For this reason, a morphological examination of primary neurons from the available *Cln3* KO brain was performed. Neurons from the KO mouse model and wild type controls were cultured for 10 days and subsequently fixed and processed for electron microscopy examination. Neuronal culture has been performed by Hannah Mitchison.

At the ultrastructural level, the same aberrant electron dense organelles seen in the mutant fibroblasts were observed; these were morphologically classified as late autophagosomes (Figure 3.18, panel D and E, white arrowheads). These were present just in the KO neurons.

Close to the TGN area, many newly formed autophagosomes were also present. They were distinguishable from the mature autophagosomes because of their inner content which is cytosolic and not electron dense (panel A , B and C indicated as AVi).

Furthermore, in the neurons from the KO model, a mitochondrial defect was also revealed that was not observed in KO MEFs. Normal and healthy mitochondria were present alongside mitochondria deformed, being of significantly bigger size (Figure 3.18, panel C). This phenotype was later confirmed by another work (Luiro et al., 2006).

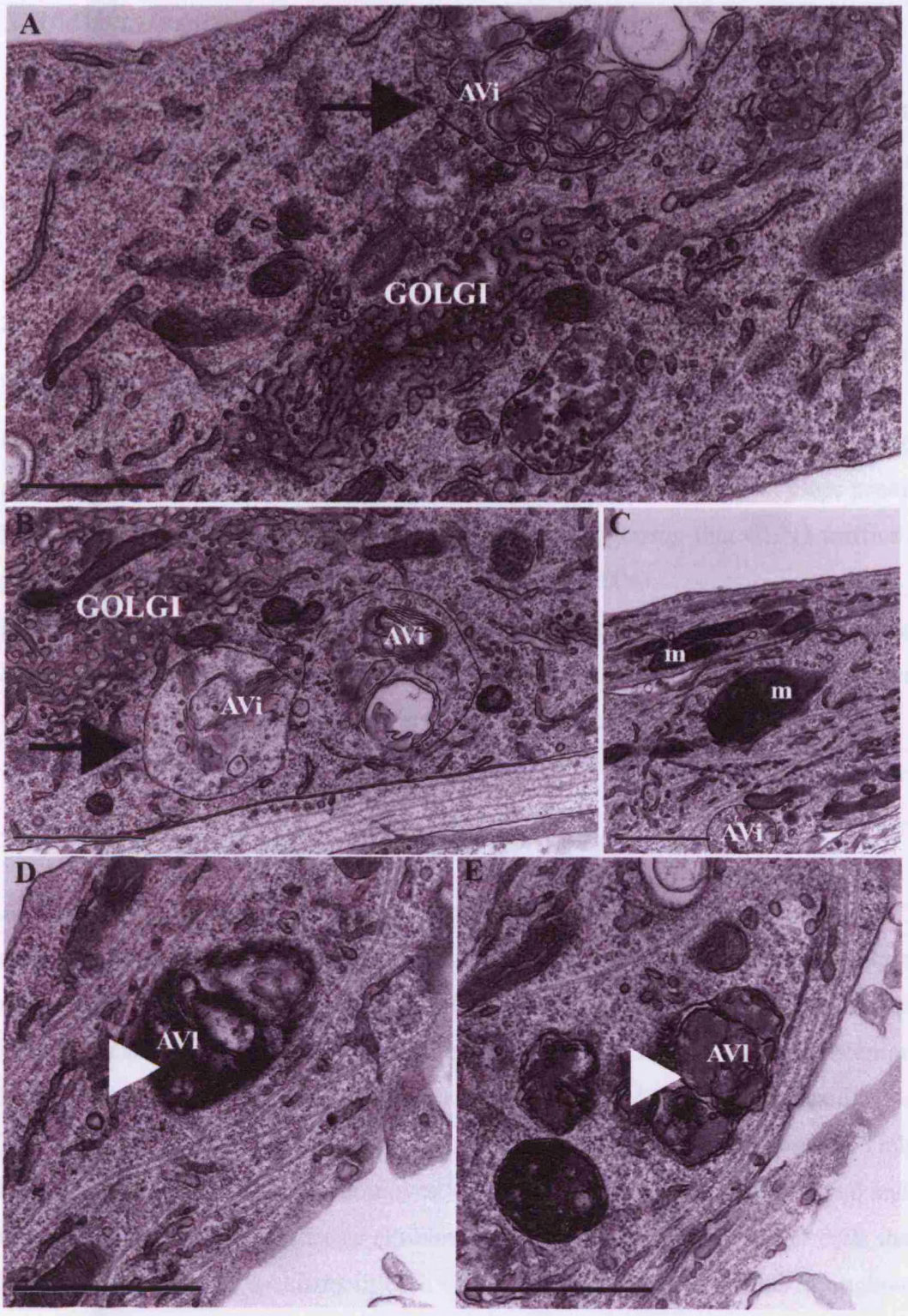

Figure 3.18 Ultrastractural examination of CLN3 KO neurons

Avi indicate early autophagosomes, white arrowheads indicate late autophagosomes (AVl) and m label mitochondria. Scale bar=1μm

3.3 Discussion

The aim of this part of the thesis was to analyze CLN3 localization at the ultrastructural level and basic phenotypes arising from CLN3 loss of function in the cells.

3.3.1 CLN3 localization at the ultrastructural level

To study its localization by electron microscopy, HeLa cells were transfected with CLN3-GFP and processed for cryo sectioning. CLN3 was found in late endosomes and lysosomes as expected but also in small vesicles (100nm) some in close proximity to the Golgi, some close to the plasma membrane suggesting that CLN3 traffics a lot in the cells between organelles(Persaud-Sawin et al., 2004).

Double labelling of CLN3-GFP HeLa cells would have been desirable in order to better classify the CLN3 compartment however because of the difficulty of locating CLN3-positive overexpressed cells by cryo we did not attempt this experiment.

3.3.2 Impairment in the endocytic pathway

A detailed survey with endocytic markers was carried out in controls and cells deficient for CLN3. In both human skin fibroblasts and mouse embryonic fibroblasts at the light level the only difference detected with endosomal markers was obtained with the early endosomal/recycling endosomal marker Rab11 and the receptor CI-MPR whereas the endosomal markers Lamp1, CD63, EEA1 were unchanged.

The CI-MPR is a fundamental receptor, which delivers hydrolases from the Golgi to the lysosomes where they get employed for degradation of lysosomal material and it is critical for lysosomal biogenesis (Pohlmann et al., 1995). In mouse KO cells the CI-MPR which normally localizes in both Golgi and endosomes scattered throughout the cytoplasm was prevalently detected in the Golgi area.

Rab11 traffics through the early and recycling compartment and it is thought to regulate endosomal/plasma membrane interactions, by controlling membrane traffic,

through recycling early endosomes. In both human and mouse CLN3 deficient cells Rab11 is almost completely distributed in the perinuclear/Golgi area. This suggests a defect in the endocytic pathway at the level of the Golgi or recycling early endosomes in CLN3 deficient cells from JNCL patient and the mouse model.

3.3.3 Impairment in autophagy

In human skin fibroblasts and CLN3 KO fibroblasts and neurons, an increased number of autophagosomes was discovered. This was confirmed in both light microscopy study and electron microscopy. An increased abnormal number of autophagosomes were present in CLN3 deficient cells.

Upregulation of the autophagic pathway due to CLN3 deficiency was also reported, after this study was already carried out, in immortalized cerebella cells from the mouse model *Cln3* $^{\Delta ex7/8}$ confirming that autophagy is misregulated when CLN3 is impaired (Cao et al., 2006).

Autophagy is a routine housekeeping process exerted by cells but it is generally difficult to see autophagosomes frequently in normal cultured conditions. As a result of CLN3 dysfunctions autophagy could be either upregulated in these cells or the maturation of autophagosomes could be arrested, blocking their removal and leading to accumulation. The major component of the storage material in JNCL is subunit c of the mitochondrial ATP synthase. Surprisingly, primary cells in culture were found to be able to accumulate the protein, implying that the storage material accumulates very quickly.

The presence of a mitochondrial protein within the endocytic compartment may be explained by the process of mitophagy, where mitochondria, subject to a very high turnover in the cells, get incorporated in autophagosomes for their ultimate removal.

The only available route in cells for a mitochondrial protein such as the subunit c protein to encounter the endocytic pathway is through fusion between endosomes/ lysosomes and autophagosomes which have previously incorporated mitochondria. These results suggest that when correct functioning of CLN3 is lost by the cells, autophagosomes accumulate that are positive for subunit c, mostly in the perinuclear

area of the cells. Accumulation of autophagosomes could be due to upregulation of the autophagic pathway resulting in an increased amount of these structures because the cells are not able to clear them, or simply because the cells are failing to deliver the necessary hydrolases through fusion of autophagosome with the organelle devoted to degradation: the lysosome.

4 The autophagic pathway in relation to loss of the CLN3 protein

The CLN3 protein is a very hydrophobic, transmembrane protein of unknown function. Chapter 3 shows that CLN3 dysfunction creates endocytic and autophagic defects, implicating it in both these intimately associated pathways.

Accumulation of autophagic vacuoles has been noted in neurodegenerative diseases, including Alzheimer disease and Parkinson's disease, but their significance is not understood (Nixon, 2006; Rubinsztein et al., 2005).

The autophagic pathway provides a double-edged sword in that it can be a promoter of cell survival, used when the cells need to remove damaged organelles or require protection during a situation of starvation, but it can also promote cell death, perhaps when it is excessive. Whether autophagy protects from disease or causes disease is unclear (Shintani and Klionsky, 2004).

In all these diseases where an abnormal amount of autophagic structures have been reported, it is unclear whether this phenomenon is the result of increased autophagic activity or decreased autophagosome maturation for example due to problems with autophagosome/lysosome fusion(Settembre et al., 2008).

The autophagic pathway can be dissected into at least 4 key steps: induction of autophagy, formation of autophagosomal membrane and maturation of the new born organelle, docking and fusion with the lysosome and vesicle breakdown (Reggiori and Klionsky, 2002). Although autophagy remains poorly understood, this part of the study focussed on an attempt to locate which step of the pathway is affected when CLN3 function is defective. In particular, the microtubule- associated protein light chain 3 (LC3), the only marker available to label maturing autophagosomes in mammalian cells and the use of the electron microscopy were the tools extensively employed in this part of the analysis.

4.1 CLN3 and fusion of autophagosomes with lysosomes

While autophagosomes are forming they acquire the microtubule-associated protein light chain 3 (LC3) and during maturation they lose LC3 while acquiring the endosomal marker Lamp1 via fusion with the late endosomes and lysosomes. To assess if this fusion step is impaired in CLN3 deficient cells, the subcellular localization of Lamp1 was analyzed in conjunction with the autophagosomal marker LC3.

4.1.1 Autophagosome-lysosome fusion in JNCL 1kb patient skin fibroblasts

Human skin fibroblasts from controls and JNCL 1kb deletion patients were cultured for not more than 20 passages and labelled for indirect immunofluorescence with the lysosomal marker Lamp1 and the autophagosomal marker LC3.

Since in wild type human skin fibroblasts the autophagosome number is low due to a low level basal rate of autophagy in this cell type, the autophagic pathway was stimulated by amino acid deprivation using EBSS media for 2 hours at 37 °C to induce the formation of new autophagosomes.

The starved and non-starved cells were fixed and stained using LC3 and Lamp1 for the indirect immunofluorescence studies as shown in Figure 4.1.

As observed in chapter 3, only a few LC3 positive vesicles representing autophagosomes were present in the non-starved wild type cells, in contrast with the 1kb deficient non-starved JNCL cells where a conspicuous number of autophagosomes were evident in the cytoplasm of the cells (Figure 4.1, upper panel). In the control cells, maybe partly due to the low number of autophagosomes it was not possible to detect any colocalization between LC3 and Lamp1.

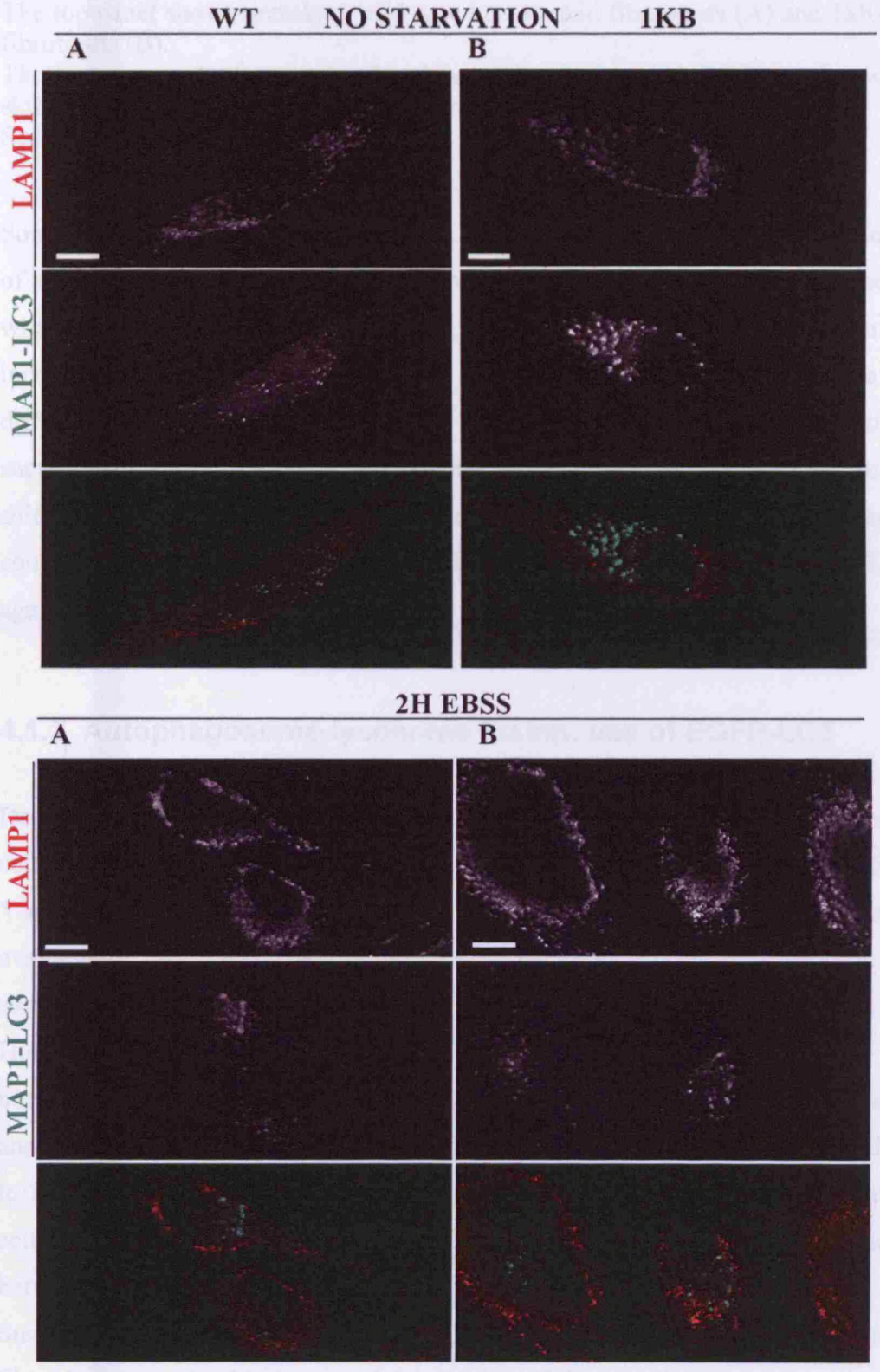

Figure 4.1 Immunofluorescence with LC3 and LAMP1 in human skin fibroblasts

The top panel shows untreated wild type human skin fibroblasts (A) and 1kb deletion fibroblasts (B).
The bottom panel shows cells after 2 hours incubation with EBSS media, wild type skin fibroblasts (A) and 1kb deletion fibroblasts (B).
Scale bar=10μm

Some of the cells were also grown for 2 hours in EBSS media to induce the formation of autophagosomes. In this case, the number of LC3 autophagosomes increases in the wild type cells but it was noted that the autophagosome number was markedly increased by starvation in the control cells, but starvation did not make such a difference to LC3-positive structures in the mutant cells. This was not quantified but suggests a state of starvation pre-existing in the mutant cells that is not so greatly shifted by amino acid deprivation, while the usual reaction to starvation occurred in control cells (Figure 4.1, lower panel). Colocalization between LAMP1 and LC3 was again, rarely seen.

4.1.2 Autophagosome-lysosome fusion: use of EGFP-LC3

Despite this, since LC3 is the only available marker to identify autophagosomes in cells we further attempted to use it. However unfortunately, the antibody from Dr. Yoshimori recognizing the endogenous form of the protein is not commercially available. It was limited in supply therefore we could not continue using it. Further studies were conducted using the overexpressed form of LC3.

Human skin fibroblasts were transfected with EGFP-LC3 using an Amaxa nucleofector device and analysed 24h later by indirect immunofluorescence. To analyze the autophagy pathway some of the cells were treated with EBSS media for 2h to induce the formation of new autophagosomes before fixation. After fixation the cells were stained with the lysosomal marker Lamp1 to analyze the association between autophagosomes and lysosomes.

Surprisingly the overexpression of LC3 in either mutant or control human skin fibroblasts considerably increased the number of the autophagosomes present (Figure 4.2) and therefore it was not possible to distinguish the same phenotype difference that

had been visible using endogenous LC3 (Figure 3.5, Chapter 3). With endogenous staining of LC3, a clear difference of the staining between wild type and mutant cells was seen; in the wild type cells the protein was visible almost entirely in the cytoplasm whereas in the mutant cells it was associated in organelles (Figure 3.5, Chapter 3). In these overexpressed cells no difference is apparent. Therefore the attempt to look direcly at autophagosome-lysosome fusion in this way was abandoned.

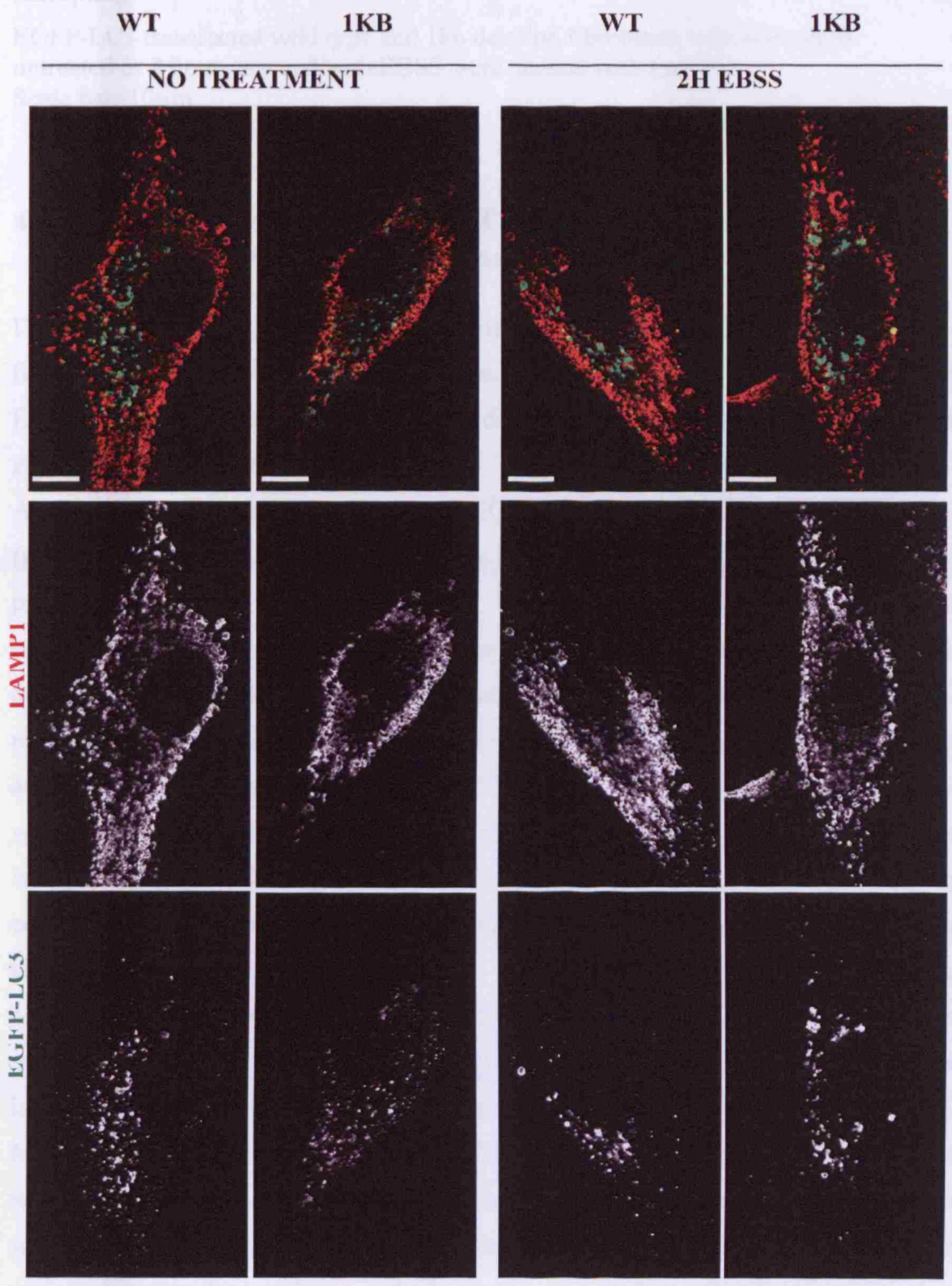
WT
1KB
WT
1KB
NO TREATMENT
2H EBSS
LAMP1
EGFP-LC3

Figure 4.2 EGFP-LC3 overexpression in human skin fibroblasts induced Autophagy.

EGFP-LC3 transfected wild type and 1kb deletion fibroblasts with starvation-untreated or 2 hours starved with EBSS were stained with Lamp1.
Scale bar=10μm

4.1.2.1 Overexpression of EGFP-LC3 in Cln3 mouse knock out primary embryonic fibroblasts

Due to the problem above, we next tried a third approach. Mouse embryonic fibroblasts (MEFs) were grown for not more than 4 passages and transfected with EGFP-LC3 using an Amaxa nucleofector device. 24 hours later cells were fixed and stained for immunofluorescence study.

As for the human skin fibroblasts, LC3-EGFP transfection in embryonic fibroblasts from either control or mutant mice notably increased the number of autophagosomes, preventing a clear distinction of the CLN3-associated expanded autophagic compartment phenotype that had been seen using the LC3 antibody for endogenous detection of the protein (Figure 4.3). The aim of this experiment was again the same, to analyse colocalization between LC3 and Lamp1 in order to investigate a putative autophagosome-lysosome fusion phenotype. In both wild type and knock out MEFs it was rare to see colocalization between the two markers but sometimes possible. More commonly, in the KO MEFs the two markers were in proximity without fully colocalizing (Figure 4.3, panel B and enlargement from the white square) suggesting that autophagosomes and lysosomes were getting close but prevented from fusing. MEFs were also starved for 2 hours with EBSS media to induce the formation of new autophagosomes (Figure 4.4). The induction of the formation of new organelles increased the number of the autophagosomes in the wild type cells whilst in the KO MEFs autophagosome number looked less altered but the size of the autophagosomes was markedly enlarged. In wild type and knock out the increase in autophagosomes was marked as a decrease in general cytoplasmic staining of LC3, and increase in vesicular perinuclear staining, which is the expected result of starvation. Any

difference in the level of colocalization between Lamp1 and LC3 was difficult to assess since this was rarely seen in either wild type or KO MEFs.

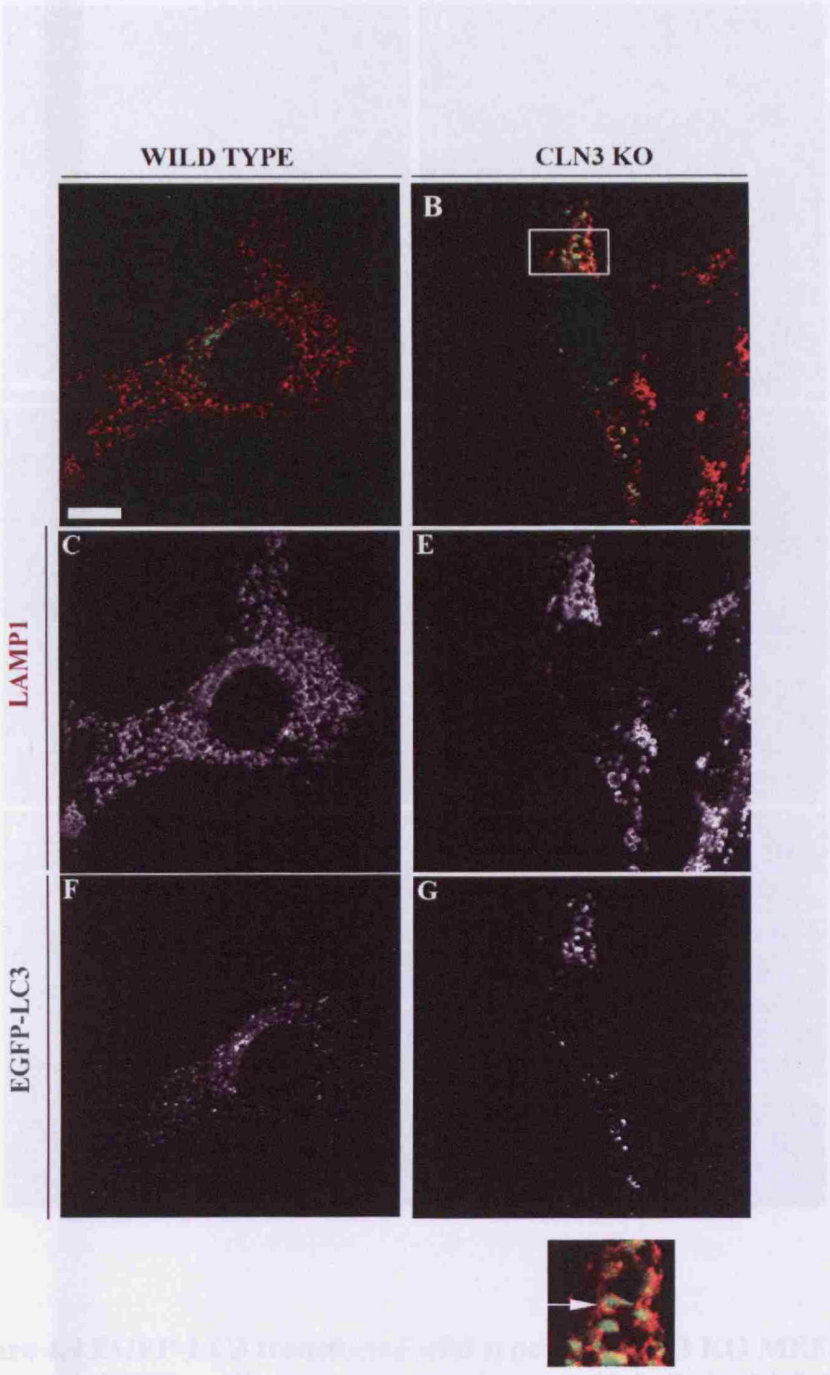

Figure 4.3 EGFP-LC3 transfected wild type and CLN3 KO MEFs labelled with LAMP1

Instert shows a magnification image from panel B. Scale bar=10μM

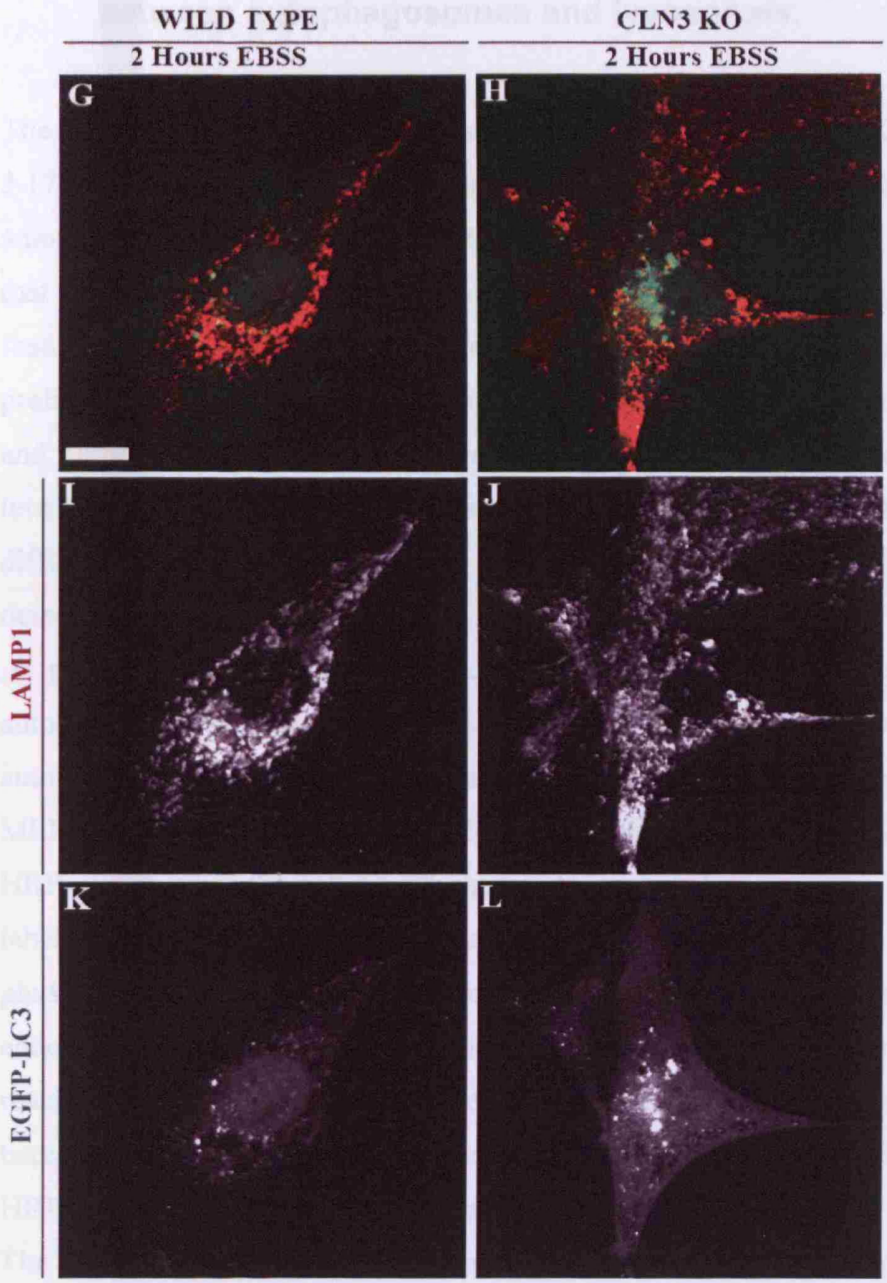

Figure 4.4 EGFP-LC3 transfected wild type and CLN3 KO MEFs starved for 2 hours with EBSS media to induce auophagy and labelled with LAMP1

EGFP-LC3 transfected mouse embryonic fibroblasts were starved for 2 hours in EBSS media to induce autophagy.
Scale bar=10μM

4.1.3 Autophagosomes in CLN3 KO MEFs have a fusion defect between autophagosomes and lysosomes.

The accumulation of subunit c positive structures in the CLN3 KO MEFs (Figure 3.17) under nonstarved conditions coupled with the increased size of the autophagosomes in starved CLN3-deficient cells compared to non starved suggested that the autophagic structures accumulate as a result of an autophagosome/lysosomal fusion impairment that leads to a failure in their clearance. We tried to look at this problem by the analysis of colocalization between the autophagosomal marker LC3 and Lamp1. However, this did not allow us to an answer to this question due to high levels of LC3 positive structures after its overexpression and the subsequent difficulties in resolving individual organelles plus the lack of an antibody which detects the endogenous protein.

A new approach was therefore adopted to assess if the interaction between the autophagic pathway and the endocytic is impaired when CLN3 is deficient. Since autophagosomes and lysosomes are connected through fusion events, WT and KO MEFs were incubated for one hour in the presence of 4mg/ml of the fluid phase tracer HRP, dissolved in the cell growth media. This incubation time was selected to ensure labelling of the whole endocytic pathway. Normally, HRP enters the cell via fluid phase endocytosis reaching endocytic structures, filling the internal lumen of endosomes, late endosomes and lysosomes. The early endosomes are normally reached by HRP after a few minutes, and the late endosomes begin to receive HRP between 10 to 15 minutes after the cells are exposed to the tracer. After 30 minutes the HRP reaches the lysosomes (Tooze and Hollinshead, 1992).

The cells were then fixed and incubated with diaminobenzidine and hydrogen peroxide to reveal the location of the HRP, postfixed and processed for electron microscopy. By electron microscopy HRP has a characteristic and distinct floccular aspect (Figure 4.5).

In the WT MEFs, after fluid phase endocytosis and HRP uptake had occurred, the tracer was found to fill the early endosomes, late endosomes and lysosomes as expected (Figure 4.5). In the CLN3 MEFs the HRP also reached these organelles but it

did not reach any of the aberrant autophagic organelles present in the mutant fibroblasts (Figure 4.6).

Therefore, the CLN3 KO cells were able to uptake the HRP by fluid phase endocyosis, but the HRP did not access those organelles that were previously identified as positive for subunit c. This suggested a delay in delivery to autophagosomes, or absence of fusion between autophagosomes and lysosomes. In particular some HRP-negative aberrant- autophagic structures in CLN3 KO MEFs were observed to be in very close proximity to HRP-positive endosomes, emphasising the hypothesis that fusion between the autophagic and endocytic pathways was not occurring efficiently (Figure 4.6, panel A, C and F).

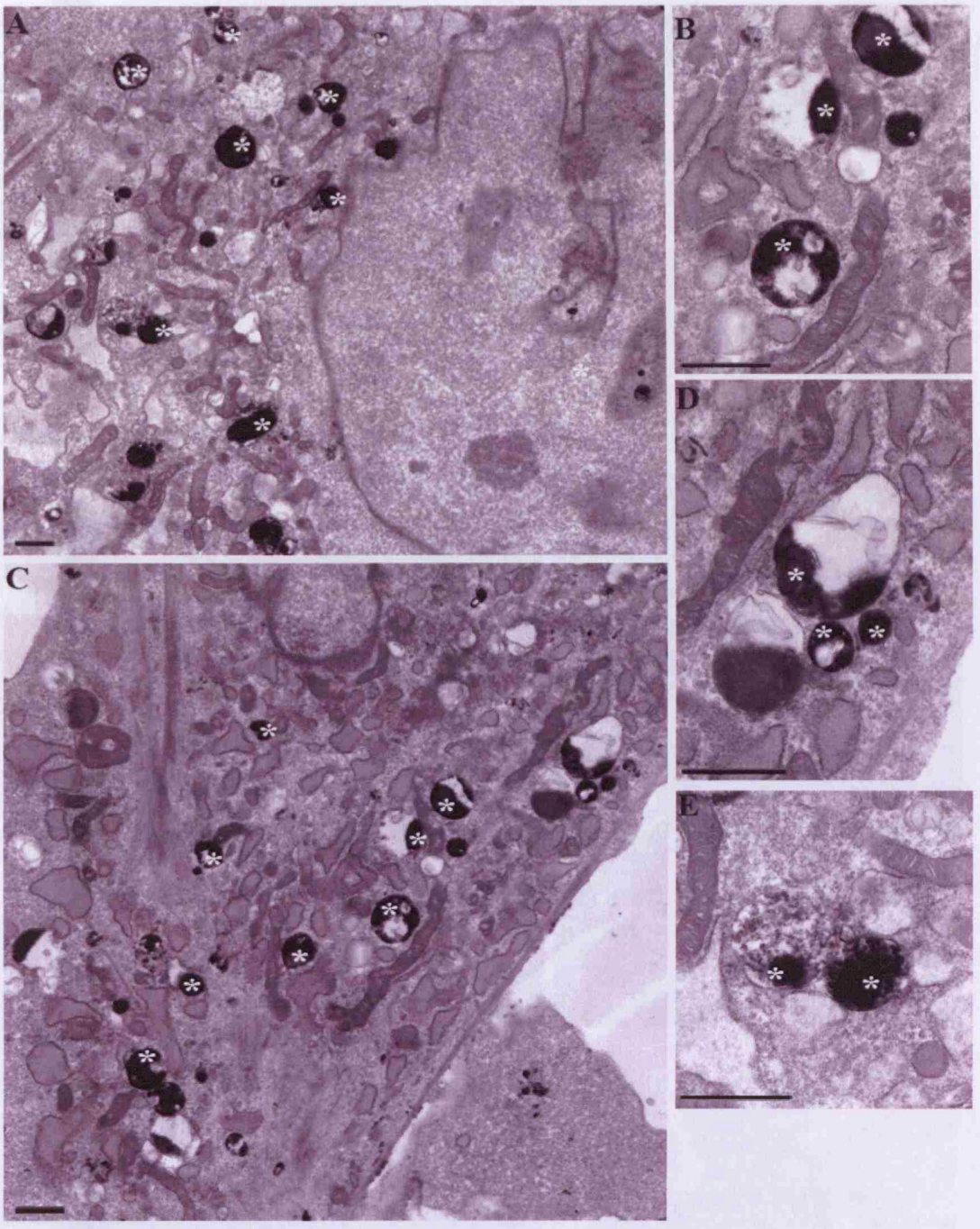

Figure 4.5 HRP feeding in wild type MEFs indicates HRP positive endosomes

* indicates positive endosomes for HRP. These are recognisable by their floccular aspect.

Scale bar=500 nM

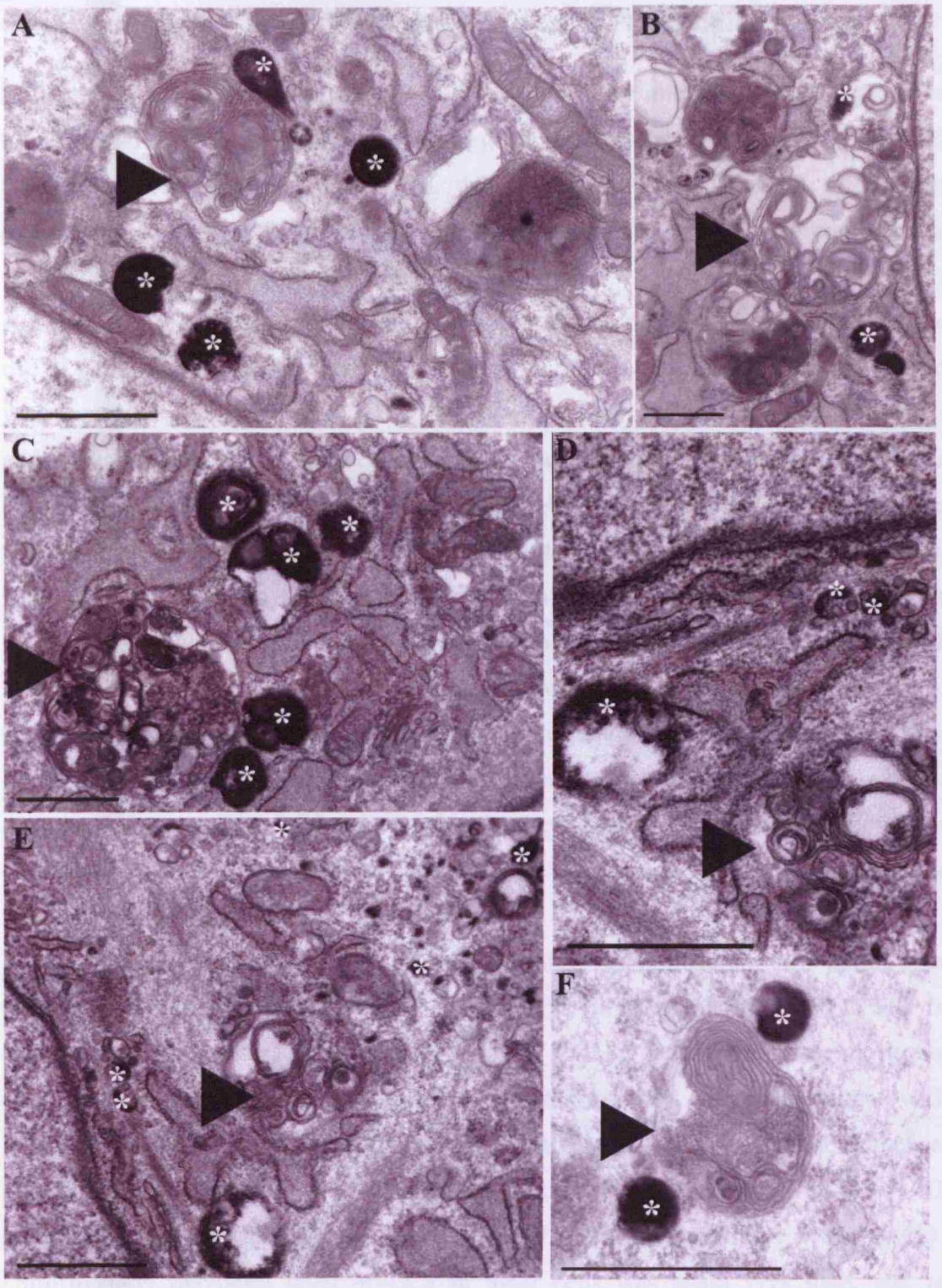

Figure 4.6 CLN3 KO Fibroblasts fed with HRP

*indicates HRP positive endosomes
Arrows heads indicate HRP negative autophagosomes. scale bar=500μm

4.1.4 Autophagy after CLN3 knock down in HeLa cells

Since the levels of over-expression of LC3 in both mice and human fibroblasts was highly variable, and the number of autophagosomes was clearly increased in the wild type cells after LC3 was transfected, these technical issues made it difficult to distinguish a robust difference in the autophagy phenotype between the control cells versus the mutant cells at the light level.

An alternative approach towards the use of mutant fibroblasts was attempted by the use of gene-silencing oligos against CLN3 in HeLa cells. HeLa cells were transfected with two rounds of small interfering RNAs (siRNA) against human CLN3 (materials and methods, Chapter 2). HeLa cells were also transfected with scrambled siRNA as a control. 24 hours after the second round of siRNA transfection cells were fixed and prepared for immunofluorescense studies. Quantification of the CLN3 knock down was obtained for all the experiments shown in this and other sections using real time PCR. In all siRNA experiments >90% knock down of CLN3 mRNA was confirmed. Analysis of the cells by confocol microscopy showed that overexpression of LC3 in this system again induced a large increase of the autophagic compartment in cells. However the level of autophagy was high in HeLa control cells and also the number of the punctae representing LC3 was variable from cell to cell. Since the expression level of LC3 was not uniform between cells this made it too complicated to compare the mock and CLN3 siRNA autophagic structures.

The expression level of LC3 in HeLa cells was observed at different time points after transfection but the level of expression was always very variable from cell to cell. In an attempt to standardize the expression level of LC3 in order to compare mock and CLN3 siRNA cells, a HeLa cell line stably expressing the LC3 protein tagged with EGFP was obtained from the Tolkovsky lab (University of Cambridge) (Bampton et al., 2005). The stable HeLa LC3-overexpressing cells were transfected with the CLN3 siRNA or scrambled siRNA and analysed, by immunofluorescence study. Unfortunately the basal level of LC3 in these cells was again very high, and in addition the levels of LC3 was very variable in different cells in the same culture.

Therefore, for similar reasons as the transient transfected cells system, the LC3 expressing stably cells were not a good model to study the maturation of the autophagy pathway and their use was abandoned.

Another HeLa cell line was obtained from the Tolkovsky group expressing both LC3-EGFP and dsRed-mito, a plasmid which labels mitochondria (Bampton et al., 2005). Damaged or old mitochondria are removed by autophagic process of mitophagy such that mitochondrial fragments can be detected in the degradative compartment. In this LC3-EGFP dsRed-mito cell line, dsRed-Mito has been shown in part to colocalize with LC3-EGFP after induction of autophagy (Bampton et al., 2005). We used this to investigate whether the removal of mitochondria by autophagy occurs in these cells after CLN3 knock down. LC3 and dsRed-Mito double stably expressing HeLa cells were transfected with CLN3 siRNA or control siRNA and fixed, 24 hours after the second round of transfection, the processed for indirect immunofluorescence. Some cells were treated for 2 hours with EBSS to induce newly formed autophagosomes by starvation (Figure 4.7). In normal growth conditions the LC3 level was variable from cell to cell as expected from the above reported work; however more LC3 positive punctae were generally seen after CLN3 knock down (bottom left Figure 4.7 left panels). Rare colocalization of ds-Red Mito and LC3 was ascertained in both mock and CLN3 depleted cells. Upon induction of starvation, overlap was more often detected between the mitochondrial marker and LC3 in both mock and CLN3 siRNA depleted cells. No gross difference in this change to staining was detected between control and siRNA treated cells. This therefore suggests that CLN3 knock down cells were able to react after starvation to form new autophagosomes enclosing mitochondria. Since there was no obvious difference between wild type and CLN3 knock down cells, we did not pursue this system further, despite not being able to determine whether this is a real co-localization or just an overlap was present.

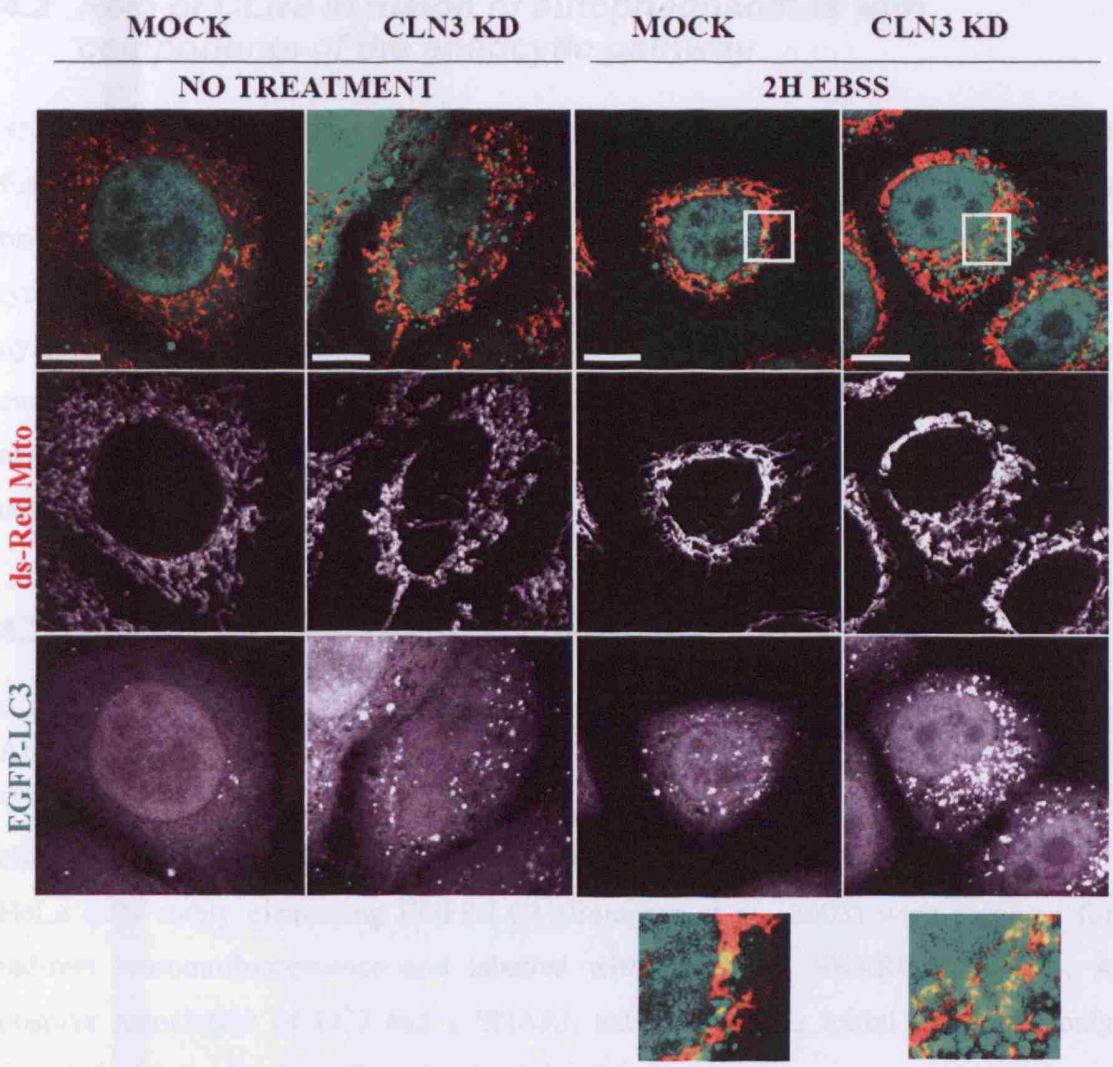

Figure 4.7 LC3-EGFP and ds-Red Mito double stably HeLa expressing cells transfected with scrambled siRNA and CLN3 siRNA

CLN3 siRNA and scrambled siRNA transfected were observed after no treatment or after 2 hours of starvation induced autophagy by culture in EBSS media. Insert shows a blow up of the indicated areas in the top panel.
Scale bar=10μm

4.2 Role of CLN3 in fusion of autophagosomes with components of the endocytic pathway

SNARE proteins are integral parts of the machinery required for recognition and fusion between membranes (Chen and Scheller, 2001). SNAREs form complexes bridging the gaps between membranes to facilitate fusion. The fusion between lysosomes and autophagosomes had been highlighted as of interest for CLN3 dysfunction so a study was made to discover if SNARE proteins present in the endocytic compartment could be identified as part of the autophagic pathway and used as tools to dissect the putative defective endocytic-autophagic fusion events in CLN3 deficient cells.

4.2.1 The Syntaxin 8 SNARE is present in maturing autophagosomes

Andrew Peden, (University of Cambridge) provided SNARE antibodies including VAMP7, VAMP8, Syntaxin 7, Syntaxin8 and VT1b (Luzio et al., 2007). These were chosen for their reported localization and role in the endocytic compartment.

HeLa cells stably expressing EGFP-LC3 (Bampton et al., 2005) were prepared for indirect immunofluorescence and labelled with individual SNARE antibodies. A positive association of LC3 and a SNARE antibody in this initial study was only detected with the Syntaxin 8 marker (not shown).

Syntaxin 8 is present in late endosomes and lysosomes and it mediates both homotypic late endosome fusion and late endosome/lysosome heterotypic fusion (Pryor et al., 2004). It forms a complex with Vt1b, syntaxin 7 and endobrevin (Antonin et al., 2000).

Since Syntaxin 8 is localized in the late endosomes and lysosomes and sometimes colocalizes with the lysosomal protein Lamp1, triple staining of Lamp1, LC3 and Syntaxin 8 was performed to analyze if the association with LC3 and Syntaxin 8 takes place after the autophagosomes are fused with the lysosomes.

HeLa cells stably expressing LC3 were fixed and labelled with Lamp1 and Syntaxin 8 (Figure 4.8).

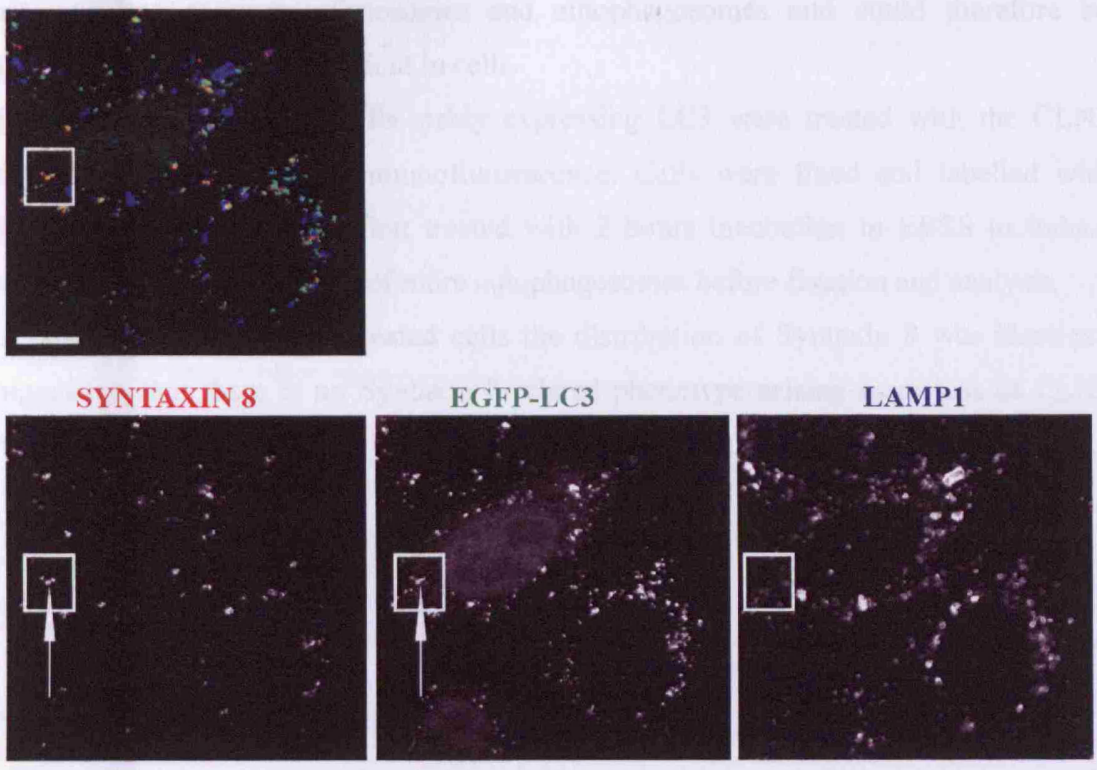

Figure 4.8 The SNARE protein Syntaxin 8 is associated with maturing autophagosomes.

LC3 stable expressing HeLa cells were fixed and labelled with the late endosomal/lysosomal marker Lamp1 and the SNARE antibody Syntaxin 8. The white box and arrow highlight a LC3 and Syntaxin 8 puncta co-staining representing a maturing autophagosome which it is not postive for Lamp1.
Scale bar=10μm

The immunofluorescence analysis showed that the SNARE protein Syntaxin 8 is present in the late endosomes, lysosomes as has been described previously (Pryor et al., 2004). In addition, Syntaxin 8 was sometimes observed in autophagic structures by colocalization with LC3 and sometimes no Lamp1 was observed in the same puncta (Figure 4.8, box).

Vt1b is specifically required for the stability of the Syntaxin 8 protein (Atlashkin et al., 2003). In Vti1b knock out mice, Syntaxin 8 is degraded and the mice present with an accumulation of autophagic structures in hepatocytes. This suggests a possible role for Syntaxin 8 in the autophagic pathway. Since Syntaxin 8 was associated with autophagosomes, we hypothesised that Syntaxin 8 could possibly have a role in fusion

between late endosomes/lysosomes and autophagosomes and could therefore be affected when CLN3 is deficient in cells.

To address this question cells stably expressing LC3 were treated with the CLN3 siRNA and prepared for immunofluorescence. Cells were fixed and labelled with Syntaxin 8 and Lamp1 or first treated with 2 hours incubation in EBSS to induce starvation and the formation of more autophagosomes before fixation and analysis.

In both mock and siRNA treated cells the distribution of Syntaxin 8 was identical, suggesting that there is no Syntaxin 8 related phenotype arising from loss of CLN3 function (Figure 4.9).

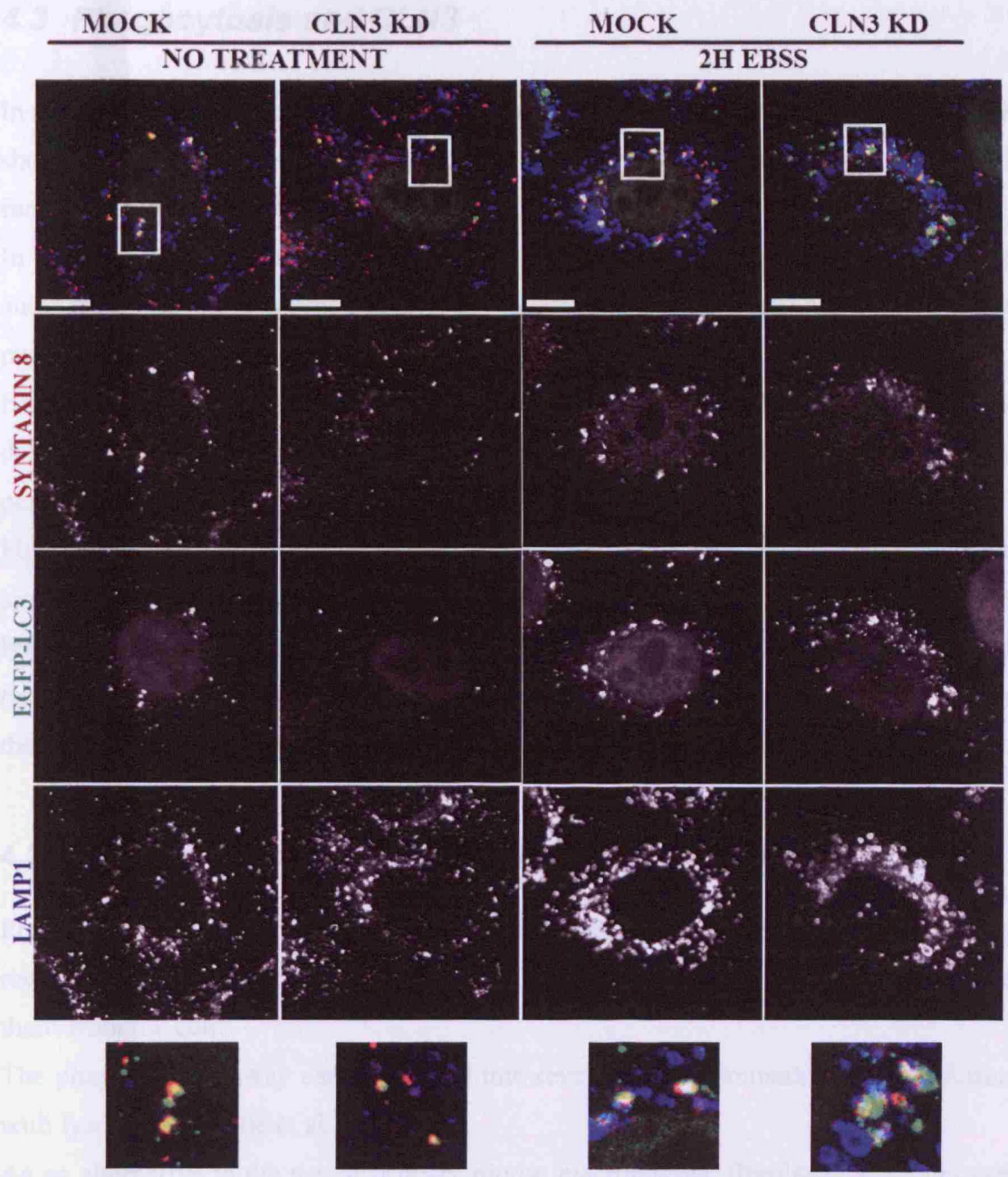

Figure 4.9 The Syntaxin 8 protein is not affected by CLN3 siRNA

EGFP-LC3 stably expressing HeLa cells were transfected with control and CLN3 siRNA. Some cells were treated for 2 hours with EBSS media to induce the formation of new autophagosomes. The boxes highlight autophagosomes puncta.
Scale bar=10μM

4.3 Phagocytosis and CLN3

In CLN3 deficient cells, the number of autophagosomes is increased and here we have shown that autophagosomal maturation may be arrested or delayed due to impaired fusion of lysosomes with autophagosomes.

In light of the multiple technical difficulties we encountered with a detailed analysis of autophagy a different approach was made to examine a cellular pathway related to but potentially more easily studied than autophagy.

For an alternative assessement of wether a lysosome fusion is defective when CLN3 is deficient, an analysis of the effect on phagoctytosis of CLN3 deficiency was performed.

Phagosomes, like autophagosomes, undergo a process of maturation which includes similarly contacts with the endo-lysosomal system and culminates in fusion with lysosomes (Tjelle et al., 2000) (Vieira et al., 2002). Importantly, fusion with lysosomes is an essential step for both phagosomes and autophagosomes which thereby receive the hydrolases necessary for the degradation of their content.

4.3.1 CLN3 KO MEFs are able to phagocytose latex beads

Professional phagocytic cells, such as macrophages, recognize pathogens via specific receptors and then employ the phagocytic pathway in order to digest and eliminate them from the cell.

The phagocytic pathway can be divided into several steps culminating with the fusion with lysosomes (Tjelle et al., 2000).

As an alternative to the use of primary mouse macrophages, fibroblasts cell lines can be used to analyse phagocytosis. These are transfected with phagocytic receptors to obtain 'engineered phagocytes' (Huynh et al., 2007) with the capacity to recognize and internalize an opsonised host. CLN3 KO and WT MEFs were transfected with the FcIIλ receptor (referred to here as FcR) (Caron and Hall, 1998) and after 24 hours were fed with 3 μM latex beads, added directly in the medium of the cells, previously opsonized with human IgG. The beads were allowed to internalize for 30 minutes at

37 C° after a brief centrifugation of the cells with the beads to first allow the beads to attach at the PM and synchronize phagocytosis. Cell were then stained with anti human IgG 480 secondary antibody, then fixed and stained with anti human IgG secondary antibody to detect the presence of the beads.
Importantly, FcR-transfected CLN3 KO MEFs were able to internalize opsonized beads (Figure 4.10).

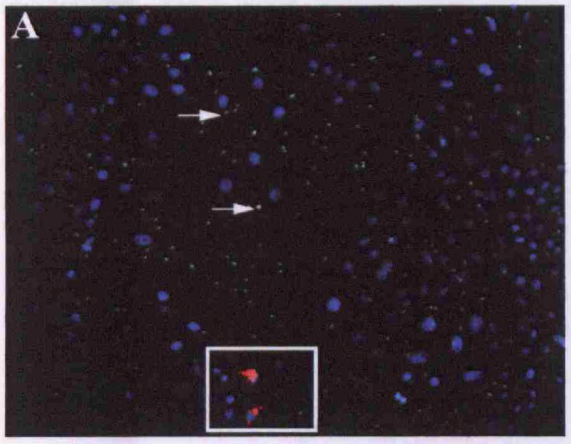

Figure 4.10 CLN3 KO MEFs are able to internalize opsonized latex beads

Cells were transfected with FcR and 24 hours later were fed with latex beads for 1 hour. Cells were fed with latex beads for 1 hour and stained with secondary antibody anti 480 IgG to label external beads, then fixed and stained with anti 680 IgG secondary antibody to label all the beads.
The white square includes two cells which have been internalized the beads.
Nuclei were stained with DAPI. White arrows indicate external beads.
Axioscop picture, magnification 20X.

4.3.2 In CLN3 deficient fibroblasts the fusion between phagosomes and endosomes is impaired

To measure and compare phagosome-lysosome fusion in transfected FcR expressing MEFs, both WT and CLN3 KO cells were transfected with the FcR construct using an Amaxa nucleofactor device. After 24 hours cells were exposed to previously human IgG-opsonized 3 μm latex beads. To synchronize phagocytosis, cells with the beads were briefly spun down.

The phagosomes were allowed one hour at 37 °C to mature and cells were brought to 4 °C and incubated with anti human IgG secondary antibody to label all the external beads. Subsequently, cells were fixed and stained with Lamp1 to assess if the phagosomes were able to fuse with lysosomes. Both WT and CLN3 KO cells were analysed by confocal microscopy and >100 internal beads were counted.

In both WT and CLN3 KO MEFs, many beads were internalized but in CLN3 deficient cells fewer internal beads were positive for Lamp1 (Figure 4.11). The internalized beads were divided into Lamp1 positive and Lamp1 negative (Table 4.1).

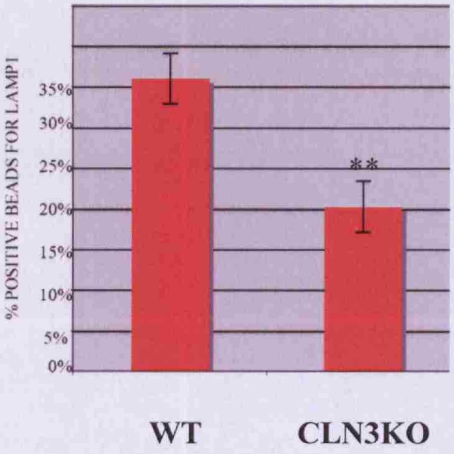

Table 4-1 Quantitation of phagosomes which undergo fusion with lysosomes as seen by Lamp1 labelling

Quantitation of the fraction of phagosomes positive for the endocytic marker Lamp1. WT and KO MEFs transfected with FcR after 24 hours were fed for 1 hour with latex beads and then prepared for immunofluorescence studies. Data are means ± SD of three experiments with ≥100 internalized phagosomes from ≥ 20 cells. Error bars represent standard errors; p=0.002.

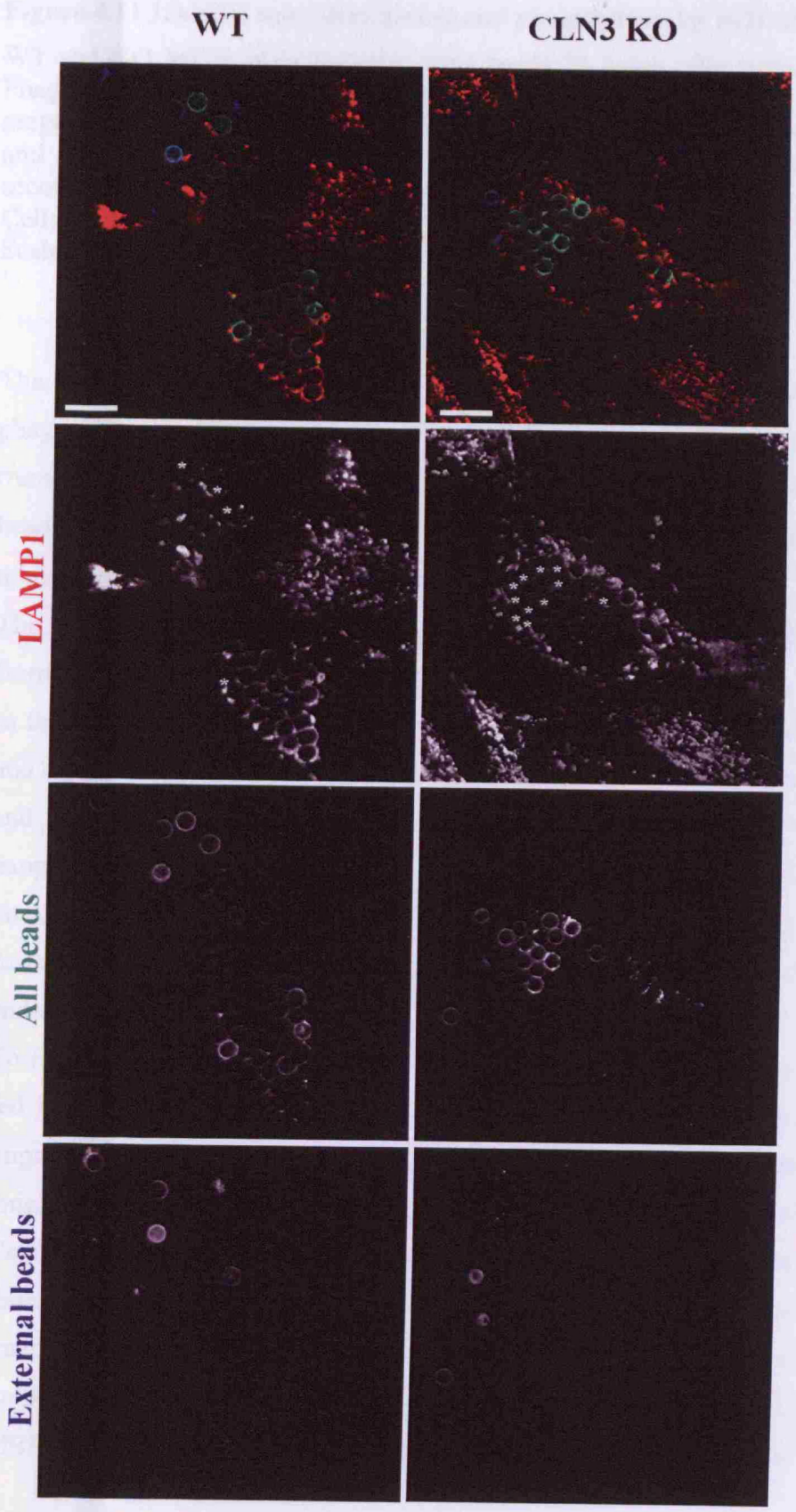
WT
CLN3 KO
LAMP1
All beads
External beads

Figure 4.11 LAMP1 immunostaining and phagocytosis by FcR transfected MEFs

WT and KO MEFs were fed with latex beads 24 hours after transfection with FcR. Phagosome maturation was allowed to proceed for 60 minutes. Cells were then prepared for indirect immunofluorescence studies. External beads were stained with anti IgG 680 secondary antibody (far red), all beads were stained with anti 488 IgG secondary antibody (green).
Cells were also stained with Lamp1 (594 anti rat secondary antibody used- red).
Scale bar=10μm

The proposed failure in proper lysosome fusion and recruitment of LAMP1 to phagosome membranes was then investigated at the ultrastructural level; FcR transfected WT and CLN3 KO MEFs were allowed to internalize opsonized latex beads for 1 hour at 37 °C and then immediately fixed and embedded for electron microscopy study.

The analysis by EM shows a very striking difference between the beads internalized from the WT cells versus the CLN3 KO cells (Figure 4.12).

In the WT cells, all the latex beads analysed were surrounded by a smooth membrane and occasionally a few vesicles were observed in between the phagosomal membrane and the latex bead, suggesting that a fusion event with the endocytic pathway had happened. In contrast, in the KO cells, between the phagosomal membrane and the latex bead, membraneous structures were accumulated, suggesting that perhaps, a fusion event had happened, presumably involving early endosomes and multivesicular endosomes, but that phagosomal maturation was arrested at this stage.

To further analyse fusion events of phagosome with the endocytic pathway, HRP was fed into cells to label late endosomes/lysosomes and to confirm the presence of an impairment in fusion between the endocytic pathway and the phagosomes.

4mg/ml of HRP was added to the media of MEFs previously transfected with FcR. Cells were incubated in HRP for 90 minutes, after which cells were washed several times and the HRP media was substituted with fresh media for 5 hours to allow the tracer to arrive to the lysosomes and to clean from early endocytic structures.

Subsequently, opsonized latex beads were exposed to the cells and after 1 hour the MEFs were fixed and processed for EM analysis. The distribution of HRP along the

surface of the bead indicates fusion. The retention of HRP within vesicles trapped against the surface of beads shows a strikingly different phenotype.

The beads (≥100) were counted (

Table **4-2**).

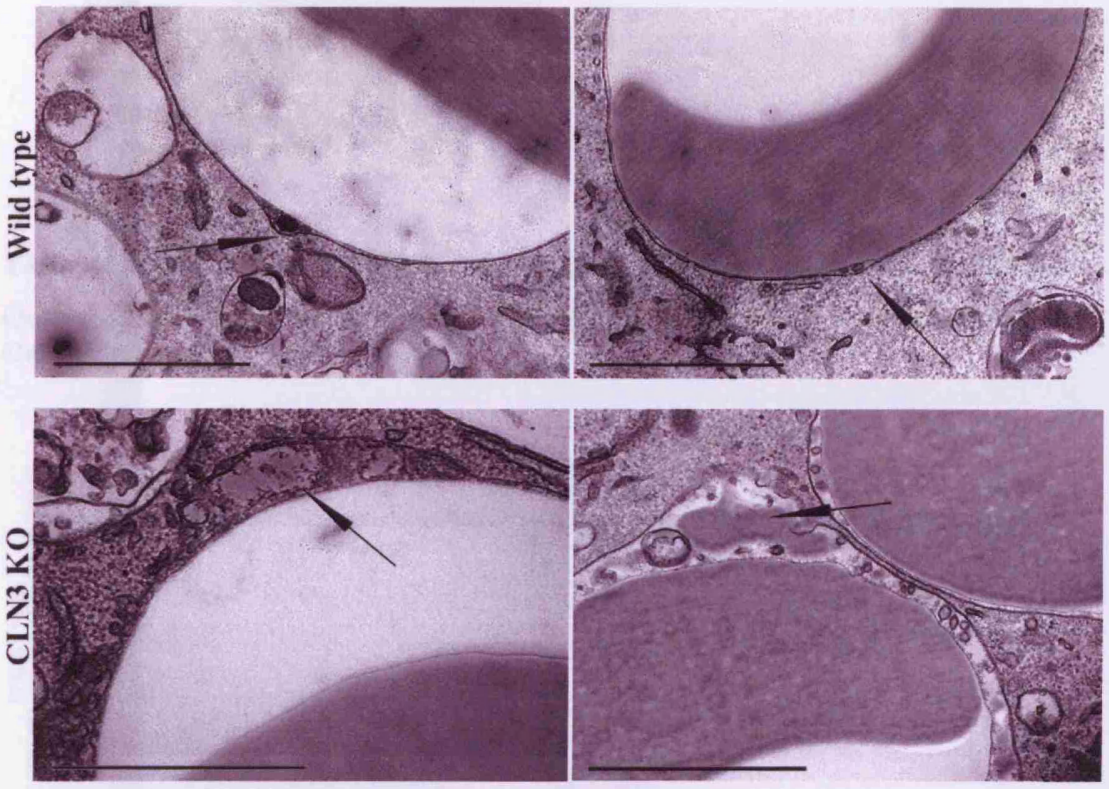

Figure 4.12 EM characterization of phagosomes from FcR transfected MEFs

Fc receptor transfected WT and CLN3 KO MEFs were fed for 1 hour with latex beads after 24 hours after transfection and then processed for electron microscopy study.
In wild type MEFs a representative image show that a fusion event of phagosome with early and perhaps late endosomes happened as suggested by vesicles visualized in between the phagosomal membrane and the bead (arrow). In the KO MEFs complex membraneous structures were instead observed in between the phagosome and the bead (arrow)
Scale bar=1μm

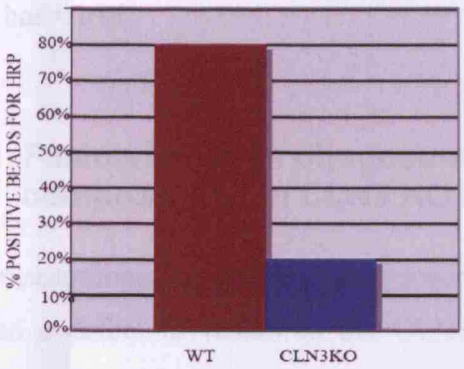

Table 4-2 Quantitation of HRP positive latex beads in FcR transfected MEFs

Quantitation of the fraction of phagosomes postive for the endocytic tracer HRP. Data are means of ≥100 phagosomes.

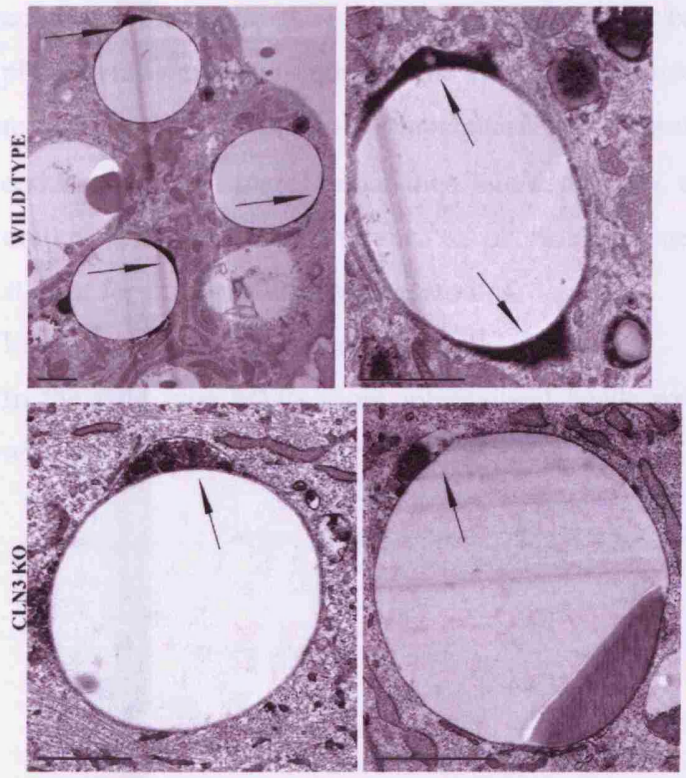

Figure 4.13 Wild type and CLN3 KO MEFs transfected with Fc receptor, fed with HRP and latex beads

Fc receptor transfected MEFs were fed with HRP for 90 minutes, chased for 5 hours and fed with latex beads for 1h. HRP is present in between the phagocytic membrane and the bead in the wild type cells (arrow). In the KO cells, in between the phagocytic membrane and the bead no HRP was present (arrow).
Scale bar=1μM

4.3.3 Fusion between phagosomes and early endosomes is also compromised in CLN3 KO MEFs

The measurement of phagosome-lysosome fusion in Fc receptor transfected MEFs showed a defect in fusion in the CLN3 KO cells. Before fusing with lysosomes, phagocytic vacuoles interact with both early and late endosomes. To determine at which stage the maturation is arrested, the early endosomal marker EEA1 was used to assess if an earlier stage of fusion between autophagosomes and endocytic pathway is also impaired.

WT and KO MEFs were transfected with FcR and 24 hours later latex beads were added to the cells, then beads and cells were briefly spun down to syncronize phagocytosis and subsequently the cells were allowed to internalize the beads for 15 minutes at 37C°. The shorter incubation time meant the majority of beads are at the endosome fusion stage, rather then late endosome, and therefore still retain the early marker EEA1 on the membrane. As previously done for Lamp1, cells were fixed and stained for immunofluorescence studies.

Internalized latex beads were counted (<100).

In the wild type MEFs more internalized beads were positive for EEA1 in contrast with the ones internalized by the CLN3 KO MEFs (Table 4-3).

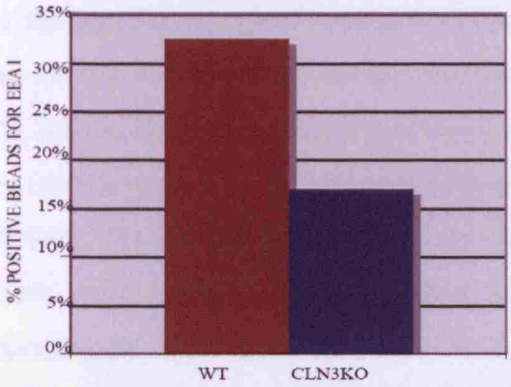

Table 4-3 Quantitation of phagosomes undergoing fusion with early endosomes

Quantitation of a fraction of phagosomes positive for the endocytic marker EEA1. Data represent ≥100 internalized beads from ≥ 20 cells.

4.4 Discussion

At the beginning of our preliminary survey an increased number of autophagosomes were observed in cells deficient for CLN3 as summarised in chapter 3.

Lysosomal storage diseases are caused by over 40 different genes and clinically they affect different organs but most often they cause severe damage to the nervous system (Neufeld, 1991). In the past three years the involvement of autophagy in lysosomal storage disorders and neurodegenerative disorders has became clearer. For example, accumulation of autophagosomes (AVs) has been reported in Batten disease caused by deficiency in cathepsin D (Koike et al., 2005) and Mucopolysaccharidosis (Settembre et al., 2007). We found in CLN3 deficient fibroblasts and neurons that autophagosomes accumulate. During the course of this work another group published related findings for CLN3 (Cao et al., 2006). We attempted to verify if the accumulation of autophagosomes was due to reduced clearance after their formation and maturation due to an absence of fusion between lysosomes and autophagosomes. In different neurodegerative conditions, such as Alzheimer disease (Nixon et al., 2005)

and Huntington disease (Rubinsztein et al., 2005), the hypothesis of defective fusion between lysosomes and autophagosomes has been reported but none of these studies conducted so far suggested a good approach to establish if this hypothesis is true. At the beginning of our study, to follow the maturation of autophagosomes in CLN3 deficient cells, a light microscopy approach was taken, using LC3 in conjunction with the lysosomal marker Lamp1, to visualize if LC3 and LAMP1 could meet or not when CLN3 is deficient. The level of LC3 in non starved wild type cells is low whereas in CLN3 deficient cells the level is higher but no colocalization with Lamp1 was detected supposing possible autophagosome maturation defect. After starvation the level of LC3 increased in both wild type and mutant cells, but the localization with Lamp1 was hardly seen, probably due to the fact that LC3 is getting rapidly degraded while the autophagosomes are maturing at the same time as Lamp1 is being acquired via endocytic fusion events. In CLN3 deficient cells after starvation, the LC3-positive autophagosomes became bigger than those in both unstarved mutant cells and starved wild type cells, indicating a defect in their maturation was likely. Starvation conditions did not have such as a dramatic effect on mutant versus wild type cells, suggesting the CLN3 deficient cells are already effectively started.

To assess the autophagic pathway in a more detailed and quantitative manner, we required an LC3 antibody to detect the endogenous protein unfortunately. Not enough of this was available to finish this part of the study to detect a fusion defect at the light level.

An increase in the number of autophagosomal membranes was demonstrated by both light microscopy and electron microscopy but the use of the EGFP-LC3 construct employed in this chapter instead of the endogenous antibody complicated the phenotype. This is because the overexpression of LC3 in fibroblasts drastically increased the basal number of autophagic vacuoles in cells, thereby removing any clear cut difference in LC3 levels by introduction of either CLN3 or starvation.

For this reason electron microscopy was employed for the visualization of the autophagic structures.

To label the structures at the ultrastructural level and determine if a connection with the endocytic pathway was impaired, a fluid phase marker of the endocytic pathway,

HRP was employed. The fluid phase marker reached the endosomes and lysosomes in both wild type and knock out cells but not the expanded autophagic compartment on KO cells. This indicates that the endocytic pathway to the lysosomes is unaffected by CLN3 dysfunction but there is a clear block in the communication between endocytic and autophagic pathways due to CLN3 deficiency.

These are the first reported findings that can confirm morphologically that an increase in the number of autophagic structures found in the lysosomal disease JNCL is related to a defect in fusion between autophagosomes and lysosomes.

The study by Cao et al., published during this work suggested that distruption at the level of autophagosomal maturation was likely, but they showed a reduction of LC3 positive structures in their CLN3 deficient cerebellar cell line and reduced endocytosis in addition to loss overlap on endocytic tracer and lysotracker.

Poor information is available on the machinery involved in fusion of autophagosomes with lysosomes and what mechanisms are used by the cells to exert these events. For this reason a survey of the SNARES, so far reported to be involved in heterotypic and homotypic fusion between endosomes/lysosomes, was carried out. Interestingly a SNARE, Syntaxin 8 reported to be important for late endosomes homotypic fusion and heterotypic late endosomes/lysosome fusion (Luzio et al., 2007) was found to colocalize with LC3 after overexpression of LC3-EGFP. This result could be potentially interesting for a more detailed analysis of this SNARE and its involvement in the autophagic pathway. No difference with the syntaxin 8 antibody was noticed after CLN3 silencing in conjunction with LC3 expression in HeLa cells and for this reason no more work on the syntaxin 8 marker was attempted. We encountered significant problems using LC3 overexpression to analyse autophagy. This was due not only to its effect in increasing the basal level of autophagy in transfected cells such that altered autophagy levels were masked, as compared staining of LC3 using the endogenous antibody. In addition, the heterogeneity of the level of LC3 expression between transfected cells, in transfection experiments prevented reproducible results.

The study of defects in autophagy and fusion events with autophagosomes and lysosomes related to CLN3 deficiency has been a challenging project since induction,

regulation and mechanisms with in the autophagic pathway are still not well understood.

It would be of interest, not only for CLN3 but also for other lysosomal storage diseases and neurodegenerative diseases, to continue this research into the autophagic pathway in Batten disease, carrying out studies on the relationship between autophagosomes and the endocytic pathway. Electron microscopy remains the best technique to visualize and differentiate the autophagosomes from lysosomes before they have met, due to the paucity of markers able to classify just the autophagosomes.
The two pathways, autophagic and endocytic, are physically well connected in cells and it is a high priority to discover the molecules involved that they share.
It will be hard to continue analysis of CLN3 and its role in both endocytic and autophagic pathways without more basic information about the molecular mechanism underlying autophagy.

4.4.1 Delay in recruitment of endocytic markers to phagosomes in CLN3 deficient cells

Since so little is known about the autophagic pathway and no easy assay of autophagic function is available, we decided to approach function of CLN3 in the endocytic pathway via the phagocytic pathway, which presumably share essentially the same fusion steps with the lysosome as the autophagic pathway.
Since in autophagy the fusion event between lysosomes and autophagosomes is impaired by loss of CLN3, we hypothesed that phagosome-lysosome fusion events could also be malfunctioning in CLN3 deficient cells.
Phagocytosis involves different steps of vesicular maturation which include a kiss and run or fusion event with endosomes and conclude with a fusion step with the lysosome (Vieira et al., 2002). The latter is a fundamental step to bestow lytic properties to the phagosomes. In view of the fact that phagocytic fusion events result in the delivery to phagosomes of membrane proteins such as Lamp1 and EEA1, we tested the possibility of an impairment of the endocytic and phagocytic pathway using those markers. We showed that the recruitment of endocytic markers to phagosomes is defective or

delayed in CLN3 deficient cells. These experiments indicated that loss of CLN3 function results in a delay in recruitment of endocytic markers to phagosomes. However these experiments did not indicate the exact time point of the delay since in our protocol, the beads were fed continuously and the analysis carried out without a chase. Since a proportion of beads remained stuck at the PM even after repeated washes, this prevented the possibility of a meaningful chase.

A similar phenotype has been observed in Lamp1/Lamp2 deficient MEFs, where cells prepared for the same experiment presented membranous accumulation between phagosomal membrane and the phagosomes suggesting a defect in phagosomal maturation i.e., the possibility of a fusion event with a MVB but not with lysosomes (Huynh et al., 2007).

The autophagic and phagocytic pathways are distinct and separate processes but both are defective when CLN3 is deficient. This is suggestived a general impairment in fusion events at the lysosomal level resulting from lack of CLN3 function.

5 Mannose 6 phosphate receptor distribution in CLN3 deficient cells

The morphological analysis of cells deficient for the CLN3 protein showed an aberrant accumulation of material in membrane-bound organelles, likely to be of autophagosomal origin, indicating a defect in the degradation of their content. Lysosomes and autophagosomes require lysosomal hydrolases to perform their degradative function.

The aim of the work presented in this chapter was to determine if impaired recruitment of the hydrolases from the Trans Golgi Network (TGN) to the lysosomes and consequent failure in lysosomal degradation was linked to mislocalization of the CI-MPR that had been observed and was the cause of CLN3 related autophagosome pathology.

The CI-MPR executes a fundamental role in the recognition and delivery of these hydrolases. Result from chapter 3 suggested impaired trafficking of CI-MPR in CLN3 deficient cells (Figure 1.7). During their transport from the ER to the Golgi, the enzymes destined to be delivered to the lysosomes are postransationally modified by the addition phosphorylated mannose residues. These are recognized by the mannose 6 phosphate receptors (MPRs) and are subsequently sorted into clathrin coated vesicles and transported to late endosomes, where the enzymes dissociate from the receptors and are subsequently delivered to lysosomes for use. The MPRs are then recycled back to the TGN for a new cycle.

In this part of the work an analysis of the route taken by the endocytosed CI-MPR, was undertaken in collaboration with Dan Metcalf in the Cutler lab.

5.1 Effect of CLN3 deficiency on CI-MPR-receptor trafficking

Following from its altered distribution in CLN3 KO mouse fibroblasts the distribution of the CI-MPR receptor was examined more closely in CLN3 siRNA treated HeLa cells to test whether the proposed impairment in the degradation ability of lysosomes and autophagosomes was due to a defect in CI-MPR trafficking and the correct sorting of hydrolases. A CD8-CI-MPR reporter construct was used in combination with CLN3 siRNA to provide a more flexible system to determine the reason for the CI-MPR defects.

5.1.1 Steady state distribution of CI-MPR in CLN3 depleted HeLa cells

To determine any effect of a loss of CLN3 on CI-MPR distribution, as in chapter 4, RNAi was performed on HeLa cells using exon 6 and exon 10 small interfering RNA (siRNA) duplex oligonucelotides to silence expression of human CLN3 (material and methods, chapter 2). HeLa cells were transfected with the siRNA using an Amaxa nucleofector device, and very little detectable mRNA was found by real time PCR 72 hours after two rounds of siRNA transfection in comparison to HeLa control cells treated with a scrambled siRNA. 85-90% knockdown was confirmed for all experiments described.

The effect of CLN3 loss on CI-MPR receptor distribution was analysed by indirect immunofluorescence and confocol microscopy, staining for endogenous CI-MPR and comparing CLN3 siRNA depleted cells versus labelled control cells as shown in Figure 5.1. From this first investigation, the CI-MPR staining in the siRNA treated cells looked more concentrated in the pericentriolar area and less dispersed in the cytoplasm.

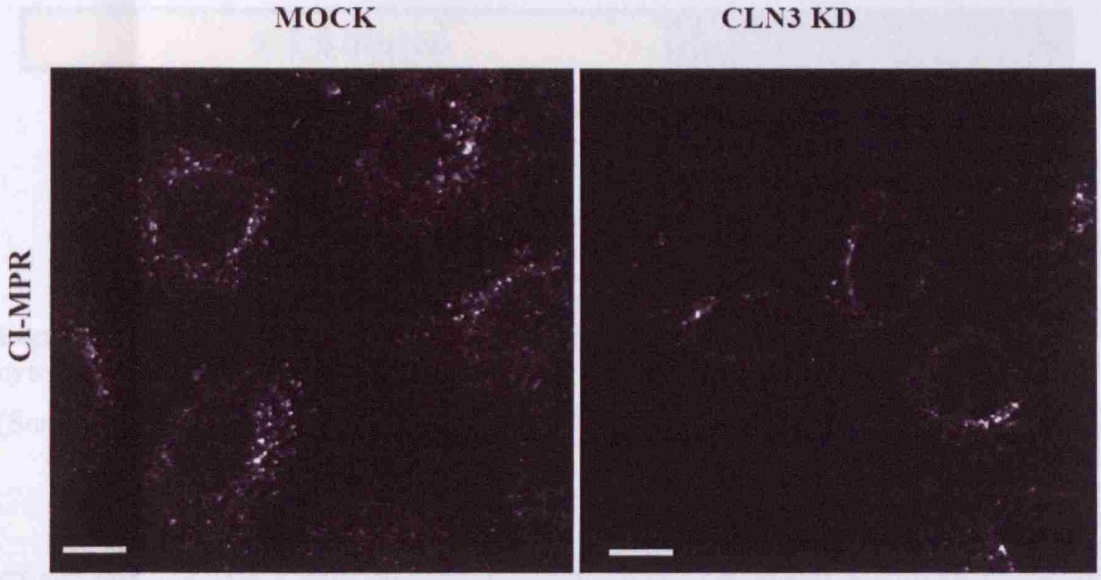

Figure 5.1 Immunofluorescence labelling of CI-MPR in CLN3 knock down HeLa cells and mock treated control cells.

Hela cells transfected with CLN3 siRNA or transfected with control were fixed after 24 hours after the second round of transfection and stained for CI-MPR antibody. Scale bar=10μm

5.1.2 Altered steady state distribution of CD8-CI-MPR chimera in CLN3 depleted HeLa cells.

To extend the analysis of CI-MPR localisation, distribution and trafficking, constructs expressing a CD8 reporter protein in which the cytoplasmic tail of CD8 was replaced with the cytoplasmic tail of the CI-MPR (Seaman, 2004) were expressed in HeLa cells (Figure 5.2). In this way the CI-MPR protein is more readily detected than endogenous CI-MPR, using a commercially available anti CD8 antibody.

Figure 5.2 The cytoplasmic tail of CD8 is replaced with the trasmembrane-cytoplasmic tail (TM/C) of CI-MPR

(Seaman, 2004)

CLN3-depleted HeLa cells and control cells were transiently transfected with the CD8-CIMPR construct and subsequently fixed and labelled by indirect immunofluorescence with antibodies against CD8. The localization was assessed by co-staining with the trans-golgi network marker TGN46.

In cells transfected with scrambled siRNA, the CI-MPR was present at the TGN as seen by the co-localization of CD8 and TGN46 (Figure 5.3, panel A). It was also distributed in a population of endosomes visualized as scattered dots positive for the CD8 antibody, present throughout the cytoplasm. In contrast, the CLN3 depleted cells had an altered CD8- CI-MPR distribution where the anti CD8 was mostly distributed at the TGN and was partially missing from the endosomes (Figure 5.3, panel B). The accumulation of CI-MPR at the TGN in CLN3 depleted cells and relative absence from peripheral endosomes suggested a defect in its cycling route.

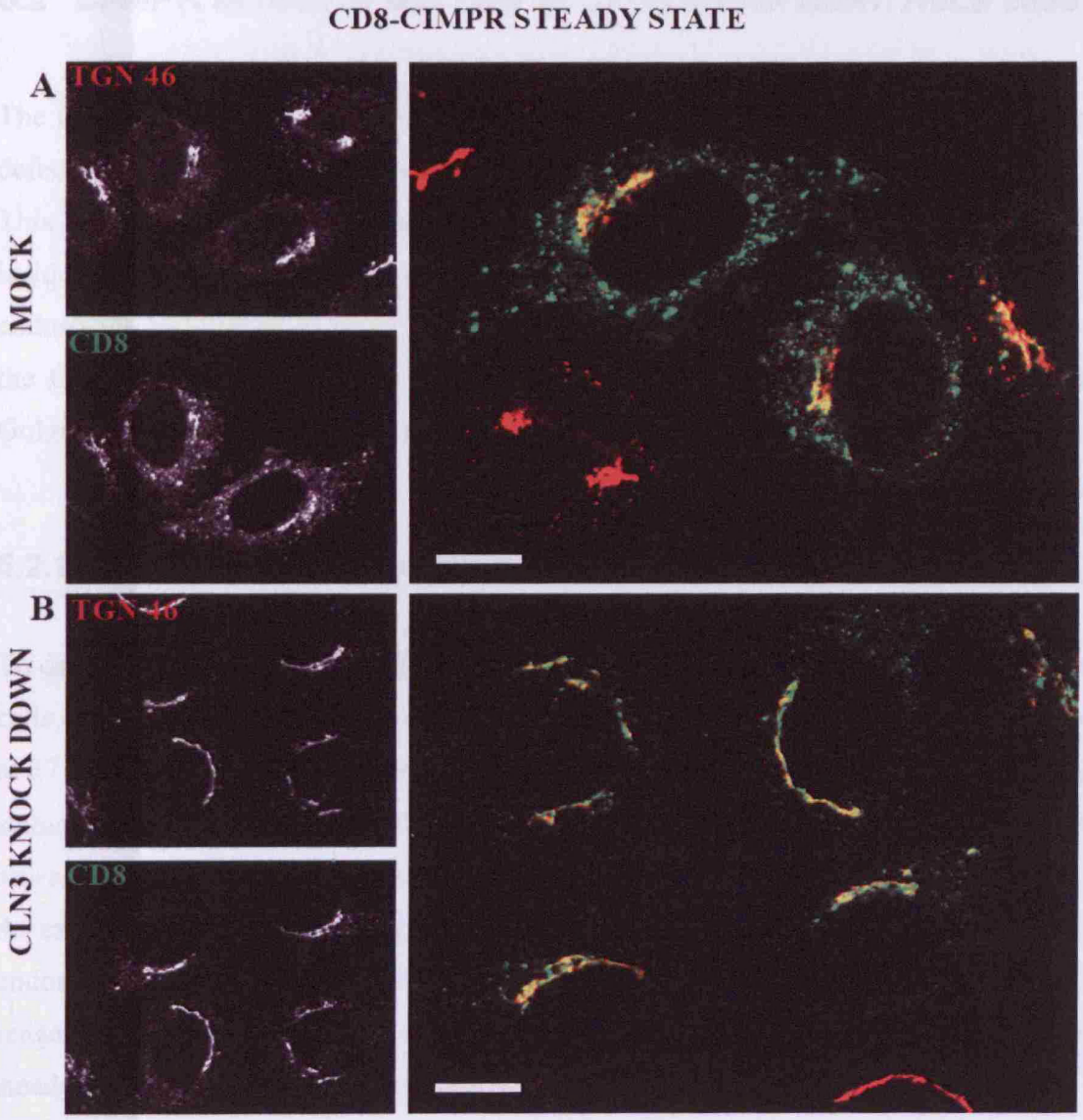

Figure 5.3 Immunofluorescence of mock transfected and CLN3 siRNA treated HeLa cells expressing CD8-CI-MPR

(A) Control cells and (B) CLN3 depleted cells labelled with TGN46 and CD8 to visualize the localization of CI-MPR in the cells. In control cells (A) CD8 is present in both Golgi and endosomes in contrast CLN3 depleted cells where the majority of the CD8 is present in the TGN.
Scale bar=10μm

5.2 CI-MPR is held in the TGN in CLN3 knock down HeLa cells

The altered steady state distribution of CI-MPR in CLN3 depleted cells suggested a defect in the trafficking of the receptor.

This is a well studied and characterized receptor that follows a complicated route inside cells that involves multiple sorting steps, trafficking via the plasma membrane, endosomes and Golgi. In order to follow the CI-MPR route in CLN3 deficient cells, the CI-MPR path was analysed from the plasma membrane to the endosomes and Golgi, by feeding the cells with the CD8 antibody.

5.2.1 Endocytosed CD8 is almost exclusively detected at the TGN

To determine if the route from the plasma membrane to the Golgi was impaired, HeLa cells depleted for CLN3 and expressing the CD8-CIMPR chimera were fed for 3 hours at 37 °C with a CD8 monoclonal antibody. After internalization, cells were fixed and stained by indirect immmunofluorescence with the trans-Golgi marker TGN46 to assess the arrival of the CD8 at the Golgi (Figure 5.4)

As expected, in scrambled siRNA control cells the CD8 was present in both TGN and endosomes as the result of the continuous feed and subsequent trafficking of the reagent in the cells, as shown in panel A. The distribution is similar to that seen for the steady state distribution of the receptor in Figure 5.3, panel A.

In contrast, the distribution of the CI-MPR in the CLN3 knock down cells was severely altered with a predominant localization at the TGN, where the CD8 accumulated with a brighter and tighter stain than in the control cells, to the detriment of the endosomal population (panel B).

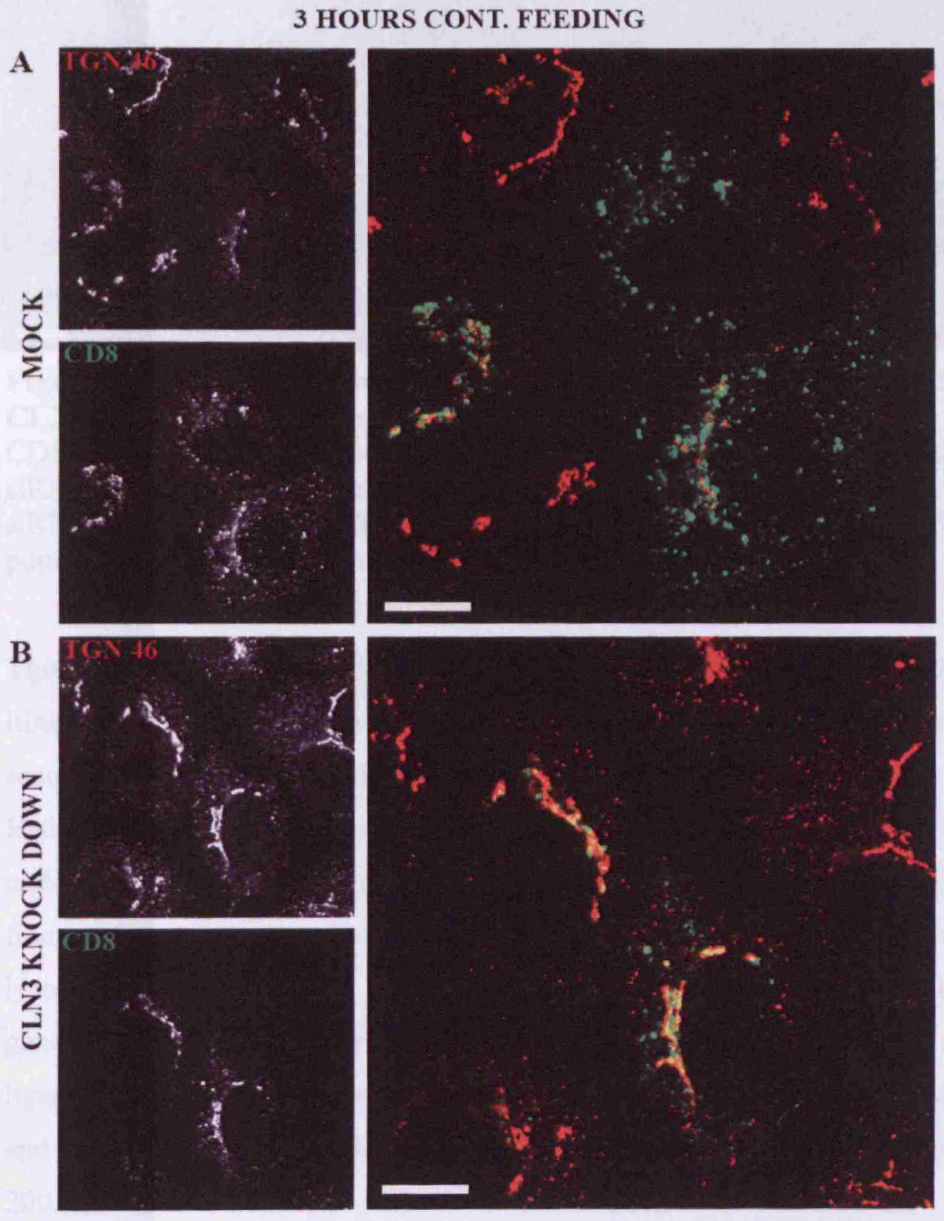

Figure 5.4 Immunofluorescence of mock transfected cells and CLN3 siRNA treated HeLa cells expressing CD8-CI-MPR and fed with the CD8 antibody for 3 hours

Cells were incubated for 3 hours continuously with the antibody CD8 prior to fixation. Cells were labelled with TGN46 followed by appropriate secondary antibodies. In mock transfected cells there is colocalization of endocytosed CD8 with the Golgi marker but a good bulk of CD8 is present also in endosomes scattered throughout the cytoplasm (A) in contrast with CLN3 depleted cells (B) where the majority of the endocytosed CD8 is present just in the TGN. Scale bar=10μm

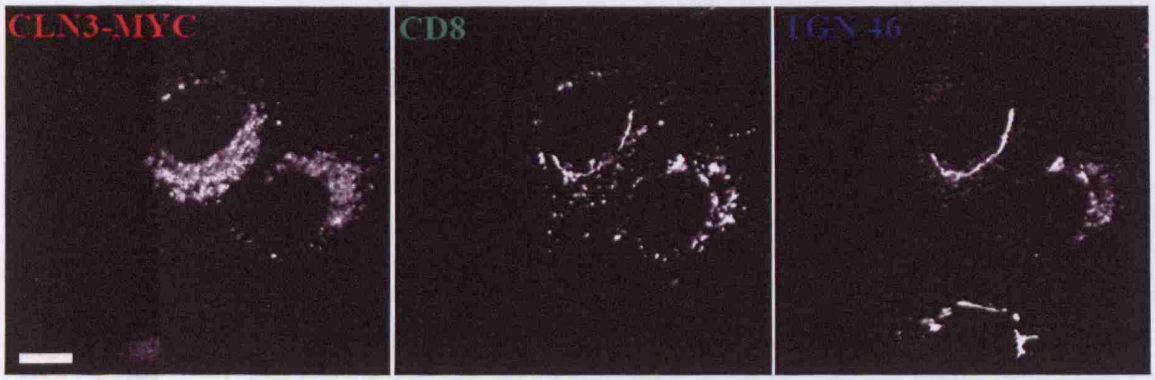

Figure 5.4 b CLN3-Myc overepression rescue the CD8-CI-MPR localization in CLN3 siRNA treated cells.
CD8-CI-MPR was localized at the TGN and in the endosomal population in CLN3 siRNA cells suggesting phenotype rescue and confirming the specificity of the CLN3 siRNA in missorting the CI-MPR at the TGN area to the detriment of the endosomal population. Scale bar=10μm

This finding raised two different questions. Firstly: which part of the trafficking itinerary of the CI-MPR was deficient resulting its accumulation at the TGN and secondly, whether the CI-MPR was getting degraded by the lysosomes.

Endocytosed CI-MPR enters sorting endosomes and subsequently recycling early endosomes. A proportion of the receptor eventually proceeds to the TGN, another fraction returns to the PM and finally a proportion of CI-MPR also goes to the lysosomes from the early endosomes(Lin et al., 2004). Only a small fraction can generally be detected in the endosomal compartment where the receptor dissociates its ligand due to acidic endosomal environement due to the acidic endosome environment and comes back to the TGN by a process involving the retromer complex (Seaman, 2005).

5.2.2 CI-MPR retention in the TGN is a specific phenotype due to CLN3 loss that can be reversed by restoring CLN3 expression

CLN3 loss caused a re-distribution of CI-MPR which could influence its primary function of delivery of hydrolases to the lysosomes and consequently limit lysosomal degradation, causing the build-up of storage material in autophagosomes and

lysosomes in CLN3 deficient cells. The specificity of the siRNA-mediated CLN3 knock down in HeLa cells was confirmed by re-introducing CLN3 to the cells by the overexpression of a Myc tagged CLN3 (Pohl er al., 2007) construct in conjunction with siRNA, during the second round of transfection in experiments. Twenty four hours after the second round of transfection with the CLN3 siRNA/mock transfection and CLN3-Myc co-transfection the cells were fed with the CD8 antibody for 3 hours, immediately fixed and labelled with the TGN 46 antibody. CD8-CI-MPR was localized at the TGN and in the endosomal population in both control and CLN3 siRNA cells suggesting phenotype rescue and confirming the specificity of the CLN3 siRNA in missorting the CI-MPR at the TGN area to the detriment of the endosomal population (Daniel Metcalf, UCL, figure 5.4b).

5.2.3 CI-MPR is not degraded by lysosomes in the CLN3 depleted cells

After being transported in coated vesicles from the TGN to late endosomes/lysosomes, the hydrolases dissociate at their destination from the CI-MPR allowing the receptor to come back to the TGN for a new cycle. In this way the receptor is recycled for re-use rather then being degraded and wasted.

In CLN3 depleted cells, the lack of CI-MPR outside of the TGN area raised the possibility that the receptor has being degraded by lysosomes instead of being returned for a new cycle. To test this hypothesis HeLa cells depleted for CLN3 and expressing the CD8-CI-MPR chimera were treated with the protease inhibitors leupeptin and pepstatin for 3 hours prior to and during the 3 hours of the CD8 antibody feeding to the cells at 37 degrees. After the protease treatment and internalization by feeding, both CLN3 knock down and control cells were fixed and stained with the TGN46 antibody to detect the Golgi compartment and Lamp1 antibody to visualize the late endosomes/lysosomes (Figure 5.5).

In control cells, the CI-MPR is detected at the TGN and in endosomal population as shown previously (panel A). In the CLN3 depleted cells, no colocalization of the CD8

antibody with the lysosomal marker Lamp1 was detected and the majority was in the TGN (panel B). This confirmed the relative lack of CI-MPR outside the TGN in knockdown cells and excluded the possibility that the CI-MPR was retained and degraded in the lysosomes.

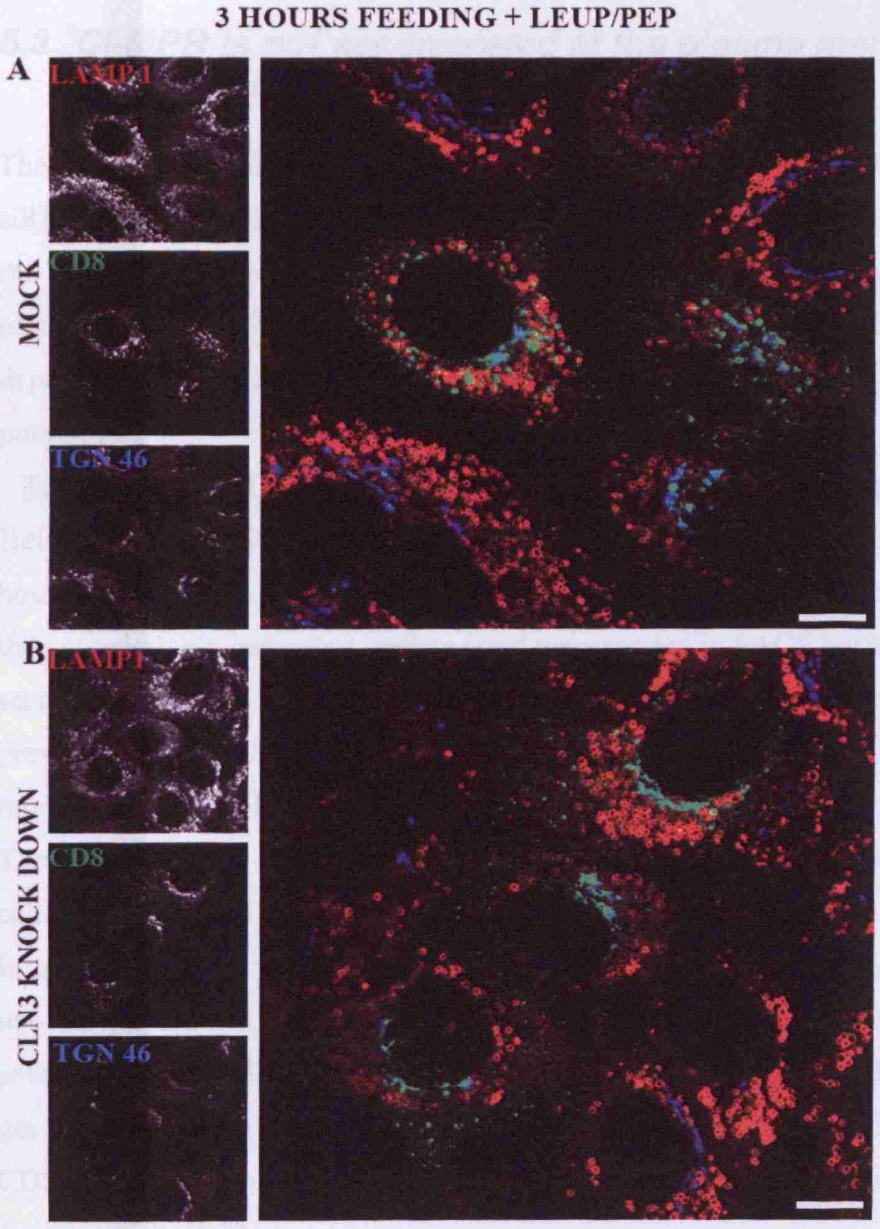

Figure 5.5 Immunofluorescence of mock and CLN3 siRNA treated HeLa cells expressing CD8-CI-MPR and fed with the CD8 antibody in the presence of protease inhibitors

Cells were treated with the protease inhibitors leupeptin and pepstatin for 3 hours prior to and during 3 hours of CD8 antibody uptake. Cells were fixed and stained with TGN46 and Lamp1. Control cells (A) showed the presence of CD8 in both TGN and endosomes in contrast with CLN3 depleted (B) cells where the CD8 antibody is almost exclusively colocalizing with TGN 46. Scale bar=10μm

5.3 CI-MPR is not accumulated at the plasma membrane in CLN3 depleted cells

The analyses by indirect immunofluorescence of CI-MPR localization in CLN3 siRNA depleted cells and corresponding controls showed a pronounced distribution at the TGN and an absence from the endosomes in the siRNA cells. It was possible that a part of the CI-MPR might be stored or retained at the plasma membrane in CLN3 depleted cells. To explain this phenotype, an analysis was performed to rule out this possibility.

To assess if the CI-MPR was accumulated at the PM, CLN3 depleted and control HeLa CD8-CI-MPR stably expressing cells were fed with the CD8 antibody for 3 hours continuously. Cells were extensively washed to remove unbound CD8 antibody, then successively harvested, pelleted and resuspended in FACS buffer, with 488 Alexa secondary antibody. Cells were incubated on ice for 30 minutes with the antibody to prevent endocytosis and immediately fixed. Cells were not permeabilized, in order to monitor just the CI-MPR pool at the PM.

The FACS analysis revealed a lower level of CI-MPR at the PM in the CLN3 depleted cells than in control cells (Figure 5.6).

In the context of previous results, the flow cytometry data suggested that the biggest pool of internalized CI-MPR in the CLN3 siRNA cells is at the TGN and that once it enters the cells, it does not cycle back to the PM. Since the internalized CD8 did not get degraded by the lysosomes nor accumulate at the PM, it is possible that all the fed CD8 is retained exclusively at the TGN; this raises the possibility that CLN3 exers its function in the TGN.

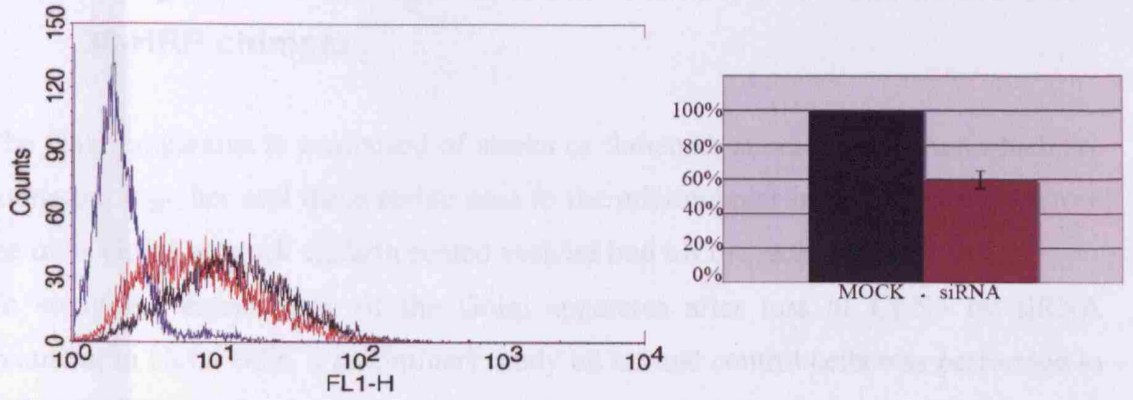

Figure 5.6Cell surface expression of CD8-CI-MPR in mock and CLN3 siRNA CD8-CI-MPR

HeLa cells stably expressing CD8-CI-MPR were fed for 3 hours with anti CD8. Cells were extensively washed and labelled with an Alexa 488nm secondary antibody, cells were then fixed in formaldehyde before analysis by FACS. Unstained cells (blue), siRNA treated cells (red), mock transfected cells (green).
The graph shows the mean of the percentage of the CD8 fluorescence at the plasma membrane ± SD for the same experiment repeated three times.

5.4 Morphology of the Golgi apparatus in control cells and in CLN3 depleted cells

Since in CLN3 depleted cells expressing the CD8-CI-MPR chimera the MRP is present almost exclusively at the TGN, this raised the possibility that a dramatic morphological defect could occur in the Golgi after CLN3 siRNA transfection which prevents the exit of the CI-MPR from the TGN.

5.4.1 Analysis of the TGN in control cells with the use of the TGN-38-HRP chimera

The Golgi apparatus is composed of stacks of flattened, adherent cisternae which are connected together and these reside next to the microtubular organizing centre. From the trans Golgi network clathrin coated vesicles bud off to reach their destination.

To study the morphology of the Golgi apparatus after loss of CLN3 by siRNA treatment in HeLa cells, a preliminary study on normal control cells was performed to define the TGN in these cells by electron microscopy using a TGN-38-HRP chimera.

HeLa cells were fixed 24 hours after transfection with the TGN-38-HRP chimera. Immediately after fixation the cells were treated with diaminobenzidine and hydrogen peroxide to reveal the location of the HRP and subsequently processed for embedding for electron microscopy (EM) as described in the material and methods (chapter 2).

The TGN-38-HRP fusion protein was efficiently targeted as seen by the presence of active HRP to the Golgi complex and in particular it was specific for the TGN network and the small vesicles budding off from it, which TGN38 cycles to (Figure 5.7). This experiment showed that the TGN-38 chimera could be successfully used as a monomer that was specific for the TGN area. Furthermore this specific definition of the TGN area showed the ultrastructure in HeLa cells with its stacks and vesicles, allowing a definition of its normal structure prior to CLN3 depletion.

TGN-38-HRP

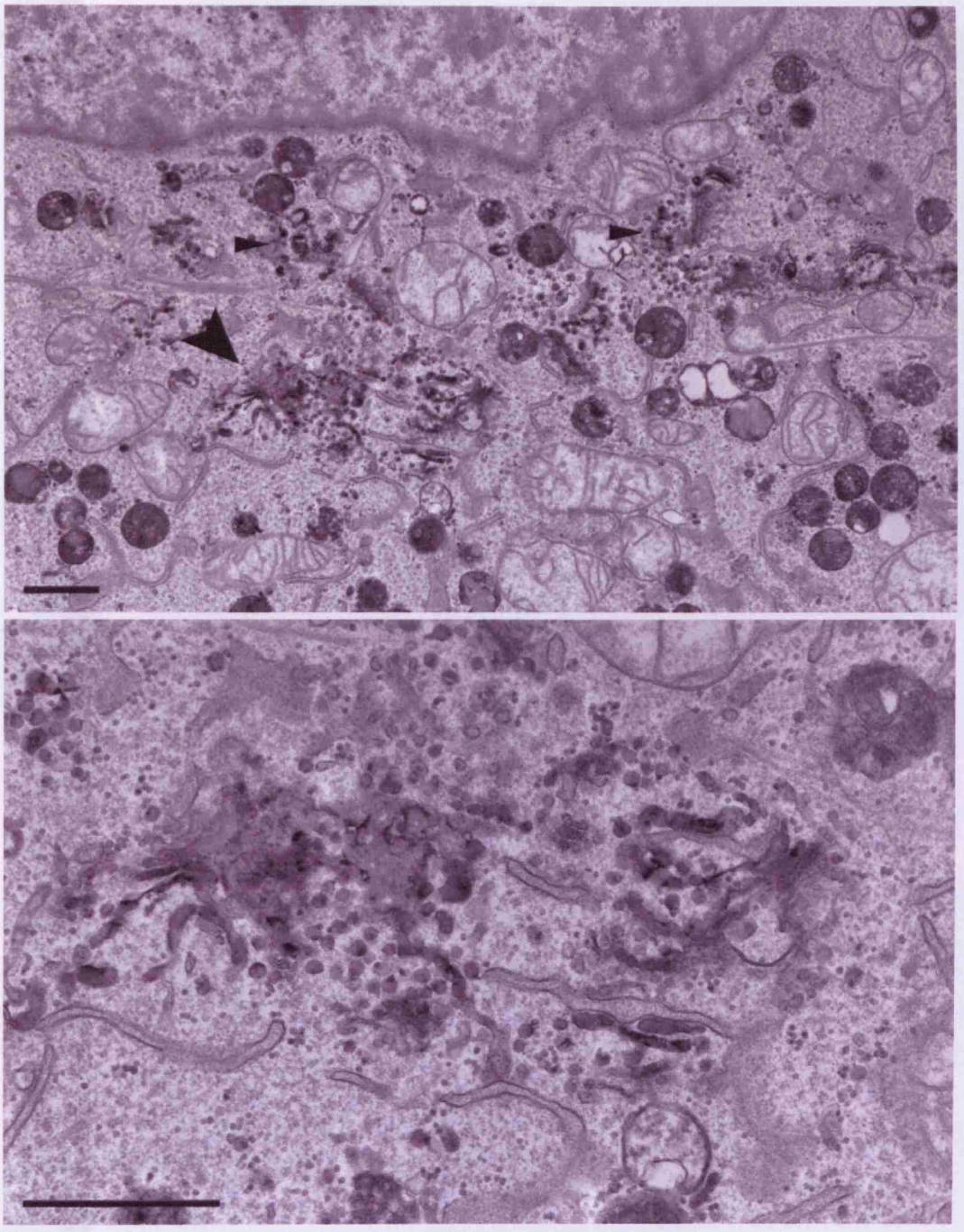

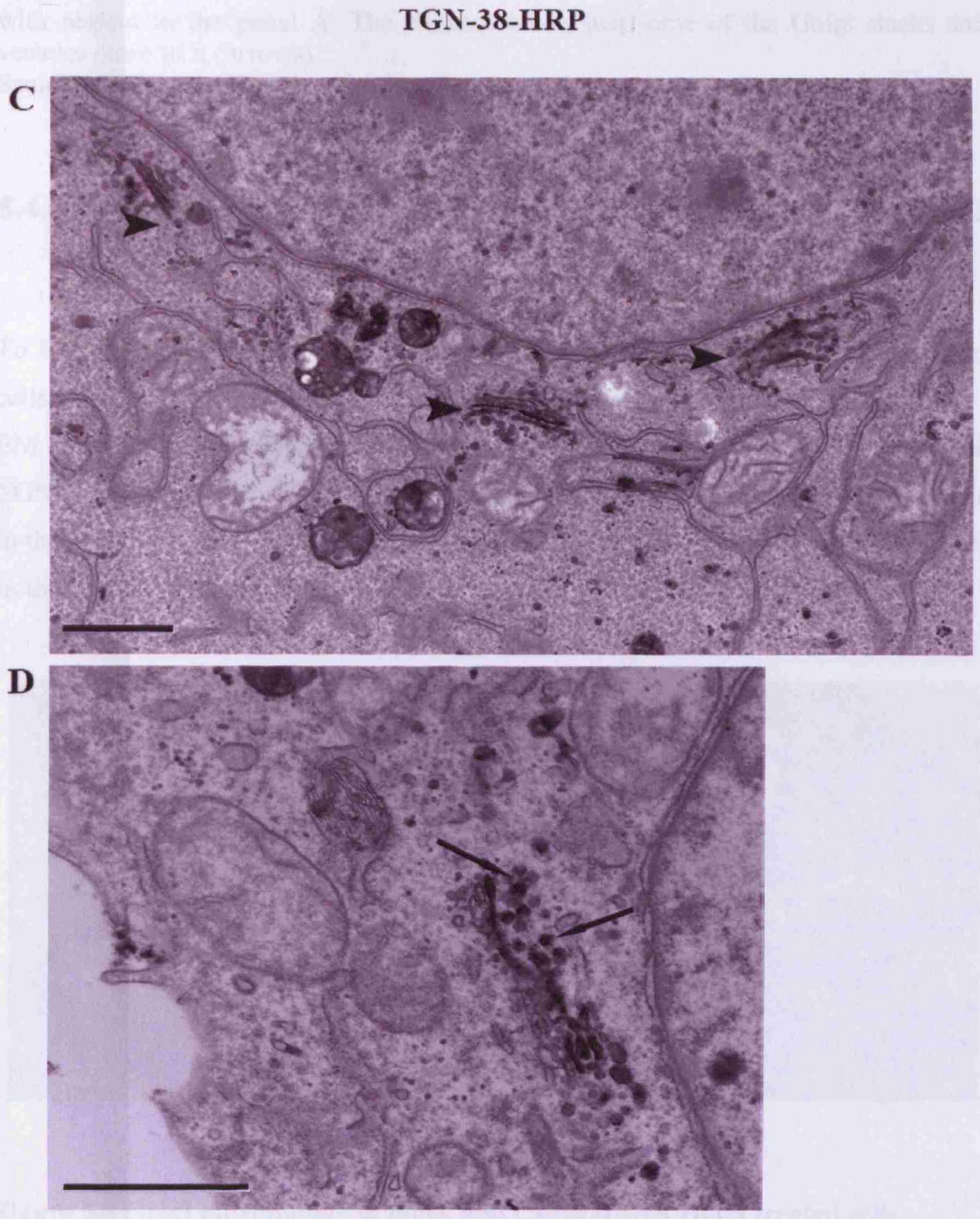

Figure 5.7 TGN-38-HRP chimera expressed in HeLa cells

Electron micrographs of HeLa cells expressing the TGN-38-HRP chimera. Panel A, Low magnification of expressing the chimera in the Golgi area, the small arrow heads indicate the TGN, where the chimera is expressed as shown by the presence of HRP. Large arrow head indicates a subset of Golgi, which is shown, at higher magnification in panel B. Panel C and Panel D shows at hight magnification the location of the TGN-38-HRP chimera in the TGN, but here the Golgi is shown in a different plane

with respect to the panel A. The chimera labels just some of the Golgi stacks and vesicles close to it (arrows).
Scale bar=100nm

5.4.2 Morphology of the Golgi apparatus is normal in CLN3 depleted HeLa cells

To test the hypothesis of a morphological defect at the TGN in CLN3 knock down cells, siRNA treated and control cells were processed for electron microscopy.
EM morphological analysis suggested that in both the mock and knock down cells, the TGN cisternae were normally organized and connected (Figure 5.8). Also, the vesicles in the TGN area were clathrin coated suggesting no evident morphological impairment in the CLN3 knock down cells compared to control cells.

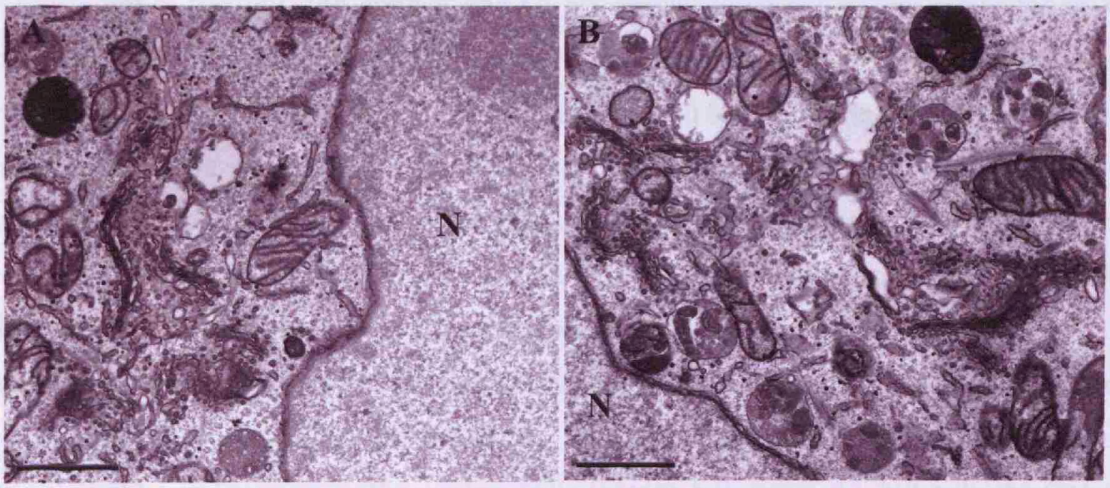

Figure 5.8 Golgi morphology in mock and CLN3 siRNA HeLa treated cells
Electron micrograph of the Golgi area in a mock transfected cell (A) and CLN3 siRNA treated cell (B). CLN3 siRNA does not change the morphology of the Golgi area. N=nucleus.
Scale bar=1000 nM

5.5 Ultrastructure localization of CIMPR in CD8 fed CLN3 depleted cells

In CLN3 depleted cells, immunofluorescence studies showed that the CI-MPR was confined to the Golgi area in contrast with control cells where it was also present in endosomes.

To better define the CI-MPR localization in CLN3 depleted conditions, the analysis of its distribution was taken to the ultrastructural level. To directly compare, in parallel, the results found so far at the light microscopy level, stable HeLa cells lines expressing CD8-CI-MPR were made and transfected with control siRNA or CLN3 siRNA. After the second round of transfections, The CD8 antibody was conjugated to HRP-Fab fragments (Zenon labelling kit) to be visible using electron microscopy after being fed to the cells for 3 hours continuously.

After 3 hours feeding, the control and CLN3 knock down cells were incubated at 4 degrees for 30 minutes in the presence of diaminobenzidine and hydrogen peroxide to reveal the location of the HRP, and subsequently fixed and embedded for electron microscopy. The specificity of the HRP-Fab fragments was first proven at the light level by indirect immunofluorescence, using an anti HRP antibody to stain the Zenon HRP-Fab fragments after the anti CD8 antibody was conjugated to them. The CD8 antibody conjugated to HRP-Fab fragments was added and left for 3 hours in the medium of the cells. Cells were then fixed and labelled with the HRP antibody. The HRP antibody recognizes the HRP-Fab fragments and labelled the TGN and a population of endosomes in the control cells (Figure 5.9, panel A), but only the Golgi area in CLN3 depleted cells (panel B). This differential localization pattern was similar to that found when anti CD8 antibody was fed to cells expressing CD8-CIMPR in conjunction with CLN3 knock down and provided evidence that the conjugation of the antibody to the Fab fragments did not alter its distribution and its normal trafficking.

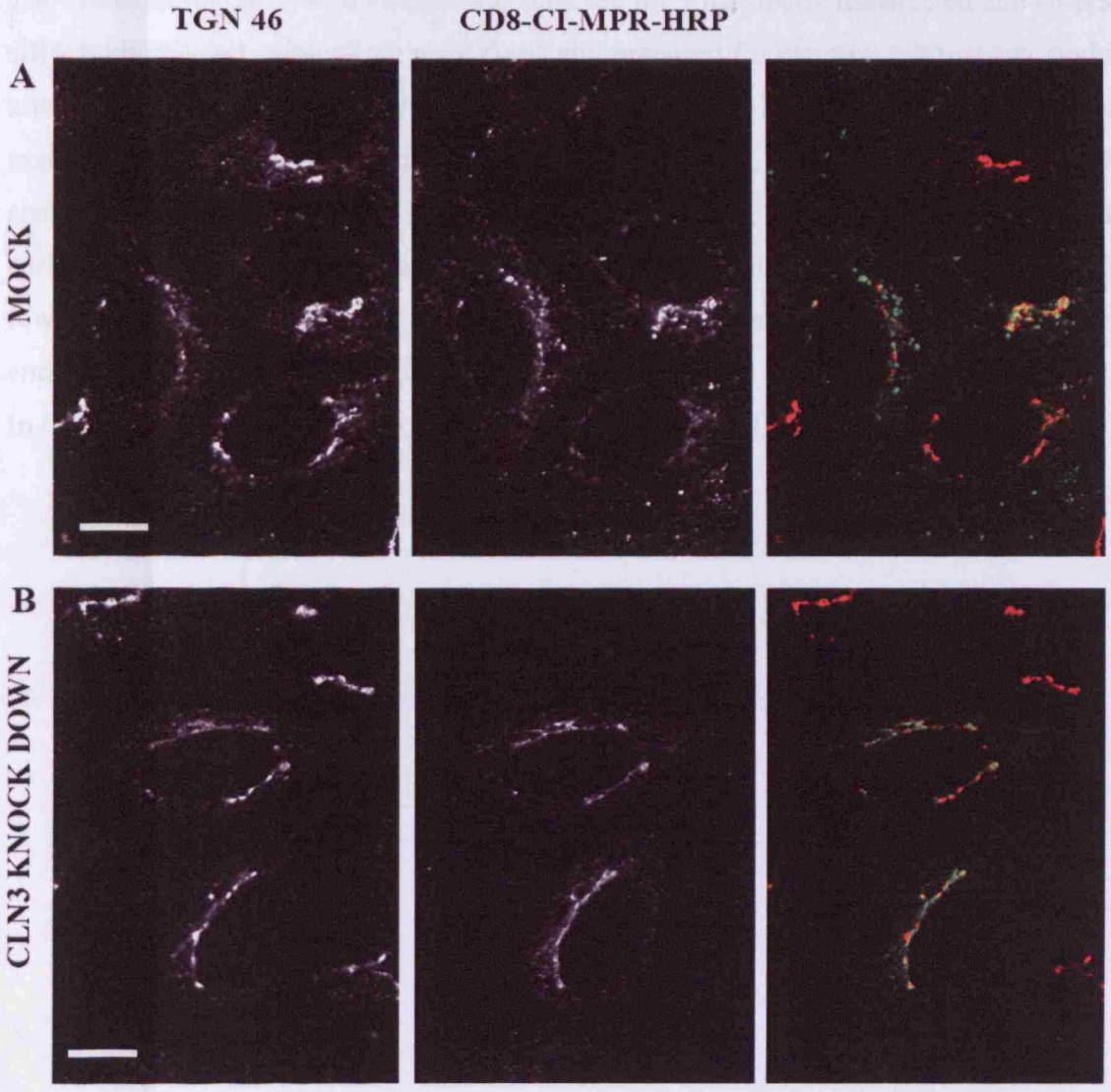

Figure 5.9 CD8-CIMPR-HRP in mock and CLN3 siRNA knock down cells

Indirect immunofluorescence of control and CLN3 depleted HeLa cells expressing the CD8-CIMPR chimera, fed for 3 hours with CD8 antibody conjugated to HRP-Fab fragments and subsequently fixed and labeled with both anti-HRP antibody, used to recognize the fragments and a TGN46 antibody. Control cells (A) and CLN3 depleted cells (B) differ, as described before in the 5.2.1 paragraph on the CD8 localization. In the control cells, the CD8 antibody is present in both Golgi and endosomes contrasting the almost exclusive TGN localization of CD8 in CLN3 deficient cells. This immunofluorescence demonstrates the specificity of the CD8 antibody upon conjugation to Fab fragments. Scale bar=10μm

The combination HRP Zenon-CD8 was then fed for 3 h in mock transfected and CLN3 siRNA transfected cells which were fixed and prepared for electron microscopy study after which the location of the HRP was revealed by the DAB reaction. In the mock treated cells, the HRP was detected in the Golgi area, in particular in the TGN cisternae (Figure 5.10, panels A and B). It was also present in populations of early/recycling endosomes (panel E), in sorting endosomes characterised by having few internal vesicles and tubules protruding from the organelles (panel D) and in late endosomal structures (panel C).

In CLN3 siRNA cells the HRP was revealed just in the TGN cisternae (Figure 5.11).

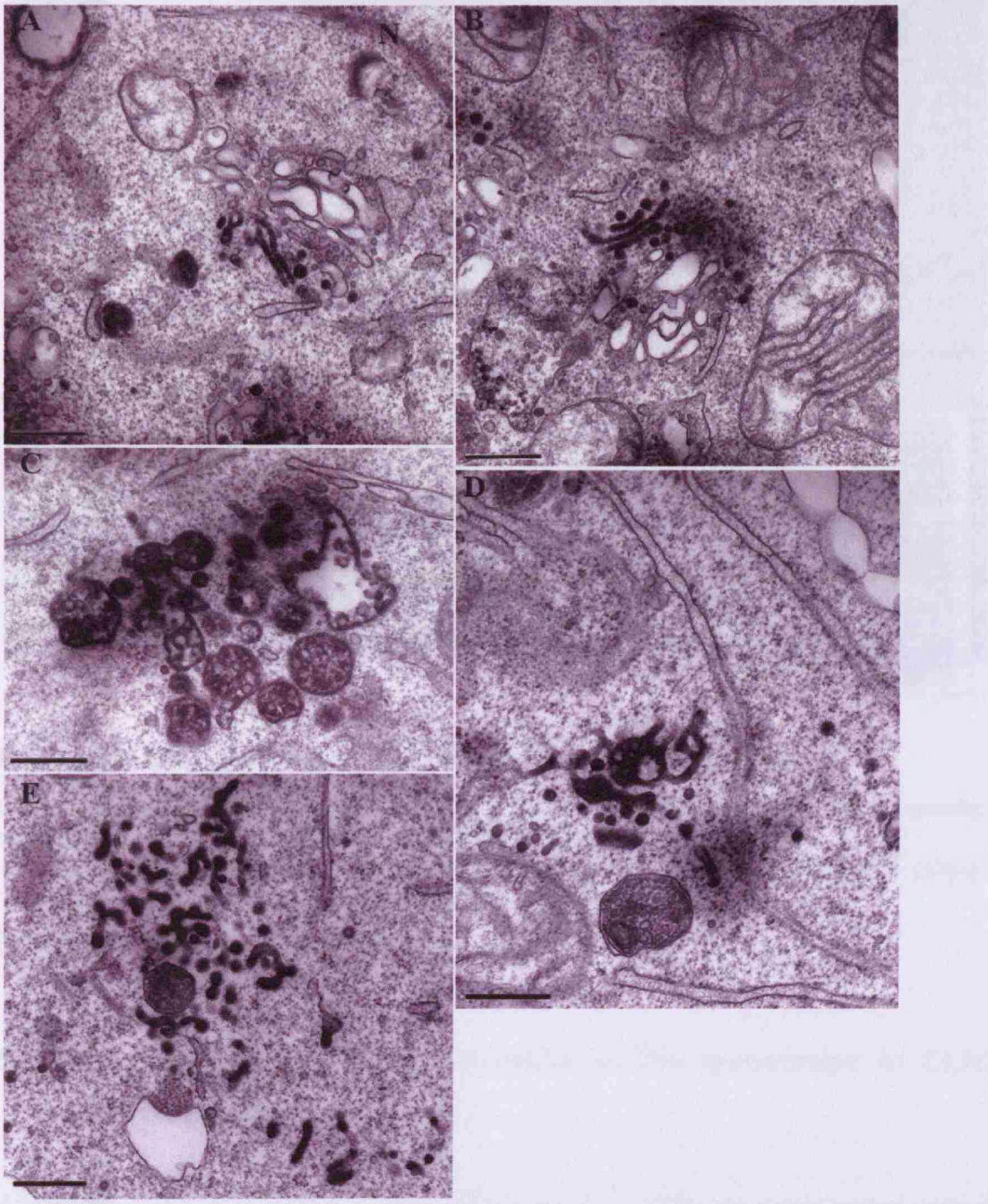

Figure 5.10 HRP Zenon-CD8 feeding in mock transfected HeLa cells

CD8 conjugated to HRP-Fab fragments was fed for 3 hours to mock transfected cells was seen in the Golgi area (panel A and B), in recycling/early endosomes (panel E), sorting endosomes (panel D), late endosomal structures (panel C) as seen by the black/floccular HRP.
N indicates the nucleus
Scale bar=100 nm

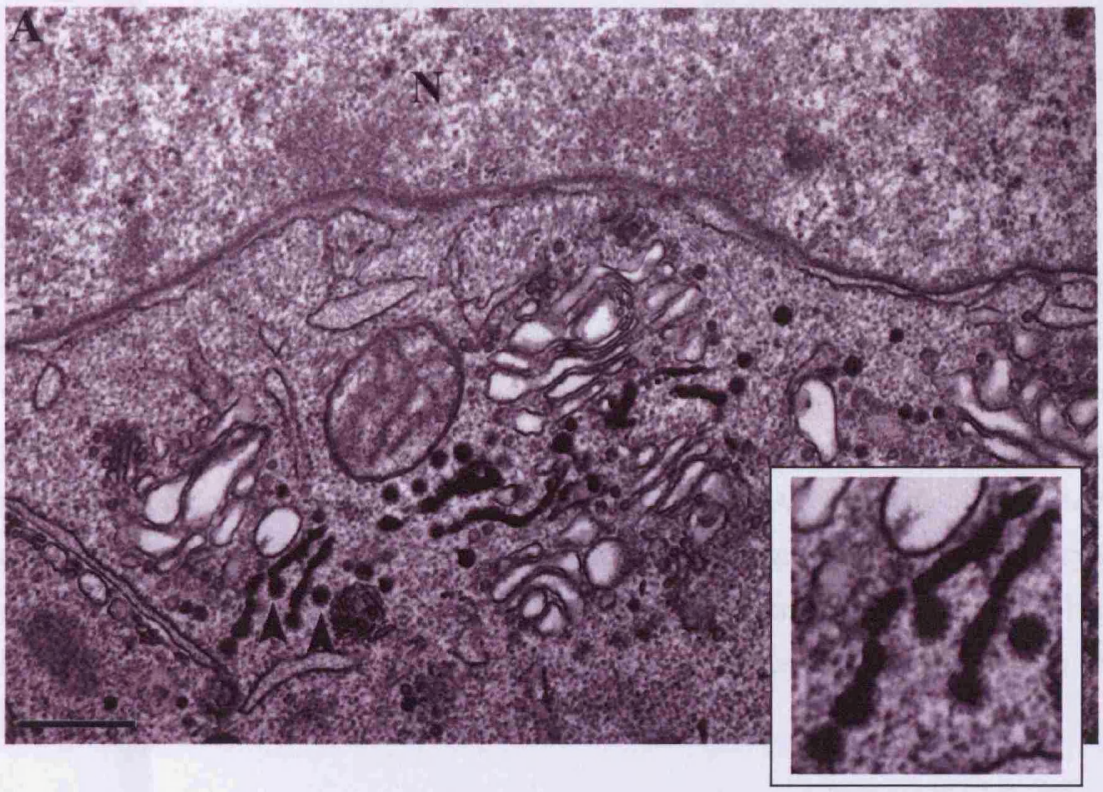

Figure 5.11 HRP-Zenon-CD8 feeding in CLN3 siRNA HeLa cells

CD8 conjugated to HRP-Fab fragments stains the TGN as seen by the black/floccular staining given after the DAB reaction. N indicates the nucleus.
The arrows indicate the presence of clathrin in the TGN area, the same portion of the TGN is shown at higher magnification in the small box.
Scale bar=100nm

5.5.1 The route from the endosomes to the lysosomes in CLN3 depleted cells

As part of its normal trafficking route a fraction of CI-MPR gets endocytosed through the PM the location where ligands destined for the lysosomes are bound and internalized. Since the bulk of the CI-MPR in CLN3 depleted cells was found mostly at the TGN to the detriment of the endosomal population it could be that, in feeding experiments, the internalized CI-MPR is mis-trafficked after CLN3 knockdown because the plasma membrane-endosomes-lysosomes route is affected.

To investigate the possibility that the route from the early endosomes to the lysosomes is affected by CLN3 knock down, cells were stimulated with fluorescent EGF, which traffics from the PM to the early endosomes and then lysosomes for its degradation passing by a specific subpopulation of multivesicular endosomes (White et al., 2006). Scrambled and CLN3 siRNA HeLa cells transiently expressing CD8-CI-MPR were grown for one hour in the absence of FCS from the media and successively pulsed with EGF for 10 minutes and chased for 30 minutes and 2 hours to analyze the presence of EGF in early endosomes and lysosomes. After the feeding, cells were processed by immunofluorescence and stained with EEA1 antibody and LAMP1 antibody (Figure 5.12). The receptor internalization or progress through the endocytic pathway was not disturbed in the knockdown cells. We found that EGF, reached both EEA1-positive endosomes and LAMP1-positive lysosomes at the same rate in the knockdown and mock-transfected HeLa cells.

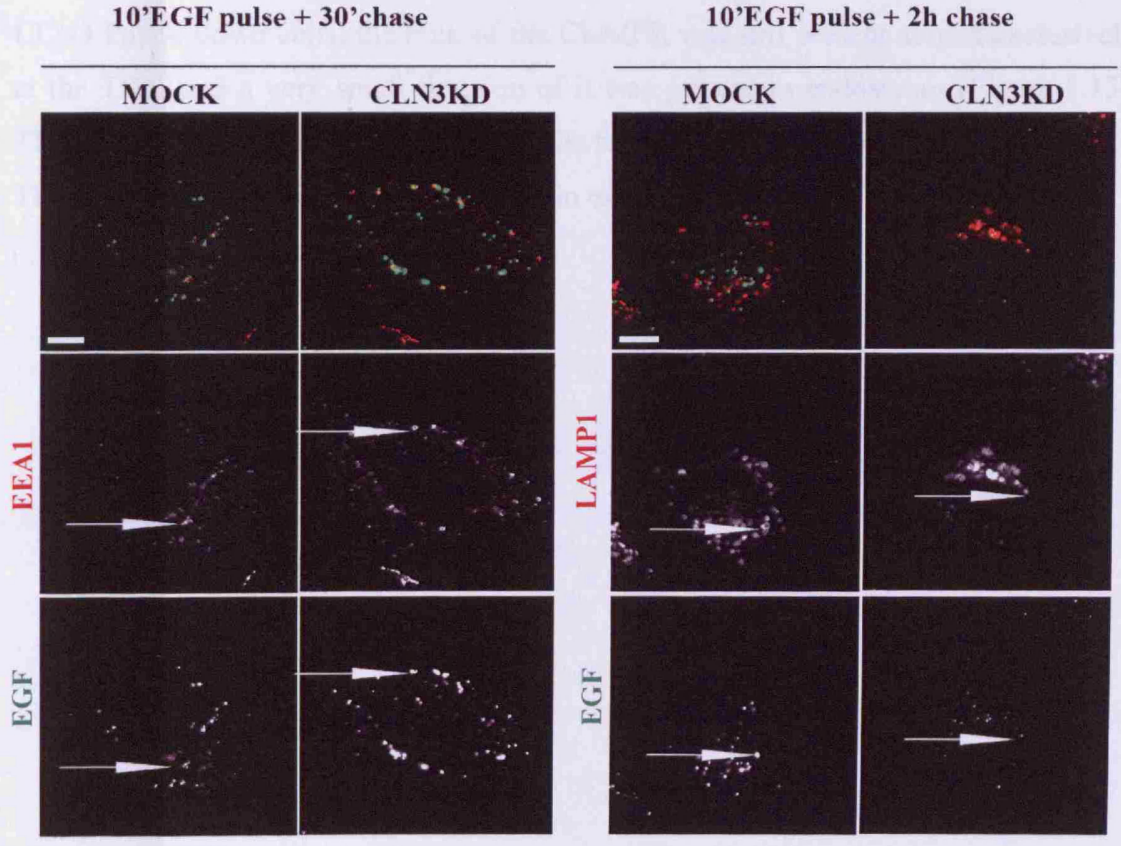

Figure 5.12 EGF enters early endosomes and lysosomes in mock and CLN3 siRNA cells.

White arrow show positive organelles for EGF and EEA1 or EGF and Lamp1. Scale bar=10μm

5.5.2 Putative role for CLN3 at the TGN exit

In an attempt to further understand which part of the CI-MPR trafficking pathway is defective in CLN3 depleted cells a further analysis was done. CLN3 depleted HeLa cells and mock transfected controls expressing the CD8–CI-MPR construct were pulsed with the CD8 antibody for 40 minutes in DMEM at 37 degrees to allow the internalization of the reagent in the cells and then chased in full media for 2,5 hours (long chase). Cells were subsequently fixed and stained with the TGN46 antibody to study the localization of the CD8 antibody. The experiment was designed to reveal whether the CI-MPR accumulating within the TGN can be chased out or not.

Figure 5.13 shows that after the long chase the CD8 antibody in the control cells was distributed, as expected in the TGN and also in the endosomal population. In the CLN3 knock down cells, the bulk of the CI-MPR was still present almost exclusively at the TGN and a very small function of it was present in endosomes (Figure 5.13). This pattern was similar to that seen in cells fed without a chase period (Figure 5.9). These data were consistent with a failure in exit from the TGN.

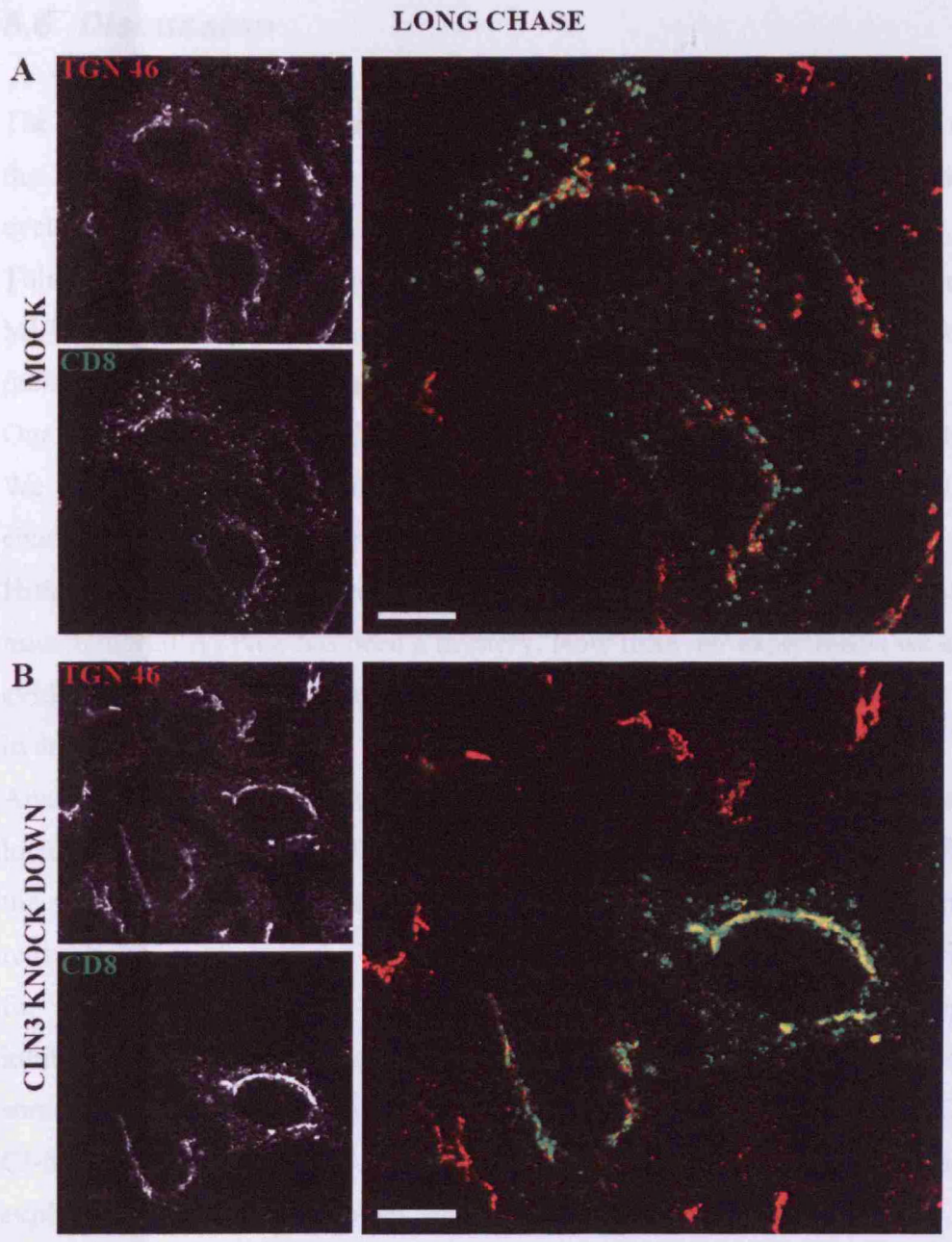

Figure 5.13 Immunofluorescence of mock and CLN3 siRNA treated HeLa cells expressing CD8-CI-MPR , fed with CD8 for 30 minutes and chased for 2,30h

Indirect immunofluorescence of control and CLN3 depleted HeLa cells expressing the CD8-CI-MPR chimera, fed for 30 minutes with CD8 and chased for 2,30 hours. Control cells (A) and CLN3 depleted cells (B) differ in CD8 localization. In the control cells, the CD8 antibody is present in both Golgi and endosomes contrasting with the almost exclusively localization of CD8 in CLN3 deficient cells. This immunofluorescence demonstrated that the anterograde route, from TGN to the endosomes is affected. Scale bar=10μM.

5.6 Discussion

The Mannose 6 phosphate receptors bind newly synthesized lysosomal hydrolases at the TGN and deliver them to prelysosomes, then release their cargo to start a new cycle (Ghosh et al., 2003a).

This study showed that cellular depletion of CLN3, using siRNA, interferes with CI-MPR localization causing its re-distribution to the TGN and thereby reducing its presence in the endosomal population.

Our data support a model where CLN3 is implicated in CI-MPR exit from the TGN.

We propose that this cellular defect can explain the phenotype of JNCL which is characterized by the cellular accumulation of undegraded material.

Hitherto, the reason why cells from JNCL patients accumulate subunit c of the mitochondrial ATPase has been a mystery. Now from our experiments we can provide evidence that this could be due to a failure of the CI-MPR to deliver lysosomal hydrolases.

Analysis of the CI-MPR was carried out after the initial finding that its steady state localisation was altered by CLN3 deficiency. This chapter showed a specific block of the CI-MPR at the TGN and that after being fed via the plasma membrane, the receptor is able to reach the TGN in CLN3 cells but it is not capable of leaving it again for a new cycle. Since it does not get degraded, as proved by adding protease inhibitors to the cells before CI-MPR feeding, the available explanation is that, somehow, CLN3 knock down is interefering with the CI-MPR exit at the TGN.

CI-MPR leaves the TGN in clathrin coated vesicles and tubules. One possible explanation is that these tubules and vesicles cannot form properly or their movement is impaired. At the ultrastructural level labelling of CI-MPR with HRP showed that in the TGN area HRP-positive clathrin coated vesicles are present and in both mock and CLN3 siRNA cells they are positive for CI-MPR. It is possible that perhaps, less CI-MPR positive vesicles are present in the CLN3 siRNA cells but this method does not allow this to be accurately quantified.

Also, the most consistent noticeable difference between mock and CLN3 siRNA cells is the dramatic reduction in CI-MPR from staining in the endosomal population.

Understanding the mechanism used by CLN3 to generate the phenotype needs further work described. CI-MPR leaves the TGN in clathrin coated vesicles with the help of AP-1 and GGAs. For the future it would be interesting to determine precisely how these are functioning in cells deficient for CLN3.

To confirm this work it would be of primary importance to understand which are the proteins partners that CLN3 protein interacts with in the cell. Attempts have been made to determine CLN3 interactors for example by yeast two hybrid analysis, but this has not been possible mainly because of the high hydrophobicity of the protein. It could be possible, on the other hand to identify which molecules are upregulated and downregulated after CLN3 siRNA treatment.

More easily, the analysis of the CI-MPR cargo should be done in CLN3 deficient cells in order to investigate the effect CLN3 has on the mobility of hydrolases towards the lysosomal compartment.

6 Autophagosomes form from TGN tubular structures and CI-MPR redistributes itself in starvation conditions

Chapter 3 and chapter 4 showed that there is an increase in the number of autophagosomes present in *Cln3* KO mouse cells and JNCL 1kb CLN3 deletion cells and that this accumulation is likely due to a defect in the clearance of autophagosomes arising from compromised fusion of lysosomes with autophagosomes.

It is believed that the fusion between lysosomes and autophagosomes is critical to the degradation of autophagic content, since of hydrolases likely come from this fusion event.

In addition Chapter 5 showed that CI-MPR, an essential receptor for hydrolase delivery, is mislocalized to the TGN in CLN3 depleted cells and that CLN3 deficiency likely perturbs its exit from the Golgi, thus impairing hydrolases delivery to endosomes. This CI-MPR phenotype does not in itself explain a fusion defect between lysosomes and autophagosomes but could create such a fusion defect. Also, a more general defect in exit from the TGN if this is the case in CLN3 depleted cells could lead to a failure to deliver fusion machinery to late endosomes/lyososomes, thus explaining or adding the fusion defect also.

In considering how a CI-MPR trafficking defect could impinge on the autophagy machinery in cells, it has been reported that, during nutrient deprivation, the CI-MPR population moves into vesicular structures (Young et al., 2006), almost completely leaving the TGN area. Since this suggests that the receptor could rearrange its cellular location when autophagy is stimulated, we have therefore investigated the trafficking of CI-MPR in cells starved to stimulate autophagy.

6.1 CI-MPR is delivered directly to autophagosomes

HeLa cells expressing CD8-CIMPR were fed with anti CD8 antibody conjugated to HRP-Fab fragments for 2 hours while being grown in EBSS media to induce starvation. After 2 hours, cells were fixed and embedded as usual for EM studies.

In starved HeLa cells, the HRP, used to reveal the Fab fragments, was present not only in the TGN but also in new-born autophagosomes, clearly identified by their internal characteristic cytosolic content (Figure 6.1). In the autophagosomal membrane the DAB deposition was strikingly present. The autophagosomes were localized in the perinuclear area and in close proximity to the Golgi. Different stages of maturation could also be easily identified by their electron density of their contents.

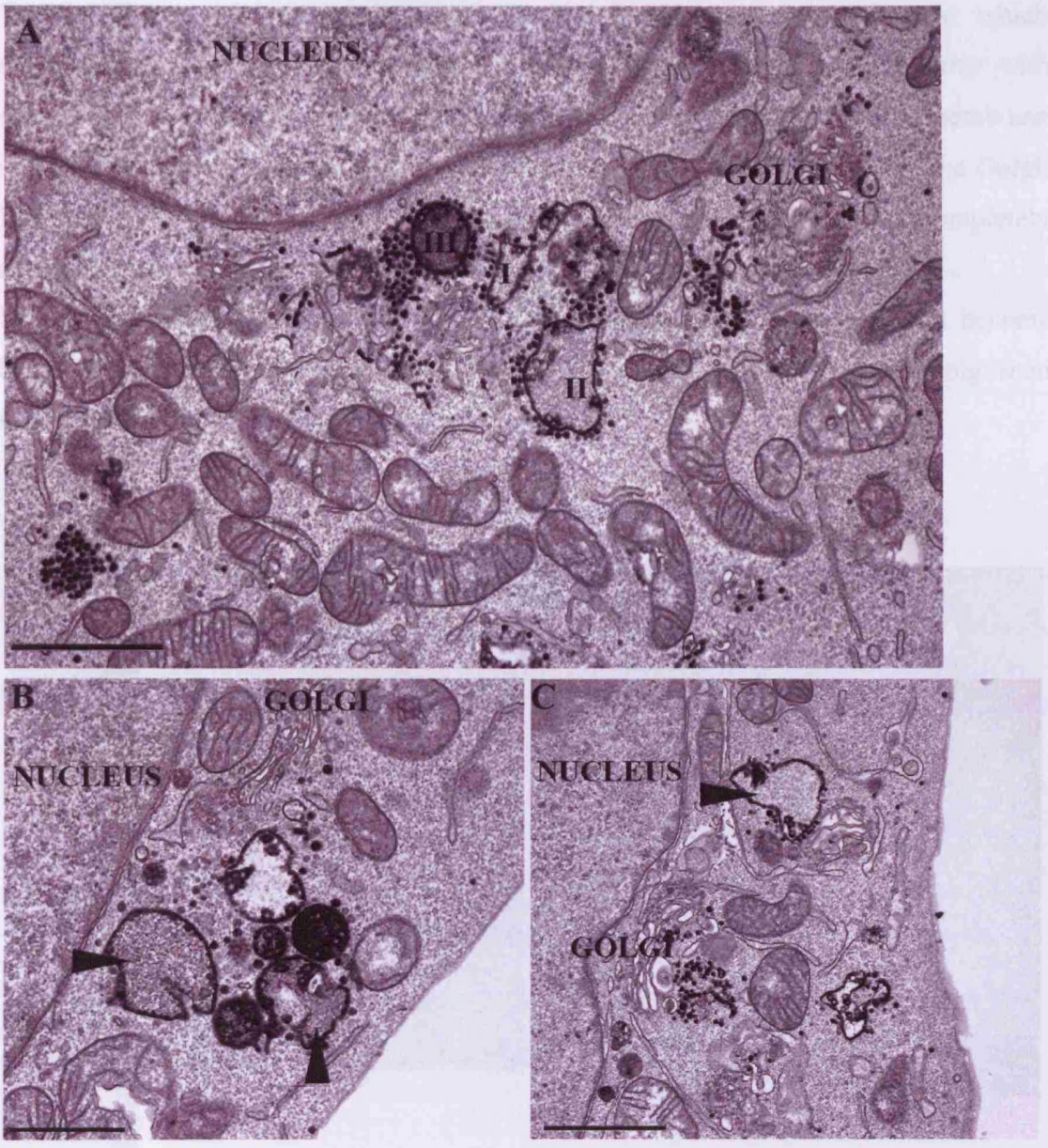

Figure 6.1 HRP-Zenon feeding of CD8-CI-MPR stably expressing HeLa cells under starvation conditions

HeLa cells expressing CD8-CI-MPR were grown for 2 hours in EBSS medium to induce starvation and fed with anti-CD8 antibody conjugated to HRP Fab fragments, then stained with DAB to visualize HRP by electron microscopy.
In A, a forming autophagosome (I), and maturing autophagosomes (II and III); in particular III is electron dense suggesting it is in an advanced stage in respect to I and II. In B and C other examples of autophagosomes are reported (arrows).
Scale bar=1μm

The early autophagosomes observed all had HRP positive membranes, which suggested that the autophagosomal membrane contains CI-MPR. This together with the proximity of newly formed organelles to the Golgi suggests that the membrane may originate from trans Golgi cisternae or tubular endosomes very close to the Golgi. In panel A of Figure 6.1, one autophagosome labelled with HRP are not completely closed (I) and the autophagic membrane is distinctively tubular (arrows).

In many starved cells, the TGN morphology was altered from normal and become become more highly arched in shape (Figure 6.2) as compared with normal Golgi seen in Figure 5.7.

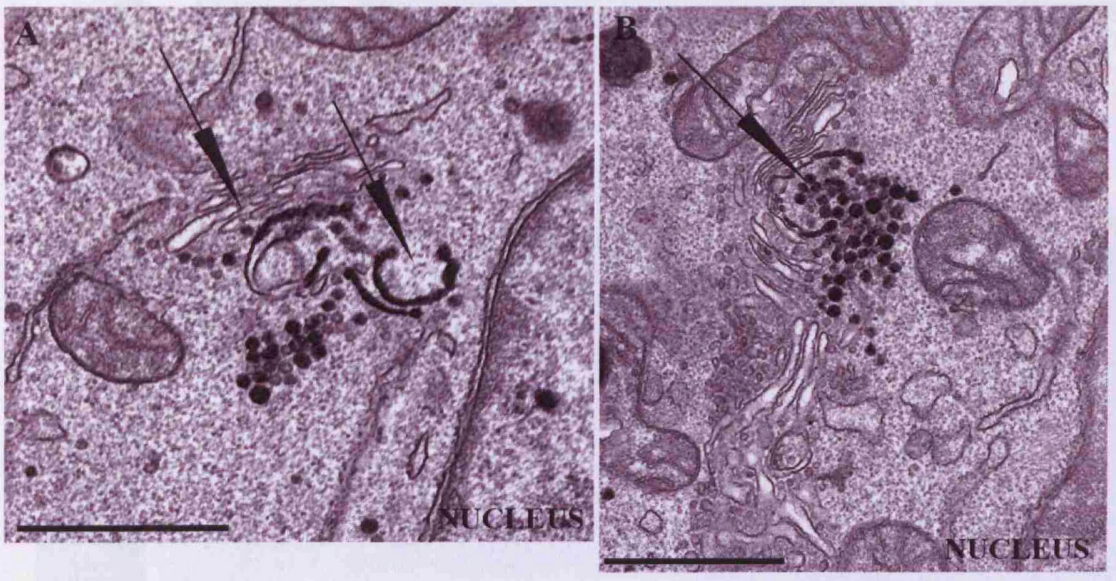

Figure 6.2 Golgi morphology of CD8-CIMPR stably expressing HeLa cells fed with HRP Zenon-CD8 under starvation conditions.

HeLa cells expressing CD8-CI-MPR were grown for 2 hours in EBSS medium to induce starvation and fed with anti-CD8 antibody conjugated to HRP Fab fragments, then stained with DAB to visualize HRP by electron microscopy.
Arrows indicate the Golgi complex. HRP visualized with DAB.
Scale bar=1μm

Further, only in starved cells, the CI-MPR receptor, in addition to its localisation at the TGN and autophagosomal membrane was also present in vesicles which were aggregated and tended to be organised in patches (Figure 6.3 panel A and B, arrow head). Sometimes they appeared to be in between the TGN apparatus and the rest of the Golgi (arrows) and sometimes further away and separated from the Golgi. The vesicles were also seen outside the newly forming autophagosome, and some were also seen inside the same autophagosomes (Figure 6.4). At first sight it seemed that the vesicles could have been entrapped with the cytosol at the moment of autophagosomal formation. However, the process seems more complicated since some vesicles were in the process of fusion or "budding in", to the newly formed organelle as suggested by the connection with the autophagosomal membrane (arrows). These vesicles could be delivering cargo, such as that carried by the CI-MPR, to the autophagosomes (Figure 6.4).

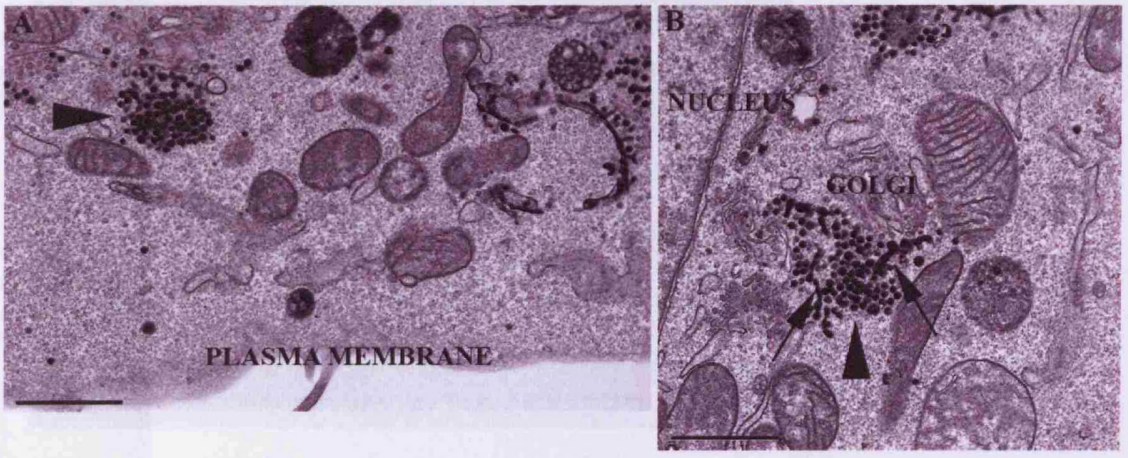

Figure 6.3 Vesicle aggregates in CD8-CIMPR stably expressing HeLa cells fed with HRP Zenon-CD8 under starvation conditions

HeLa cells expressing CD8-CI-MPR were grown for 2 hours in EBSS medium to induce starvation and fed with anti-CD8 antibody conjugated to HRP Fab fragments, then stained with DAB to visualize HRP by electron microscopy.
Arrows indicate clusters of vesicles. HRP visualized with DAB.
Scale bar=1μm

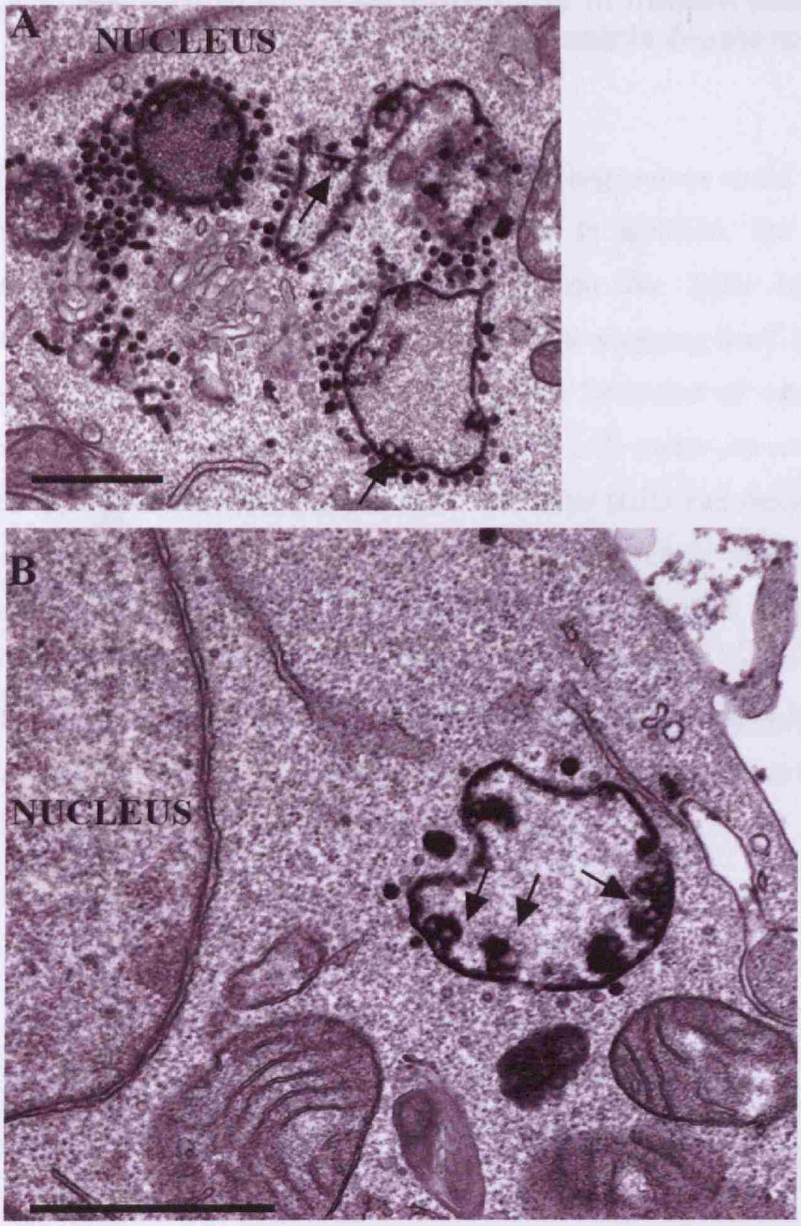

Figure 6.4 Vesicles in proximity to and inside newly formed autophagosomes in CD8-CIMPR stably expressing HeLa cells fed with HRP Zenon-CD8 under starvation conditions

HeLa cells expressing CD8-CI-MPR were grown for 2 hours in EBSS medium to induce starvation and fed with anti-CD8 antibody conjugated to HRP Fab fragments, then stained with DAB to visualize HRP by electron microscopy.
Arrow indicate vesicle presumably in the process of 'budding in" newly formed autophagosomes. HRP visualized with DAB.
Scale bar=1μm

6.1.1 Starvation induced autophagy in human skin fibroblasts, shows that the formation of vesicle clusters is not cell dependent

The observations above suggested that autophagosomes could arise from the TGN or endosomes where the CI-MPR cycles to. In addition, the presence of vesicular aggregates suggest a vesicular route from the TGN to the newly forming autophagosomes rather then the TGN directly wrapping itself into an autophagosomal sourronding membrane. To examine if the formation of vesicle aggregates was a characteristic and a specific feature of HeLa cells under starvation conditions, another cell type was analysed. Human skin fibroblasts (BR3 cell line) were also subjected to 2 hours of nutrient deprivation and prepared for electron microscopy. At the EM level, double membrane bound autophagosomes were detected in proximity to the Golgi (Figure 6.5) and many vesicles were detected inside the newly formed autophagosomes and also in their proximity (panel A, C and D). In some cells it was also possible to see in maturing autophagosomes not only cytosol with vesicles, but also organelles such as mitochondria and ER (panel B).

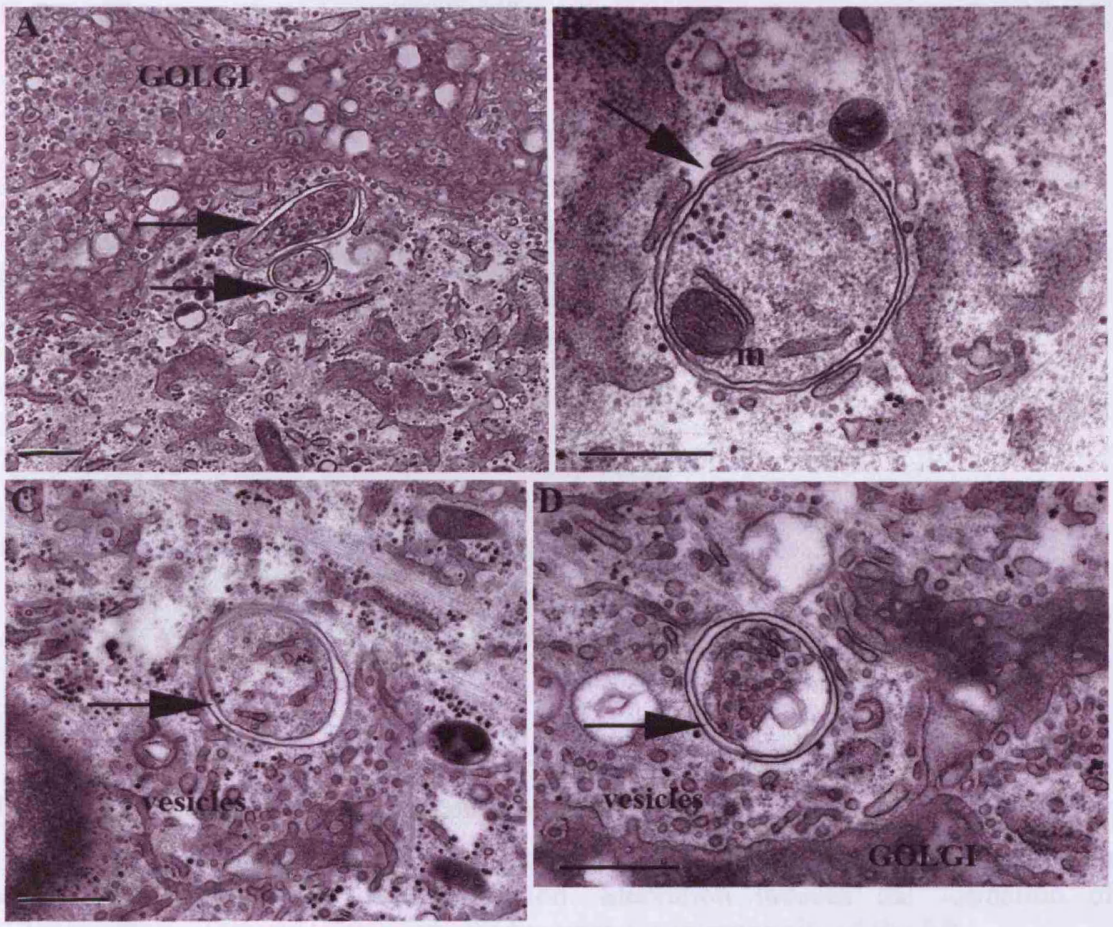

Figure 6.5 Autophagosome formation in human skin fibroblasts under starvation conditions

Human skin fibroblasts grown for not more than 20 passages, were treated for 2 hours with EBSS media to induce starvation. Starvation induces the formation of autophagosomes in the proximity of the Golgi. Many vesicles cluster around them and are present in the same newly formed organelles.
Arrows indicate autophagosomes, m=mitochondria
Scale bar=0.5μm

The forming autophagosomes were often seen in very close proximity to the ER (Figure 6.6).

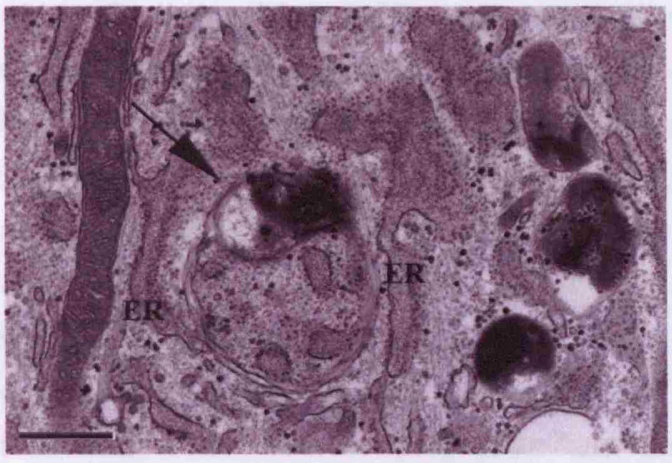

Figure 6.6 Autophagosome in close proximity to the ER

Human skin fibroblasts grown for not more than 20 passages, were treated for 2 hours with EBSS media to induce starvation. Starvation induces the formation of autophagosome (arrow). Often autophagosomes are in proximity of the ER.
Scale bar=0.5μm

6.2 Discussion

Stable CD8-CI-MPR-expressing HeLa cells were used to visualize the localization of CI-MPR after feeding of anti-CD8 conjugated to Zenon-HRP-Fab fragments to cells in starvation conditions. It was found that CI-MPR changes its localization after induction of autophagy. As shown in chapter 5 by electron microscopy, CD8-CI-MPR is present in the TGN, in a few clathrin coated vesicles in the TGN area, and in endosomes. After starvation, we observed that CI-MPR was now present in many small vesicles organized in patches and along the newly forming autophagosomes that were not present under normal growth conditions.

In particular, the newly formed autophagosmal membranes were positive for CI-MPR, indicating that the formation of the autophagosomal membrane may arise by fusion of vesicles budded from the TGN or associated endosomes. This morphology emphasized how the TGN is in close association with newly forming autophagosomes, which are distinguished by their cytosolic content. One of the main unanswered questions about autophagy is the source of the autophagosomal membrane. Golgi and ER have been suggested already as possible autophagosomal membrane sources (Mijaljica et al., 2006) but there is no firm proof to confirm this hypothesis. These results provide evidence to suggest that that the major source of autophagosome membranes in HeLa cells could be the TGN. In fibroblasts where autophagy was induced by starvation in the same way as for HeLa cells, we found that the ultrastructure of the forming autophagosomes was different. In particular, in fibroblasts a characteristic phagophore and early autophagosome with double membrane was observed, in contrast to HeLa cells, where early autophagosomes were single-membrane bound and the traditionally reported phagophore with layers of membranes was not found. Also, in HeLa cells the TGN occasionally showed membrane protrusions and it is possible to speculate that the membranes that arise from these could be autophagosomal membranes.

The most striking finding was probably the unexpected clustering of CI-MPR positive vesicles.

In starved cells autophagosomes undergo ultrastructural changes as they form and mature. This can include an increase in density and contents and changes in size. After induction of starvation with EBSS media, newly formed structures can be observed and their content is initially cytosolic.

The presence of CI-MPR in autophagosomes has already been addressed in the literature, and it has been established that the receptor is present in low levels, along with acid phosphatase and cathepsins in maturing autophagosomes (Tooze et al., 1990).

In mature autophagosomes, the level of cathepsins, especially cathepsin D, and CI-MPR are much higher (Tooze et al., 1990). Here, by using a very sensitive EM approach we have uncovered new details on CI-MPR recruitment to the

autophagosomes as they mature have been defined and form the basis for further investigation.

It has been reported that the CI-MPR does not appear to be increased after the induction of autophagy (Tooze et al., 1990). However it was found that the receptors localization shifts, into vesicles organized in patches.

Moreover, the proximity of the CI-MPR vesicles to the newly formed autophagosomes was striking. In addition, the CI-MPR positive vesicles were found inside the autophagosomes, not just randomly distributed inside the autophagic organelles but specifically adjacent to their internal edges. It is not clear why these vesicles are present inside the autophagosomes but it could be speculated that they may contain not only CI-MPR but other molecules needed for the maturation of the autophagosomes.

7 Summary, discussion and future work

In this thesis we attempted to discover the function of CLN3 by determing the phenotypes arising from its loss as seen at the light and ultrastructural level of morphology. From this descriptive work we hoped to infer CLN3 function.
Discovery of the function of CLN3 is fundamental to understand the basis of Juvenile Batten disease. Two major findings were observed and described, one regarding the abnormal accumulation of autophagosomes (chapter 3 and 4) in CLN3 cells and the other concerning the block of CI-MPR in the TGN (chapter 5). Furthermore, a small study was made of the origin of autophagosome membranes in relation to CI-MPR (chapter 6) and TGN.

7.1 Lysosome and autophagosome meeting point

Similarly to what has been shown for Batten disease, other neurodegenerative diseases present with an abnormal accumulation of autophagic vacuoles, establishing that the autophagic pathway exerts a primary role in neurodegeneration. (Nixon et al., 2005) (Rubinsztein et al., 2005) (Nixon, 2006)
In addition, it has been postulated that the autophagosome accumulation seen in some lysosomal storage diseases is due to defective clearance by autophagosome-lysosome fusion (Settembre et al., 2007) even if the mechanism still remains to be clarified (Settembre et al., 2008). Few hypotheses have been made, but one possible mechanism is an impairment of vesicular trafficking due to defects in microtubules, which has been shown to cause a block in autophagosome-lysosome fusion when disrupted (Kochl et al., 2006; Webb et al., 2004). A link between CLN3 and microtubules has been made, since CLN3 overexpression causes the microtubular binding protein HOOK1 to dissociate from microtubules and to aggregate(Luiro et al., 2004).
In phagocytosis, a different, but clearly related pathway, fusion between lysosomes and phagosomes is arrested due to a defective lysosomal distribution in cells deficient for Lamp1/Lamp2. The lysosomes in these cells are more dispersed than in the wild

type due to altered dynein-mediated transport of lysosomes which is depressed in Lamp-KO cells (Huynh et al., 2007).

Another possible mechanism underlying autophagic compartment expansion in lysosomal storage disorders involves changes in the lipid composition in the lysosome membranes leading to impairment of fusogenic and transport mechanism. This could occur in cholesterol and glycosphingolipids accumulating lysosomal storage disorders such as Niemann Pick disease (Ko et al., 2005) (Sobo et al., 2007). Thirdly and more applicable to JNCL, a defect in endosomal trafficking could also be responsible for perturbing autophagosomal maturation (Settembre et al., 2008).

It is possible the basis of this phenomena could be due to a combination of these effects.

To determine which step in autophagosome maturation is affected in cells after loss of CLN3 in JNCL, both light and electron microscopy approaches were employed. A good approach to investigate if the relationship between lysosomes and autophagosomes was found using HRP feeding and electron microscopy. This showed that none of the autophagosomes accumulating in CLN3 MEFs KO were reached by an endocytic tracer. Previously, it was reported using pancreatic cells that autophagosomes fuse with components of the endocytic pathway just 20 minutes after induction of autophagy (Tooze et al., 1990). Here we allowed more than one hour for the tracer to reach the entire endocytic machinery (Tooze et al., 1990) but it was able just to fill the endocytic pathway, not the JNCL autophagosomes.

Also subunit c, the mitochondrial marker which accumulates in JNCL patient cells, was found just in the autophagosomes and not in the lysosomes by cryo electron microscopy.

We therefore propose that the autophagic pathway in CLN3 deficient cells is arrested and either no fusion or very delayed fusion occurs with the components of the endocytic pathway. Sparse Lamp1 gold particles were found in cryo sections labelling the autophagosomes. It is believed that Lamp1 is recruited to autophagosomes as a consequence of fusion with lysosomes but no fusion was observed between endosomes and autophagosomes in CLN3 deficient cells so it would be possible that Lamp1 could get partially recruited directly to autophagosomes via TGN. We here

proved that the maturation of the autophagosomes is arrested in CLN3 deficient cells and no fusion events of autophagosomes with lysosomes occurs or it is very delayed.

Since it is currently only possible to examine the relationship between autophagosomes and endosomes using electron microscopy due to the paucity of autophagosomal markers we decided to investigate if phagocytosis, another pathway which involves fusion events and a tight relationship to the endocytic pathway, is impaired in JNCL due to impaired fusion with endosomes. Phagosomes need to fuse with endosomes to mature (Tjelle et al., 2000; Vieira et al., 2002) in a similar way to autophagosomes (Bampton et al., 2005). In CLN3 deficient cells a striking delay in fusion events occurred between phagosomes both late and early endosomes was observed.

Light and electron microscopy evidence suggested that the interaction between phagosomes with lysosomes was impaired, as was observed for the autophagic pathway. Although autophagic and phagocytic pathways cannot be direcly compared due to the differences in origin of phagosomes and autophagosomes, both do have in common the necessity for these multiple interactions with the endocytic pathway.

To continue the work on autophagy it would be very helpful to have to hand new markers which specifically recognize the organelles from their intitial formation. Otherwise accurate analysis relies on electron microscopy study. In particular it is critical to understand at which point CLN3 is recruited to the autophagosomal membrane. In addition, there are other components that should be investigate, for example Lamp2 (Eskelinen et al., 2002) which has been shown to exert a role in fusion between phagosomes and lysosomes.

7.1.1 SNARE mediated membrane fusion

To better study fusion defects, it would also be critical to identify new SNAREs which must be present in the membranes of the autophagosomes. There are over 30 SNARE family members in mammalian cells and each one is found in a distinct subcellular compartment (Chen and Scheller, 2001).

In this work the presence of Syntaxin 8 was identified in LC3 positive organelles. Syntaxin 8 forms a complex with Vtlb, endobrevin/Vamp8 and Syntaxin 7; and it is localized mostly in late endosomes/lysososomes (Pryor et al., 2004). In LC3-EGFP stable expressing cells we observed the presence of Syntaxin 8 in autophagosomes, and sometimes Syntaxin 8 was found colocalizing with LC3 before Lampl was recruited.

No difference in Syntaxin 8 distribution was observed after CLN3 knock down. Syntaxin 8 stability is due to another SNARE, Vtlb. In Vtlb KO mice, Syntaxin 8 levels are reduced due to degradation of the protein and cells from the liver presented an abnormal accumulation of autophagosome and MVBs (Atlashkin et al., 2003). Vtlb may control the stability of Syntaxin 8 and the interaction of the two SNAREs could somehow exert a role in the fusion of autophagosomes with MVBs or lysosomes. For this reason it would be of great interest to analyse in detail both Syntaxin 8 and Vtlb in relation to autophagy to better understand and its mechanism and the interconnections with endosomes.

7.1.2 Phagocytosis defects in CLN3 deficient cells

Phagocytosis was found to be defective in CLN3 KO mouse embryonic fibroblasts transfected with FcR and allowed to internalize latex beads opsonized with human IgG (Chapter 4). We showed that CLN3 deficient cells are able to internalize latex beads but a delay of fusion events occurs as was demonstrated by delay of recruitment of endocytic markers to maturing phagosomes.

To further this phagocytosis study in the future, it would be worth looking at professional phagocytic cells isolated from *Cln3* mice, rather than engineered phagocytic fibroblasts.

A major defect in phagocytosis has not been reported in patients with Batten disease, although bacterial respiratory infections have been noted in Finnish patients (Dr. Laura Aberg, University of Helsinki, personal communication). The leading symptom in JNCL/Batten disease is blindness associated with retinitis pigmentosa and photoreceptor cell death. The retinal pigment epithelia cells are a major site of

phagocytosis, digesting shed photoreceptor outer segments. RPE cells have not been reported to be deficient in Batten disease, but phagocytosis in the *Cln3* $^{\Delta ex1/6}$ mice is currently being examined by EM in collaboration with Dr Clare Futter (UCL).

Previously examined samples from *Cln3* KO brains showed an accumulation of large amounts of storage material in microglial cells, suggesting that these professional phagocytes are able to phagocytose properly but are not able to digest (Mitchison and Turmaine, unpublished). Similar microglial storage accumulation is seen in JNCL brains by many. Both *Cln3* KO mouse and *Cln3*$^{\Delta ex7/8}$ show prominent and enlarged microglia in brain (Pontikis et al., 2004) (Pontikis et al., 2005) similar to JNCL brains (Tyynela et al., 2004).

As demonstrated in chapter 4, using engineered phagocytic cells, the defect is probably a deficiency in fusion of phagosomes with the endocytic compartment.

In conclusion, it is necessary to continue investigating the phagocytic pathway, since this could be responsible in part, for cell death in JNCL patients.

7.2 Batten disease and CI-MPR

After CLN3 depletion, CI-MPR is almost exclusively localized at the TGN.

Anti-CD8 antibody feeding in CLN3 siRNA HeLa cells that were also transfected with CD8-CIMPR showed re-localization of CI-MPR to the Golgi area resulting from CLN3 depletion. In particular, a 30 minute pulse of CD8 antibody in these cells with a more than 2 hours chase, resulted in an even tight localization of CI-MPR at the TGN. Together this indicates that CI-MPR is specifically blocked in the TGN after CLN3 knock down.

One of the CI-MPR functions is to deliver hydrolases to the lysosomes. If the trafficking of this essential receptor is impaired it could result in reduced hydrolase delivery to the lysosomes with a knock on effect of increased secretion of hydrolases. Time did not allow an analysis of cargo delivery in CLN3 depleted cells, but an important assay would be investigating targeting and secretion of cathepsin D and other lysosomal hydrolases.

CI-MPR binds the hydrolases at the TGN and is directed to endosomes in clathrin coated vesicles (CCV) that bud from the TGN.

It was reported that CLN3 localization to lysosomes is dependent on direct interaction with AP-1 and AP-3 (Kyttala et al., 2005) although this remains controversial (Storch et al., 2004). If AP-1 directly interacts with CLN3, it could be that this interaction is crucial to the exit of CI-MPR from the clathrin-coated vesicles. It will be critical in future to understand how the proteins involved in CI-MPR exit from the TGN and CLN3 interact.

After CLN3 siRNA, we found that CI-MPR re-distributes localizing almost exclusively at the TGN. Electron microscopy analysis showed that CI-MPR is present not only along the TGN ribbon but also in clathrin coated vesicles in the TGN area. A quantification of these clathrin coated vesicles and also vesicles that are not clathrin coated is crucial to continue this work on understanding if CI-MPR is less present in these vesicles. In the scenario that there is less CI-MPR present in clathrin coated vesicles it would be worth checking the level of GGAs, since they have been shown to be likely to be important for bringing CI-MPR to CCVs and so are closely involved in budding events.

In future work it would also be of vital importance to repeat and confirm by EM experiments on CI-MPR localization using an antibody that can recognize the endogenous protein. Electron microscopy experiments provided evidence that CI-MPR is localized at the TGN but investigation of the endogenous protein would be more meaningful and might supply more information about the exact distribution. It is possible that the overexpression of the CD8-CI-MPR construct used here could cause the CI-MPR to "fill" in all of the TGN ribbon, and thereby prevent discovery of a subdomain.

TGN exit is the main defect observed after CLN3 siRNA. From the TGN, membrane carriers and clathrin coated vesicles form and bud off in order to be transported to the PM or endosomes respectively. At the TGN a segregation process occurs and different cargos are sorted into different carriers. For example the VSGV protein is sorted at the Golgi into carriers and not in clathrin coated vesicles for destination at the PM; these constitutive secretory carriers do not colocalize with CI-MPR or Furin (Polishchuk et

al., 2003). The VSVG protein could be used as a control in future work, to prove the specificity or not of the role of CLN3 in blocking CI-MPR exit. In conclusion, it remains to be determined if the block at the TGN caused by CLN3 is specific for CI-MPR; other receptors may also be impaired, such as sorLA or sortillin.

Knock down of GGAs or AP-1 causes a bypass of TGN-lysosome targeting and causes hydrolases to be secreted. It would be desirable to test whether after CLN3 knock down there is secretion of lysosome hydrolases. In particular cathepsin D which is employed in subunit c degradation.

It has been shown that CLN3 deficiency causes defects in cathepsin D processing but it still remains to be established whether this enzyme is actually secreted from CLN3 deficient cells (Golabek et al., 2000) (Fossale et al., 2004).

In conclusion, two important question marks remain for the role of CLN3 in the CI-MPR block at the TGN: establishing the relationship between the two proteins and also their interaction scheme with the GGA and AP-1 proteins.

It was recently reported that depletion of Vps24 (ESCRTIII) increases the amount of CI-MPR and the receptor localizes in the Golgi. Further, the Golgi is fragmented suggesting that Vps24 controls recycling to the Golgi of one or more factors that mantain its integrity (Raiborg et al., 2007). Since in our hands, loss of CLN3 does not fragment the Golgi but tightens up the ribbon, we would argue that a different mechanism is being used.

7.3 Autophagy: a new clue to the origin of autophagosomal membrane

One of the major phenotypic characteristics in CLN3 deficient cells is the accumulation of autophagosomes.

CI-MPR recruitment to autophagosomes has been analysed in pancreatic cells and it was observed that a low level of CI-MPR was present in maturing autophagosomes but a higher level was found in autophagosomes fused with lysosomes (Tooze et al., 1990).

In chapter 6 we tried to link the CI-MPR block caused by CLN3 deficiency and the formation of autophagosomes by inducing starvation in CD8-CI-MPR expressing cells and simultaneously feeding CD8 conjugated to HRP-Fab fragments.

In this study we could confirm the presence of CI-MPR in maturing autophagosomes in HeLa cells. Additionally we noticed that CI-MPR is recruited very early after the formation of autophagosomes, likely even before a fusion with endosomes had occurred, as judged on morphological criteria.

We also found that after starvation, CI-MPR distributes itself in vesicles that are located in near proximity to the TGN, most often organized in clusters. The EM clearly implied that the CI-MPR positive vesicles are destined for delivery to the autophagosomes. It seems possible that vesicles-based delivery of CI-MPR is necessary for the initial formation of the autophagosomes.

It is also possible to speculate that, in Batten disease the autophagosomal maturation defect is due not only to missing interactions between autophagosomes and endosomes but also due a defect in formation revealed by the missing delivery of CI-MPR.

It would be challenging to understand the function of the CI-MPR containing vesicles. One hypothesis is that these vesicles could bring proton pumps to the autophagosomes, for their initial acidification: it was reported that acidification occurs while the autophagosomes mature by staining with DAMP (Tooze et al., 1990) and that autophagosomal acidification could in fact occur before the fusion of autophagosomes with the lysosomes.

Futher experiments are required to confirm which molecules the CI-MPR-positive vesicles are bringing to the autophosomes and it is intriguing to consider that autophagosomes might be maturing independently of the endocytic pathway.

It would be of interest to investigate the only transmembrane protein conserved across species, member of the Atg family called Atg9 (Noda et al., 2000). This transmembrane protein localizes at the PAS and in the cytosol in yeast, and traffics between PAS and non-PAS structures (usually mitochondria) thus potentially being involved in autophagosome formation (Reggiori et al., 2005). In mammalian cells Atg9 traffics from the TGN, from where it is usually presented to endosomes in starvation conditions, but it is not found in mitochondria (Young et al., 2006). ULK1

(Atg1) siRNA inhibits the starvation-induced redistribution of Atg9 and it stays in the TGN. It was reported in the same work that after starvation CI-MPR traffics in the same way as Atg9, when the CI-MPR TGN population moves to the endosomes in starvation conditions (Young et al., 2006). It would be extremely interesting to observe Atg9 behaviour in CLN3 depleted cells.

Due to paucity of markers there is currently no way to distinguish (except by morphology), the initial stage of autophagosome formation since even LC3 gets recruited late and is therefore not a good early marker. Additionally, in conventional cryo-fixation samples the preservation is not good enough to distinguish the first stages of autophagosomal maturation. In addition, new techniques need to be developed. In chapter 6 we suggested that the TGN changes morphology after induction of autophagy and sometimes protrusions are observed. It would therefore be of great interest to apply the high pressure freezing technique to improve the resolution of the TGN (Zenner et al., 2007). Another development that should also be considered is a new approach combining high pressure freezing with the use of less conventional resin that allows gold particle staining for immunolocalisation purposes (Hawes et al., 2007).

Bibliography

(1995). Isolation of a novel gene underlying Batten disease, CLN3. The International Batten Disease Consortium. *Cell* **82**, 949-57.

Antonin, W., Holroyd, C., Tikkanen, R., Honing, S. and Jahn, R. (2000). The R-SNARE endobrevin/VAMP-8 mediates homotypic fusion of early endosomes and late endosomes. *Mol Biol Cell* **11**, 3289-98.

Atlashkin, V., Kreykenbohm, V., Eskelinen, E. L., Wenzel, D., Fayyazi, A. and Fischer von Mollard, G. (2003). Deletion of the SNARE vti1b in mice results in the loss of a single SNARE partner, syntaxin 8. *Mol Cell Biol* **23**, 5198-207.

Bampton, E. T., Goemans, C. G., Niranjan, D., Mizushima, N. and Tolkovsky, A. M. (2005). The dynamics of autophagy visualized in live cells: from autophagosome formation to fusion with endo/lysosomes. *Autophagy* **1**, 23-36.

Barbero, P., Bittova, L. and Pfeffer, S. R. (2002). Visualization of Rab9-mediated vesicle transport from endosomes to the trans-Golgi in living cells. *J Cell Biol* **156**, 511-8.

Bensaoula, T., Shibuya, H., Katz, M. L., Smith, J. E., Johnson, G. S., John, S. K. and Milam, A. H. (2000). Histopathologic and immunocytochemical analysis of the retina and ocular tissues in Batten disease. *Ophthalmology* **107**, 1746-53.

Berg, T. O., Fengsrud, M., Stromhaug, P. E., Berg, T. and Seglen, P. O. (1998). Isolation and characterization of rat liver amphisomes. Evidence for fusion of autophagosomes with both early and late endosomes. *J Biol Chem* **273**, 21883-92.

Cao, Y., Espinola, J. A., Fossale, E., Massey, A. C., Cuervo, A. M., MacDonald, M. E. and Cotman, S. L. (2006). Autophagy is disrupted in a knock-in mouse model of juvenile neuronal ceroid lipofuscinosis. *J Biol Chem* **281**, 20483-93.

Caron, E. and Hall, A. (1998). Identification of two distinct mechanisms of phagocytosis controlled by different Rho GTPases. *Science* **282**, 1717-21.

Chang, J. W., Choi, H., Kim, H. J., Jo, D. G., Jeon, Y. J., Noh, J. Y., Park, W. J. and Jung, Y. K. (2007). Neuronal vulnerability of CLN3 deletion to calcium-induced cytotoxicity is mediated by calsenilin. *Hum Mol Genet* **16**, 317-26.

Chattopadhyay, S., Ito, M., Cooper, J. D., Brooks, A. I., Curran, T. M., Powers, J. M. and Pearce, D. A. (2002). An autoantibody inhibitory to glutamic acid decarboxylase in the neurodegenerative disorder Batten disease. *Hum Mol Genet* **11**, 1421-31.

Chattopadhyay, S., Roberts, P. M. and Pearce, D. A. (2003). The yeast model for Batten disease: a role for Btn2p in the trafficking of the Golgi-associated vesicular targeting protein, Yif1p. *Biochem Biophys Res Commun* **302**, 534-8.

Chen, Y. A. and Scheller, R. H. (2001). SNARE-mediated membrane fusion. *Nat Rev Mol Cell Biol* **2**, 98-106.

Collins, R. F., Schreiber, A. D., Grinstein, S. and Trimble, W. S. (2002). Syntaxins 13 and 7 function at distinct steps during phagocytosis. *J Immunol* **169**, 3250-6.

Cooper, J. D. (2003). Progress towards understanding the neurobiology of Batten disease or neuronal ceroid lipofuscinosis. *Curr Opin Neurol* **16**, 121-8.

Cotman, S. L., Vrbanac, V., Lebel, L. A., Lee, R. L., Johnson, K. A., Donahue, L. R., Teed, A. M., Antonellis, K., Bronson, R. T., Lerner, T. J. et al. (2002). Cln3(Deltaex7/8) knock-in mice with the common JNCL mutation exhibit progressive neurologic disease that begins before birth. *Hum Mol Genet* **11**, 2709-21.

Croopnick, J. B., Choi, H. C. and Mueller, D. M. (1998). The subcellular location of the yeast Saccharomyces cerevisiae homologue of the protein defective in the juvenile form of Batten disease. *Biochem Biophys Res Commun* **250**, 335-41.

Downey, G. P., Botelho, R. J., Butler, J. R., Moltyaner, Y., Chien, P., Schreiber, A. D. and Grinstein, S. (1999). Phagosomal maturation, acidification, and inhibition of bacterial growth in nonphagocytic cells transfected with FcgammaRIIA receptors. *J Biol Chem* **274**, 28436-44.

Duclos, S., Diez, R., Garin, J., Papadopoulou, B., Descoteaux, A., Stenmark, H. and Desjardins, M. (2000). Rab5 regulates the kiss and run fusion between phagosomes and endosomes and the acquisition of phagosome leishmanicidal properties in RAW 264.7 macrophages. *J Cell Sci* **113 Pt 19**, 3531-41.

Dunn, W. A., Jr. (1990a). Studies on the mechanisms of autophagy: formation of the autophagic vacuole. *J Cell Biol* **110**, 1923-33.

Dunn, W. A., Jr. (1990b). Studies on the mechanisms of autophagy: maturation of the autophagic vacuole. *J Cell Biol* **110**, 1935-45.

Dunn, W. A., Jr. (1994). Autophagy and related mechanisms of lysosome-mediated protein degradation. *Trends Cell Biol* **4**, 139-43.

Dyken, P. R. (1988). Reconsideration of the classification of the neuronal ceroid-lipofuscinoses. *Am J Med Genet Suppl* **5**, 69-84.

Eliason, S. L., Stein, C. S., Mao, Q., Tecedor, L., Ding, S. L., Gaines, D. M. and Davidson, B. L. (2007). A knock-in reporter model of Batten disease. *J Neurosci* **27**, 9826-34.

Eskelinen, E. L., Illert, A. L., Tanaka, Y., Schwarzmann, G., Blanz, J., Von Figura, K. and Saftig, P. (2002). Role of LAMP-2 in lysosome biogenesis and autophagy. *Mol Biol Cell* **13**, 3355-68.

Ezaki, J., Takeda-Ezaki, M., Koike, M., Ohsawa, Y., Taka, H., Mineki, R., Murayama, K., Uchiyama, Y., Ueno, T. and Kominami, E. (2003). Characterization of Cln3p, the gene product responsible for juvenile neuronal ceroid lipofuscinosis, as a lysosomal integral membrane glycoprotein. *J Neurochem* **87**, 1296-308.

Ezaki, J., Wolfe, L. S. and Kominami, E. (1995). Defect of proteolysis of mitochondrial ATP synthase subunit C in neuronal ceroid lipofuscinosis. *Gerontology* **41 Suppl 2**, 259-69.

Fossale, E., Wolf, P., Espinola, J. A., Lubicz-Nawrocka, T., Teed, A. M., Gao, H., Rigamonti, D., Cattaneo, E., MacDonald, M. E. and Cotman, S. L. (2004). Membrane trafficking and mitochondrial abnormalities precede subunit c deposition in a cerebellar cell model of juvenile neuronal ceroid lipofuscinosis. *BMC Neurosci* **5**, 57.

Fratti, R. A., Backer, J. M., Gruenberg, J., Corvera, S. and Deretic, V. (2001). Role of phosphatidylinositol 3-kinase and Rab5 effectors in phagosomal biogenesis and mycobacterial phagosome maturation arrest. *J Cell Biol* **154**, 631-44.

Fukuda, T., Ewan, L., Bauer, M., Mattaliano, R. J., Zaal, K., Ralston, E., Plotz, P. H. and Raben, N. (2006). Dysfunction of endocytic and autophagic pathways in a lysosomal storage disease. *Ann Neurol* **59**, 700-8.

Gachet, Y., Codlin, S., Hyams, J. S. and Mole, S. E. (2005). btn1, the Schizosaccharomyces pombe homologue of the human Batten disease gene CLN3, regulates vacuole homeostasis. *J Cell Sci* **118**, 5525-36.

Ghosh, P., Dahms, N. M. and Kornfeld, S. (2003a). Mannose 6-phosphate receptors: new twists in the tale. *Nat Rev Mol Cell Biol* **4**, 202-12.

Ghosh, P., Griffith, J., Geuze, H. J. and Kornfeld, S. (2003b). Mammalian GGAs act together to sort mannose 6-phosphate receptors. *J Cell Biol* **163**, 755-66.

Goebel, H. H. (1995). The neuronal ceroid-lipofuscinoses. *J Child Neurol* **10**, 424-37.

Goebel, H. H., Schochet, S. S., Jaynes, M., Bruck, W., Kohlschutter, A. and Hentati, F. (1999). Progress in neuropathology of the neuronal ceroid lipofuscinoses. *Mol Genet Metab* **66**, 367-72.

Golabek, A. A., Kaczmarski, W., Kida, E., Kaczmarski, A., Michalewski, M. P. and Wisniewski, K. E. (1999). Expression studies of CLN3 protein (battenin) in fusion with the green fluorescent protein in mammalian cells in vitro. *Mol Genet Metab* **66**, 277-82.

Golabek, A. A., Kida, E., Walus, M., Kaczmarski, W., Michalewski, M. and Wisniewski, K. E. (2000). CLN3 protein regulates lysosomal pH and alters intracellular processing of Alzheimer's amyloid-beta protein precursor and cathepsin D in human cells. *Mol Genet Metab* **70**, 203-13.

Haltia, M., Rapola, J. and Santavuori, P. (1973). Infantile type of so-called neuronal ceroid-lipofuscinosis. Histological and electron microscopic studies. *Acta Neuropathol (Berl)* **26**, 157-70.

Harding, T. M., Hefner-Gravink, A., Thumm, M. and Klionsky, D. J. (1996). Genetic and phenotypic overlap between autophagy and the cytoplasm to vacuole protein targeting pathway. *J Biol Chem* **271**, 17621-4.

Haskell, R. E., Carr, C. J., Pearce, D. A., Bennett, M. J. and Davidson, B. L. (2000). Batten disease: evaluation of CLN3 mutations on protein localization and function. *Hum Mol Genet* **9**, 735-44.

Haskell, R. E., Derksen, T. A. and Davidson, B. L. (1999). Intracellular trafficking of the JNCL protein CLN3. *Mol Genet Metab* **66**, 253-60.

Hawes, P., Netherton, C. L., Mueller, M., Wileman, T. and Monaghan, P. (2007). Rapid freeze-substitution preserves membranes in high-pressure frozen tissue culture cells. *J Microsc* **226**, 182-9.

Hirst, J., Seaman, M. N., Buschow, S. I. and Robinson, M. S. (2007). The role of cargo proteins in GGA recruitment. *Traffic* **8**, 594-604.

Holopainen, J. M., Saarikoski, J., Kinnunen, P. K. and Jarvela, I. (2001). Elevated lysosomal pH in neuronal ceroid lipofuscinoses (NCLs). *Eur J Biochem* **268**, 5851-6.

Honing, S., Sosa, M., Hille-Rehfeld, A. and von Figura, K. (1997). The 46-kDa mannose 6-phosphate receptor contains multiple binding sites for clathrin adaptors. *J Biol Chem* **272**, 19884-90.

Huynh, K. K., Eskelinen, E. L., Scott, C. C., Malevanets, A., Saftig, P. and Grinstein, S. (2007). LAMP proteins are required for fusion of lysosomes with phagosomes. *Embo J* **26**, 313-24.

Isosomppi, J., Vesa, J., Jalanko, A. and Peltonen, L. (2002). Lysosomal localization of the neuronal ceroid lipofuscinosis CLN5 protein. *Hum Mol Genet* **11**, 885-91.

Jager, S., Bucci, C., Tanida, I., Ueno, T., Kominami, E., Saftig, P. and Eskelinen, E. L. (2004). Role for Rab7 in maturation of late autophagic vacuoles. *J Cell Sci* **117**, 4837-48.

Jahreiss, L., Menzies, F. M. and Rubinsztein, D. C. (2008). The itinerary of autophagosomes: From peripheral formation to kiss-and-run fusion with lysosomes. *Traffic*.

Janes, R. W., Munroe, P. B., Mitchison, H. M., Gardiner, R. M., Mole, S. E. and Wallace, B. A. (1996). A model for Batten disease protein CLN3: functional implications from homology and mutations. *FEBS Lett* **399**, 75-7.

Jarvela, I., Lehtovirta, M., Tikkanen, R., Kyttala, A. and Jalanko, A. (1999). Defective intracellular transport of CLN3 is the molecular basis of Batten disease (JNCL). *Hum Mol Genet* **8**, 1091-8.

Jarvela, I., Sainio, M., Rantamaki, T., Olkkonen, V. M., Carpen, O., Peltonen, L. and Jalanko, A. (1998). Biosynthesis and intracellular targeting of the CLN3 protein defective in Batten disease. *Hum Mol Genet* **7**, 85-90.

Jolly, R. D., Brown, S., Das, A. M. and Walkley, S. U. (2002). Mitochondrial dysfunction in the neuronal ceroid-lipofuscinoses (Batten disease). *Neurochem Int* **40**, 565-71.

Kabeya, Y., Mizushima, N., Ueno, T., Yamamoto, A., Kirisako, T., Noda, T., Kominami, E., Ohsumi, Y. and Yoshimori, T. (2000). LC3, a mammalian homologue of yeast Apg8p, is localized in autophagosome membranes after processing. *Embo J* **19**, 5720-8.

Kametaka, S., Okano, T., Ohsumi, M. and Ohsumi, Y. (1998). Apg14p and Apg6/Vps30p form a protein complex essential for autophagy in the yeast, Saccharomyces cerevisiae. *J Biol Chem* **273**, 22284-91.

Kasper, D., Planells-Cases, R., Fuhrmann, J. C., Scheel, O., Zeitz, O., Ruether, K., Schmitt, A., Poet, M., Steinfeld, R., Schweizer, M. et al. (2005). Loss of the chloride channel ClC-7 leads to lysosomal storage disease and neurodegeneration. *Embo J* **24**, 1079-91.

Katz, M. L., Shibuya, H., Liu, P. C., Kaur, S., Gao, C. L. and Johnson, G. S. (1999). A mouse gene knockout model for juvenile ceroid-lipofuscinosis (Batten disease). *J Neurosci Res* **57**, 551-6.

Kida, E., Kaczmarski, W., Golabek, A. A., Kaczmarski, A., Michalewski, M. and Wisniewski, K. E. (1999). Analysis of intracellular distribution and trafficking of the CLN3 protein in fusion with the green fluorescent protein in vitro. *Mol Genet Metab* **66**, 265-71.

Kihara, A., Kabeya, Y., Ohsumi, Y. and Yoshimori, T. (2001). Beclin-phosphatidylinositol 3-kinase complex functions at the trans-Golgi network. *EMBO Rep* **2**, 330-5.

Kim, J., Huang, W. P., Stromhaug, P. E. and Klionsky, D. J. (2002). Convergence of multiple autophagy and cytoplasm to vacuole targeting components to a perivacuolar membrane compartment prior to de novo vesicle formation. *J Biol Chem* **277**, 763-73.

Kim, Y., Ramirez-Montealegre, D. and Pearce, D. A. (2003). A role in vacuolar arginine transport for yeast Btn1p and for human CLN3, the protein defective in Batten disease. *Proc Natl Acad Sci U S A* **100**, 15458-62.

Klionsky, D. J. (2005). The molecular machinery of autophagy: unanswered questions. *J Cell Sci* **118**, 7-18.

Klionsky, D. J., Cregg, J. M., Dunn, W. A., Jr., Emr, S. D., Sakai, Y., Sandoval, I. V., Sibirny, A., Subramani, S., Thumm, M., Veenhuis, M. et al. (2003). A unified nomenclature for yeast autophagy-related genes. *Dev Cell* **5**, 539-45.

Klionsky, D. J. and Emr, S. D. (2000). Autophagy as a regulated pathway of cellular degradation. *Science* **290**, 1717-21.

Klumperman, J., Hille, A., Veenendaal, T., Oorschot, V., Stoorvogel, W., von Figura, K. and Geuze, H. J. (1993). Differences in the endosomal distributions of the two mannose 6-phosphate receptors. *J Cell Biol* **121**, 997-1010.

Ko, D. C., Milenkovic, L., Beier, S. M., Manuel, H., Buchanan, J. and Scott, M. P. (2005). Cell-autonomous death of cerebellar purkinje neurons with autophagy in Niemann-Pick type C disease. *PLoS Genet* **1**, 81-95.

Kochl, R., Hu, X. W., Chan, E. Y. and Tooze, S. A. (2006). Microtubules facilitate autophagosome formation and fusion of autophagosomes with endosomes. *Traffic* **7**, 129-45.

Koenig, H. (1964). Neuronal lipofuscin in disease. Its relation to lysosomes. *Trans Am Neurol Assoc* **89**, 212-3.

Koike, M., Shibata, M., Waguri, S., Yoshimura, K., Tanida, I., Kominami, E., Gotow, T., Peters, C., von Figura, K., Mizushima, N. et al. (2005). Participation of autophagy in storage of lysosomes in neurons from mouse models of neuronal ceroid-lipofuscinoses (Batten disease). *Am J Pathol* **167**, 1713-28.

Kominami, E., Ezaki, J. and Wolfe, L. S. (1995). New insight into lysosomal protein storage disease: delayed catabolism of ATP synthase subunit c in Batten disease. *Neurochem Res* **20**, 1305-9.

Kornfeld, S. (1992). Structure and function of the mannose 6-phosphate/insulinlike growth factor II receptors. *Annu Rev Biochem* **61**, 307-30.

Kornfeld, S. and Mellman, I. (1989). The biogenesis of lysosomes. *Annu Rev Cell Biol* **5**, 483-525.

Kovacs, A. D., Weimer, J. M. and Pearce, D. A. (2006). Selectively increased sensitivity of cerebellar granule cells to AMPA receptor-mediated excitotoxicity in a mouse model of Batten disease. *Neurobiol Dis* **22**, 575-85.

Kremmidiotis, G., Lensink, I. L., Bilton, R. L., Woollatt, E., Chataway, T. K., Sutherland, G. R. and Callen, D. F. (1999). The Batten disease gene product (CLN3p) is a Golgi integral membrane protein. *Hum Mol Genet* **8**, 523-31.

Kyttala, A., Ihrke, G., Vesa, J., Schell, M. J. and Luzio, J. P. (2004). Two motifs target Batten disease protein CLN3 to lysosomes in transfected nonneuronal and neuronal cells. *Mol Biol Cell* **15**, 1313-23.

Kyttala, A., Lahtinen, U., Braulke, T. and Hofmann, S. L. (2006). Functional biology of the neuronal ceroid lipofuscinoses (NCL) proteins. *Biochim Biophys Acta* **1762**, 920-33.

Kyttala, A., Yliannala, K., Schu, P., Jalanko, A. and Luzio, J. P. (2005). AP-1 and AP-3 facilitate lysosomal targeting of Batten disease protein CLN3 via its dileucine motif. *J Biol Chem* **280**, 10277-83.

Le Borgne, R. and Hoflack, B. (1997). Mannose 6-phosphate receptors regulate the formation of clathrin-coated vesicles in the TGN. *J Cell Biol* **137**, 335-45.

Levine, B. and Kroemer, G. (2008). Autophagy in the Pathogenesis of Disease. *Cell* **132**, 27-42.

Lin, S. X., Mallet, W. G., Huang, A. Y. and Maxfield, F. R. (2004). Endocytosed cation-independent mannose 6-phosphate receptor traffics via the endocytic recycling compartment en route to the trans-Golgi network and a subpopulation of late endosomes. *Mol Biol Cell* **15**, 721-33.

Liou, W., Geuze, H. J., Geelen, M. J. and Slot, J. W. (1997). The autophagic and endocytic pathways converge at the nascent autophagic vacuoles. *J Cell Biol* **136**, 61-70.

Livak, K. J. and Schmittgen, T. D. (2001). Analysis of relative gene expression data using real-time quantitative PCR and the 2(-Delta Delta C(T)) Method. *Methods* **25**, 402-8.

Lucocq, J. and Walker, D. (1997). Evidence for fusion between multilamellar endosomes and autophagosomes in HeLa cells. *Eur J Cell Biol* **72**, 307-13.

Luiro, K., Kopra, O., Blom, T., Gentile, M., Mitchison, H. M., Hovatta, I., Tornquist, K. and Jalanko, A. (2006). Batten disease (JNCL) is linked to disturbances in mitochondrial, cytoskeletal, and synaptic compartments. *J Neurosci Res* **84**, 1124-38.

Luiro, K., Kopra, O., Lehtovirta, M. and Jalanko, A. (2001). CLN3 protein is targeted to neuronal synapses but excluded from synaptic vesicles: new clues to Batten disease. *Hum Mol Genet* **10**, 2123-31.

Luiro, K., Yliannala, K., Ahtiainen, L., Maunu, H., Jarvela, I., Kyttala, A. and Jalanko, A. (2004). Interconnections of CLN3, Hook1 and Rab proteins link Batten disease to defects in the endocytic pathway. *Hum Mol Genet* **13**, 3017-27.

Luzio, J. P., Pryor, P. R. and Bright, N. A. (2007). Lysosomes: fusion and function. *Nat Rev Mol Cell Biol* **8**, 622-32.

Mao, Q., Foster, B. J., Xia, H. and Davidson, B. L. (2003a). Membrane topology of CLN3, the protein underlying Batten disease. *FEBS Lett* **541**, 40-6.

Mao, Q., Xia, H. and Davidson, B. L. (2003b). Intracellular trafficking of CLN3, the protein underlying the childhood neurodegenerative disease, Batten disease. *FEBS Lett* **555**, 351-7.

Margraf, L. R., Boriack, R. L., Routheut, A. A., Cuppen, I., Alhilali, L., Bennett, C. J. and Bennett, M. J. (1999). Tissue expression and subcellular localization of CLN3, the Batten disease protein. *Mol Genet Metab* **66**, 283-9.

Martinez-Vicente, M. and Cuervo, A. M. (2007). Autophagy and neurodegeneration: when the cleaning crew goes on strike. *Lancet Neurol* **6**, 352-61.

Medd, S. M., Walker, J. E. and Jolly, R. D. (1993). Characterization of the expressed genes for subunit c of mitochondrial ATP synthase in sheep with ceroid lipofuscinosis. *Biochem J* **293 (Pt 1)**, 65-73.

Meyer, C., Zizioli, D., Lausmann, S., Eskelinen, E. L., Hamann, J., Saftig, P., von Figura, K. and Schu, P. (2000). mu1A-adaptin-deficient mice: lethality, loss of AP-1 binding and rerouting of mannose 6-phosphate receptors. *Embo J* **19**, 2193-203.

Mijaljica, D., Prescott, M. and Devenish, R. J. (2006). Endoplasmic reticulum and Golgi complex: Contributions to, and turnover by, autophagy. *Traffic* **7**, 1590-5.

Mitchison, H. M., Bernard, D. J., Greene, N. D., Cooper, J. D., Junaid, M. A., Pullarkat, R. K., de Vos, N., Breuning, M. H., Owens, J. W., Mobley, W. C. et al. (1999). Targeted disruption of the Cln3 gene provides a mouse model for Batten disease. The Batten Mouse Model Consortium [corrected]. *Neurobiol Dis* **6**, 321-34.

Mitchison, H. M., Lim, M. J. and Cooper, J. D. (2004). Selectivity and types of cell death in the neuronal ceroid lipofuscinoses. *Brain Pathol* **14**, 86-96.

Mitchison, H. M., Munroe, P. B., O'Rawe, A. M., Taschner, P. E., de Vos, N., Kremmidiotis, G., Lensink, I., Munk, A. C., D'Arigo, K. L., Anderson, J. W. et al. (1997). Genomic structure and complete nucleotide sequence of the Batten disease gene, CLN3. *Genomics* **40**, 346-50.

Mizushima, N., Ohsumi, Y. and Yoshimori, T. (2002). Autophagosome formation in mammalian cells. *Cell Struct Funct* **27**, 421-9.

Mousavi, S. A., Kjeken, R., Berg, T. O., Seglen, P. O., Berg, T. and Brech, A. (2001). Effects of inhibitors of the vacuolar proton pump on hepatic heterophagy and autophagy. *Biochim Biophys Acta* **1510**, 243-57.

Narayan, S. B., Rakheja, D., Tan, L., Pastor, J. V. and Bennett, M. J. (2006). CLN3P, the Batten's disease protein, is a novel palmitoyl-protein Delta-9 desaturase. *Ann Neurol* **60**, 570-7.

Narayan, S. B., Tan, L. and Bennett, M. J. (2007). Intermediate levels of neuronal palmitoyl-protein Delta-9 desaturase in heterozygotes for murine Batten disease. *Mol Genet Metab.*

Neufeld, E. F. (1991). Lysosomal storage diseases. *Annu Rev Biochem* **60**, 257-80.

Nixon, R. A. (2006). Autophagy in neurodegenerative disease: friend, foe or turncoat? *Trends Neurosci* **29**, 528-35.

Nixon, R. A., Wegiel, J., Kumar, A., Yu, W. H., Peterhoff, C., Cataldo, A. and Cuervo, A. M. (2005). Extensive involvement of autophagy in Alzheimer disease: an immuno-electron microscopy study. *J Neuropathol Exp Neurol* **64**, 113-22.

Noda, T., Kim, J., Huang, W. P., Baba, M., Tokunaga, C., Ohsumi, Y. and Klionsky, D. J. (2000). Apg9p/Cvt7p is an integral membrane protein required for transport vesicle formation in the Cvt and autophagy pathways. *J Cell Biol* **148**, 465-80.

Palmer, D. N., Fearnley, I. M., Walker, J. E., Hall, N. A., Lake, B. D., Wolfe, L. S., Haltia, M., Martinus, R. D. and Jolly, R. D. (1992). Mitochondrial ATP synthase subunit c storage in the ceroid-lipofuscinoses (Batten disease). *Am J Med Genet* **42**, 561-7.

Pearce, D. A., Ferea, T., Nosel, S. A., Das, B. and Sherman, F. (1999). Action of BTN1, the yeast orthologue of the gene mutated in Batten disease. *Nat Genet* **22**, 55-8.

Pearce, D. A. and Sherman, F. (1997). BTN1, a yeast gene corresponding to the human gene responsible for Batten's disease, is not essential for viability, mitochondrial function, or degradation of mitochondrial ATP synthase. *Yeast* **13**, 691-7.

Persaud-Sawin, D. A., McNamara, J. O., 2nd, Rylova, S., Vandongen, A. and Boustany, R. M. (2004). A galactosylceramide binding domain is involved in trafficking of CLN3 from Golgi to rafts via recycling endosomes. *Pediatr Res* **56**, 449-63.

Phillips, S. N., Benedict, J. W., Weimer, J. M. and Pearce, D. A. (2005). CLN3, the protein associated with batten disease: structure, function and localization. *J Neurosci Res* **79**, 573-83.

Poet, M., Kornak, U., Schweizer, M., Zdebik, A. A., Scheel, O., Hoelter, S., Wurst, W., Schmitt, A., Fuhrmann, J. C., Planells-Cases, R. et al. (2006). Lysosomal storage disease upon disruption of the neuronal chloride transport protein ClC-6. *Proc Natl Acad Sci U S A* **103**, 13854-9.

Pohl, S., Mitchison, H. M., Kohlschutter, A., Diggelen, O. V., Braulke, T. and Storch, S. (2007). Increased expression of lysosomal acid phosphatase in CLN3-defective cells and mouse brain tissue. *J Neurochem.*

Pohlmann, R., Boeker, M. W. and von Figura, K. (1995). The two mannose 6-phosphate receptors transport distinct complements of lysosomal proteins. *J Biol Chem* **270**, 27311-8.

Polishchuk, E. V., Di Pentima, A., Luini, A. and Polishchuk, R. S. (2003). Mechanism of constitutive export from the golgi: bulk flow via the formation, protrusion, and en bloc cleavage of large trans-golgi network tubular domains. *Mol Biol Cell* **14**, 4470-85.

Pontikis, C. C., Cella, C. V., Parihar, N., Lim, M. J., Chakrabarti, S., Mitchison, H. M., Mobley, W. C., Rezaie, P., Pearce, D. A. and Cooper, J. D. (2004). Late onset neurodegeneration in the Cln3-/- mouse model of juvenile neuronal ceroid lipofuscinosis is preceded by low level glial activation. *Brain Res* **1023**, 231-42.

Pontikis, C. C., Cotman, S. L., MacDonald, M. E. and Cooper, J. D. (2005). Thalamocortical neuron loss and localized astrocytosis in the Cln3Deltaex7/8 knock-in mouse model of Batten disease. *Neurobiol Dis* **20**, 823-36.

Probst, O. C., Ton, P., Svoboda, B., Gannon, A., Schuhmann, W., Wieser, J., Pohlmann, R. and Mach, L. (2006). The 46-kDa mannose 6-phosphate receptor does not depend on endosomal acidification for delivery of hydrolases to lysosomes. *J Cell Sci* **119**, 4935-43.

Pryor, P. R., Mullock, B. M., Bright, N. A., Lindsay, M. R., Gray, S. R., Richardson, S. C., Stewart, A., James, D. E., Piper, R. C. and Luzio, J. P. (2004). Combinatorial SNARE complexes with VAMP7 or VAMP8 define different late endocytic fusion events. *EMBO Rep* **5**, 590-5.

Puertollano, R., Aguilar, R. C., Gorshkova, I., Crouch, R. J. and Bonifacino, J. S. (2001). Sorting of mannose 6-phosphate receptors mediated by the GGAs. *Science* **292**, 1712-6.

Punnonen, E. L., Autio, S., Marjomaki, V. S. and Reunanen, H. (1992). Autophagy, cathepsin L transport, and acidification in cultured rat fibroblasts. *J Histochem Cytochem* **40**, 1579-87.

Raiborg, C., Malerod, L., Pedersen, N. M. and Stenmark, H. (2007). Differential functions of Hrs and ESCRT proteins in endocytic membrane trafficking. *Exp Cell Res.*

Ramirez-Montealegre, D. and Pearce, D. A. (2005). Defective lysosomal arginine transport in juvenile Batten disease. *Hum Mol Genet* **14**, 3759-73.

Raught, B., Gingras, A. C. and Sonenberg, N. (2001). The target of rapamycin (TOR) proteins. *Proc Natl Acad Sci U S A* **98**, 7037-44.

Ravikumar, B., Vacher, C., Berger, Z., Davies, J. E., Luo, S., Oroz, L. G., Scaravilli, F., Easton, D. F., Duden, R., O'Kane, C. J. et al. (2004). Inhibition of mTOR induces autophagy and reduces toxicity of polyglutamine expansions in fly and mouse models of Huntington disease. *Nat Genet* **36**, 585-95.

Reggiori, F. and Klionsky, D. J. (2002). Autophagy in the eukaryotic cell. *Eukaryot Cell* **1**, 11-21.

Reggiori, F., Shintani, T., Nair, U. and Klionsky, D. J. (2005). Atg9 cycles between mitochondria and the pre-autophagosomal structure in yeasts. *Autophagy* **1**, 101-9.

Rider, J. A. and Rider, D. L. (1999). Thirty years of Batten disease research: present status and future goals. *Mol Genet Metab* **66**, 231-3.

Riederer, M. A., Soldati, T., Shapiro, A. D., Lin, J. and Pfeffer, S. R. (1994). Lysosome biogenesis requires Rab9 function and receptor recycling from endosomes to the trans-Golgi network. *J Cell Biol* **125**, 573-82.

Rubinsztein, D. C., DiFiglia, M., Heintz, N., Nixon, R. A., Qin, Z. H., Ravikumar, B., Stefanis, L. and Tolkovsky, A. (2005). Autophagy and its possible roles in nervous system diseases, damage and repair. *Autophagy* **1**, 11-22.

Santavuori, P. (1988). Neuronal ceroid-lipofuscinoses in childhood. *Brain Dev* **10**, 80-3.

Seaman, M. N. (2004). Cargo-selective endosomal sorting for retrieval to the Golgi requires retromer. *J Cell Biol* **165**, 111-22.

Seaman, M. N. (2005). Recycle your receptors with retromer. *Trends Cell Biol* **15**, 68-75.

Seigel, G. M., Lotery, A., Kummer, A., Bernard, D. J., Greene, N. D., Turmaine, M., Derksen, T., Nussbaum, R. L., Davidson, B., Wagner, J. et al. (2002). Retinal pathology and function in a Cln3 knockout mouse model of juvenile Neuronal Ceroid Lipofuscinosis (batten disease). *Mol Cell Neurosci* **19**, 515-27.

Settembre, C., Fraldi, A., Jahreiss, L., Spampanato, C., Venturi, C., Medina, D., Pablo, R. D., Tacchetti, C., Rubinsztein, D. C. and Ballabio, A. (2007). A Block of Autophagy in Lysosomal Storage Disorders. *Hum Mol Genet.*

Settembre, C., Fraldi, A., Rubinsztein, D. C. and Ballabio, A. (2008). Lysosomal storage diseases as disorders of autophagy. *Autophagy* **4**, 113-4.

Shintani, T. and Klionsky, D. J. (2004). Autophagy in health and disease: a double-edged sword. *Science* **306**, 990-5.

Siintola, E., Topcu, M., Aula, N., Lohi, H., Minassian, B. A., Paterson, A. D., Liu, X. Q., Wilson, C., Lahtinen, U., Anttonen, A. K. et al. (2007). The novel neuronal ceroid lipofuscinosis gene MFSD8 encodes a putative lysosomal transporter. *Am J Hum Genet* **81**, 136-46.

Siintola, E., Topcu, M., Kohlschutter, A., Salonen, T., Joensuu, T., Anttonen, A. K. and Lehesjoki, A. E. (2005). Two novel CLN6 mutations in variant late-infantile neuronal ceroid lipofuscinosis patients of Turkish origin. *Clin Genet* **68**, 167-73.

Sobo, K., Le Blanc, I., Luyet, P. P., Fivaz, M., Ferguson, C., Parton, R. G., Gruenberg, J. and van der Goot, F. G. (2007). Late endosomal cholesterol accumulation leads to impaired intra-endosomal trafficking. *PLoS ONE* **2**, e851.

Steinfeld, R., Reinhardt, K., Schreiber, K., Hillebrand, M., Kraetzner, R., Brück, W., Saftig, P. and Gärtner, J. (2006). Cathepsin D Deficiency Is Associated with a Human Neurodegenerative Disorder. *American Journal of Human Genetics* **78, in press.**

Storch, S., Pohl, S. and Braulke, T. (2004). A dileucine motif and a cluster of acidic amino acids in the second cytoplasmic domain of the batten disease-related CLN3 protein are required for efficient lysosomal targeting. *J Biol Chem* **279**, 53625-34.

Storch, S., Pohl, S., Quitsch, A., Falley, K. and Braulke, T. (2007). C-terminal prenylation of the CLN3 membrane glycoprotein is required for efficient endosomal sorting to lysosomes. *Traffic* **8**, 431-44.

Suzuki, K., Kirisako, T., Kamada, Y., Mizushima, N., Noda, T. and Ohsumi, Y. (2001). The pre-autophagosomal structure organized by concerted

functions of APG genes is essential for autophagosome formation. *Embo J* **20**, 5971-81.

Tanaka, Y., Guhde, G., Suter, A., Eskelinen, E. L., Hartmann, D., Lullmann-Rauch, R., Janssen, P. M., Blanz, J., von Figura, K. and Saftig, P. (2000). Accumulation of autophagic vacuoles and cardiomyopathy in LAMP-2-deficient mice. *Nature* **406**, 902-6.

Taschner, P. E., de Vos, N. and Breuning, M. H. (1997). Cross-species homology of the CLN3 gene. *Neuropediatrics* **28**, 18-20.

Tjelle, T. E., Lovdal, T. and Berg, T. (2000). Phagosome dynamics and function. *Bioessays* **22**, 255-63.

Tooze, J., Hollinshead, M., Ludwig, T., Howell, K., Hoflack, B. and Kern, H. (1990). In exocrine pancreas, the basolateral endocytic pathway converges with the autophagic pathway immediately after the early endosome. *J Cell Biol* **111**, 329-45.

Tooze, S. and Hollinshead, M. (1992). In AtT20 and HeLa cells brefeldin A induces the fusion of tubular endosomes and changes their distribution and some of their endocytic properties. *J Cell Biol* **118 (4)**, 813-30.

Tortorella, L. L., Schapiro, F. B. and Maxfield, F. R. (2007). Role of an acidic cluster/dileucine motif in cation-independent mannose 6-phosphate receptor traffic. *Traffic* **8**, 402-13.

Tyynela, J., Cooper, J. D., Khan, M. N., Shemilts, S. J. and Haltia, M. (2004). Hippocampal pathology in the human neuronal ceroid-lipofuscinoses: distinct patterns of storage deposition, neurodegeneration and glial activation. *Brain Pathol* **14**, 349-57.

Vesa, J., Chin, M. H., Oelgeschlager, K., Isosomppi, J., DellAngelica, E. C., Jalanko, A. and Peltonen, L. (2002). Neuronal ceroid lipofuscinoses are connected at molecular level: interaction of CLN5 protein with CLN2 and CLN3. *Mol Biol Cell* **13**, 2410-20.

Vieira, O. V., Botelho, R. J. and Grinstein, S. (2002). Phagosome maturation: aging gracefully. *Biochem J* **366**, 689-704.

Waguri, S., Dewitte, F., Le Borgne, R., Rouille, Y., Uchiyama, Y., Dubremetz, J. F. and Hoflack, B. (2003). Visualization of TGN to endosome

trafficking through fluorescently labeled MPR and AP-1 in living cells. *Mol Biol Cell* **14**, 142-55.

Webb, J. L., Ravikumar, B. and Rubinsztein, D. C. (2004). Microtubule disruption inhibits autophagosome-lysosome fusion: implications for studying the roles of aggresomes in polyglutamine diseases. *Int J Biochem Cell Biol* **36**, 2541-50.

Weimer, J. M., Custer, A. W., Benedict, J. W., Alexander, N. A., Kingsley, E., Federoff, H. J., Cooper, J. D. and Pearce, D. A. (2006). Visual deficits in a mouse model of Batten disease are the result of optic nerve degeneration and loss of dorsal lateral geniculate thalamic neurons. *Neurobiol Dis.*

White, I. J., Bailey, L. M., Aghakhani, M. R., Moss, S. E. and Futter, C. E. (2006). EGF stimulates annexin 1-dependent inward vesiculation in a multivesicular endosome subpopulation. *Embo J* **25**, 1-12.

Xie, Z. and Klionsky, D. J. (2007). Autophagosome formation: core machinery and adaptations. *Nat Cell Biol* **9**, 1102-9.

Yamamoto, A., Tagawa, Y., Yoshimori, T., Moriyama, Y., Masaki, R. and Tashiro, Y. (1998). Bafilomycin A1 prevents maturation of autophagic vacuoles by inhibiting fusion between autophagosomes and lysosomes in rat hepatoma cell line, H-4-II-E cells. *Cell Struct Funct* **23**, 33-42.

Yorimitsu, T. and Klionsky, D. J. (2005). Autophagy: molecular machinery for self-eating. *Cell Death Differ* **12 Suppl 2**, 1542-52.

Young, A. R., Chan, E. Y., Hu, X. W., Kochl, R., Crawshaw, S. G., High, S., Hailey, D. W., Lippincott-Schwartz, J. and Tooze, S. A. (2006). Starvation and ULK1-dependent cycling of mammalian Atg9 between the TGN and endosomes. *J Cell Sci* **119**, 3888-900.

Yu, W. H., Cuervo, A. M., Kumar, A., Peterhoff, C. M., Schmidt, S. D., Lee, J. H., Mohan, P. S., Mercken, M., Farmery, M. R., Tjernberg, L. O. et al. (2005). Macroautophagy--a novel Beta-amyloid peptide-generating pathway activated in Alzheimer's disease. *J Cell Biol* **171**, 87-98.

Zenner, H. L., Collinson, L. M., Michaux, G. and Cutler, D. F. (2007). High-pressure freezing provides insights into Weibel-Palade body biogenesis. *J Cell Sci* **120**, 2117-25.

Acknowledgements-Ringraziamenti

I have spent more than three years in the LMCB. How can I describe this time with a few words? Three years spent in between joy, laughter and tears. I am leaving now but I will not leave behind the friendships that I have made here.
I have met a lot of special people and I would like to thank them all...so this thesis is dedicated to all of them...

To Hannah and Dan

Thanks to Hannah and Dan for giving me the chance to learn and improve in these three years. It has been a great learning experience and I feel I have grown hugely and I'm now ready to move on (and go as far away as possible!).
Thinking about my first days in the lab makes me laugh. I had not clue on how to grow cells, no clue about CLN3.... mmm no clue about English either!
These have been 3 passionate years with all the ups and downs of a PhD. I understand it was a bit hard working with me, as I know I can be a bit "intense" sometimes.

Hannah, thanks a lot for the big help on correcting this thesis. I hope you will carry on working on Batten disease.
Thank you so much.

Thanks to Lucy Collinson, one of the people I admire the most and that has passed me her passion for electron microscopy. She has been a great teacher to me

la mia meta' mela, e' stato importante per me avere uno stimolo cosi' forte vicino che mi ha portato a migliorare ed andare avanti e che so, continuera' a starmi accanto

Helen, my adoptive sister. I feel that an era is finishing: you are moving to distant Cambridge and I don't know where I will end up. Thanks for the good times we had together from the water fights to all the rest...
The students:
Emma,Tom favorito, Silene, Andy, Douggy, Emily (Emily-for all the samba classes) for all the time we passed together in and out of the LMCB. I won't miss you because I'll keep seeing you.

Rosy,
I am glad I had the chance to spend more time with you after you left the LMCB. .. I wrote this thesis on viva music notes!

Kim, for all the small presents you made for me, for sharing the office with me, for helping me in the lab and for listening to my complaints on many occasions

Danilos, thanks for helping me sort out a bit of science. Thanks to you I also know that it is possible to be open and collaborative with people, the important thing is to choose the right ones! Keep on going with the IPs on neurons!

Tom N and Krupa you made me laugh on many occasions and that is what really matters in the routine of the lab! Tom N thanks for your help...especially with the FACS!

I would like to thank my committee: Yuki, Mark and Antonella, you have helped me when I needed you.
I would particularly like to thank Antonella for the lunghe chiacchierate. Grazie per essere stata a sentire tutte le mie peripezie e per avermi dato dei consigli importanti quando ne avevo davvero bisogno.

Giovanna, grazie anche a te per essere stata a sentirmi e a consigliarmi.

Mark Turmain who helped me at the start of my PhD with his great knowledge on EM.

Marnie. I missed you in the lab after you left, and of course, "you were also a couple of steps ahead of me (ahahah)".

Jemima for the EM help and general discussion.
Annegret for EM discussions.
Lars for the FACS help

I also would like to thank the people who made my life (a witch and their 2 assistants) horrible during my PhD because they taught me how to resist! and they didn't put me off anyway!Ahahah

Giulia, la nuova amica

Ai miei genitori e mia sorella che pur essendo lontani mi sono stati vicini come sempre

Carol e Giovanni, grazie per il vostro sostegno morale in questi anni. Carol, come suocera non sei tanto male ma non capisco perche' non vuoi ammettere che lo spettacolo con le maschere non ti sia piaciuto.

Le mie amiche che non vedo piu' ma a cui voglio tanto bene, Ele, Andro, Paola. A chi e' diventata mamma di un bimbo, a chi e' pazza che piu' pazza non si puo' e a chi semplicemente auguro un periodo migliore di questo. Mi ricordo di voi anche se siamo state lontane negli ultimi 4 anni e so che ci sarete sempre per me.